CHARACTERIZATION OF THE SARS-COV-2 NSP13 HELICASE

Christine Hum

Department of Chemistry and Biomolecular Sciences
Faculty of Science
University of Ottawa

Thesis submitted to the University of Ottawa in partial fulfillment of
the requirements for the Master's Degree in Chemistry

Abstract

Severe acute respiratory syndrome coronavirus 2 (SARS-CoV-2) is the etiological agent responsible for the coronavirus disease of 2019 (COVID-19) pandemic, which has infected millions of people worldwide. To date, several vaccines and antivirals have been developed against SARS-CoV-2; however, its tendency to mutate rapidly poses a continued threat to human health. As such, the development of better pan-coronavirus therapeutics is still required. Recently, the SARS-CoV-2 non-structural protein 13 (Nsp13) helicase has been shown to be an attractive therapeutic target given its high conservation rate among coronaviruses and indispensable role in viral replication. Based on this, we sought to further study the biochemical mechanisms behind Nsp13's binding and unwinding activities, along with its interactions with host cells, to provide further insight for future therapeutic development.

To study the binding and unwinding activity of Nsp13, we site-specifically incorporated the non-canonical amino acid (ncAA) *p*-azido-*L*-phenylalanine (AzF) into Nsp13 to act as a bioorthogonal handle for fluorescent labelling. We identified five potential sites for AzF incorporation in Nsp13 and assessed their reactivities towards a conjugated Cy5 fluorophore through strain-promoted alkyne-azide cycloaddition (SPAAC). Further experiments were also performed to ensure that the unwinding activity was not adversely affected before these Nsp13-AzF constructs were utilized in fluorescence resonance energy transfer (FRET)-based binding assays. Ultimately, the F81AzF construct was identified to be the most suitable for monitoring the binding of Nsp13 to a series of nucleic acid substrates in a distance-dependent manner by FRET. The next steps of this project would be to implement F81AzF in single-molecule FRET (smFRET) experiments to directly monitor the positioning and dynamics of this helicase on its substrate.

In addition, interactions between Nsp13 and host cellular and biological processes were investigated to provide further insight into potential mechanisms that can be exploited for novel therapeutic development. From transcriptomic profiling analyses of A549 cells, we uncovered that Nsp13 influences microRNA (miRNA) expression and signalling pathways; in particular, miR-146a, a potent mediator of inflammation and immune responses, was found to be induced upon Nsp13-overexpression. Further experiments revealed that this may lead to the inhibition of NF-κB signalling, through the repression of the upstream targets TRAF6 and IRAK1, to suppress the production of proinflammatory cytokines and facilitate viral infection. Collectively, from this work, we propose that further exploration of these miR-146a-mediated signalling pathways may present alternative strategies for antiviral investigations.

Statement of Work

All of the work presented in this thesis is my own and I take full responsibility for its contents. All experiments and data analyses were performed by me.

Acknowledgements

I would like to start by expressing my sincerest gratitude to Dr. John Pezacki for his invaluable guidance and positive encouragement throughout my graduate degree. The countless opportunities you have provided me, along with your continued mentorship has helped me grow both professionally and personally. I would also like to thank Dr. Christopher Boddy and Dr. Adam Damry for your constructive insights as part of my Thesis Advisory Committee. I am also extremely grateful to Dr. John Pezacki, Dr. Roberto Chica, and all the members of the Advanced Protein Engineering, Training, Internships, Courses, and Exhibition (APRENTICE) program for providing generous funding and additional training during my studies. The opportunities to learn novel cutting-edge research and network with fascinating researchers and students from all over the world is beyond anything I could have hoped for during my graduate career.

I would also like to thank all the past and present members of the Pezacki lab for your unwavering support and encouragement – you all truly made coming to work every day an absolute joy. Specifically, I would like to thank my lab mentors Dr. Nadine Ahmed and Dr. Noreen Ahmed for taking me under your wings and providing me with your endless expertise and encouragement. Thank you to my lab-mates and friends Dr. Shadi Masoud, Dr. Roxana Filip, Kaitlyn Morrill, Gabriel Sullivan, Jordan Pham, Salmaan Chummun, Étienne Bélanger, David Lefebvre, Eryn Lundrigan, Tiffany Stern, Parrish Evers, Spencer Uguccioni, Elexa Scott, and Mariam Serhan for always being willing to discuss ideas (both science and non-science related) and lend a helping hand. Our many coffee breaks and various excursions outside the lab are the definite highlights of my time in the lab.

I would also like to thank all my family and friends. Despite not completely understanding my research, your unconditional support and reassurance definitely kept me going throughout this experience.

Table of Contents

List of Figures

List of Tables

List of Abbreviations

Abbreviation	Description
AzF	*p*-azido-*L*-phenylalanine
COVID-19	Coronavirus disease of 2019
Cy3	Cyanine 3
Cy5	Cyanine 5
DBCO	Dibenzocyclooctyne
ds	Double-stranded
FRET	Fluorescence (Förster) resonance energy transfer
HCoV	Human coronavirus
IFN	Interferon
IRAK1	Interleukin-1 receptor-associated kinase 1
MERS-CoV	Middle East respiratory syndrome coronavirus
miRNA/miR	MicroRNA
mRNA	Messenger RNA
ncAA	Noncanonical amino acid
NF-κB	Nuclear factor kappa-light-chain-enhancer of activated B cells
Nsp	Non-structural protein
Nsp13	Non-structural protein 13
nt	Nucleotide
NTPase	Nucleoside triphosphatase
RdRp	RNA-dependent RNA polymerase
RTC	Replication-transcription complex
SARS-CoV	Severe acute respiratory syndrome coronavirus
SARS-CoV-2	Severe acute respiratory syndrome coronavirus 2
smFRET	Single-molecule fluorescence resonance energy transfer
SPAAC	Strain-promoted alkyne-azide cycloaddition
ss	Single-stranded
TLR	Toll-like receptors
TRAF6	TNF receptor-associated factor 6
UTR	Untranslated region

WT	Wild type
ZBD	Zinc binding domain

Chapter 1

General Introduction

1.1 The COVID-19 Pandemic

The newly emerged human coronavirus (HCoV), named severe acute respiratory syndrome coronavirus 2 (SARS-CoV-2), is the causative agent responsible for the recent coronavirus disease of 2019 (COVID-19) pandemic[1–3]. Originating from Wuhan, China in late 2019, this virus has infected over 671 million people and caused over 6.8 million deaths across 229 countries as of February 4, 2023[4,5]. While some COVID-19 patients remain asymptomatic or present with mild flu-like symptoms, others develop severe respiratory distress, cardiac complications, renal failure, septic shock, other long-term health complications, and even death[6]. In addition to acute infection, a phenomenon known as "long covid" has been observed, whereby, recovered individuals continue to present symptoms several months after clearance of the initial infection[7]. Over the past few years, several vaccines have been developed and approved for use, with over 13 billion vaccine doses having been administered worldwide to date[8,9]. There have also been significant advancements in the development of antiviral therapeutics against SARS-CoV-2 infection, expedited through the employment of previous research on coronaviruses[10–13]. Early in the pandemic, the initial strategy for developing antivirals centred around drug repurposing as it was a timely and cost-effective strategy against the imminent threat[14]. Since then, the strategies for developing new drugs include blocking viral entry into host cells, inhibiting viral replication, and mediating cytokine signalling[14–16]. However, despite the development of vaccines and therapeutics against SARS-CoV-2, this virus remains a significant threat to human health, highlighting the need

to better understand this virus' mechanism of pathogenesis and interactions with host signalling pathways to develop more effective therapeutics against novel SARS-CoV-2 variants.

1.2 SARS-CoV- 2 Genome and Life Cycle

Coronaviruses are a group of pathogenic enveloped viruses that belong to the family Coronaviridae in the order Nidovirales[17,18]. They are divided into four genera with Alpha- and Betacoronavirus being the only ones that infect humans[18]. Previous highly pathogenic HCoVs include the severe acute respiratory syndrome coronavirus (SARS-CoV) identified in 2002 and the Middle East respiratory syndrome coronavirus (MERS-CoV) identified 2013[18–21]. SARS-CoV-2 presents high sequence similarity with SARS-CoV (around 80%) and similar cell tropism in the lower respiratory tract by infecting pulmonary epithelial alveolar type II cells[22,23]. Notably, both these coronaviruses gain entry to the cell through the interactions of their spike glycoprotein with the angiotensin-converting enzyme 2 (ACE2) receptor of the host[24,25]. This interaction, along with other host factors such as the transmembrane protease serine 2 (TMPRSS2), the lysosomal cathepsins B/L, and neuropilin-1, promote viral uptake and fusion at the cellular or endosomal membrane [24,26,27].

Following entry into host cells, the viral genome is released into the cell cytoplasm where it starts its replicative cycle. SARS-CoV-2 possesses a large single-stranded positive-sense RNA genome estimated to be around 26-31 kb in length[17]. The genome is organized into 11 open reading frames (ORF) surrounded by a 5′ and 3′ untranslated region (UTR) (**Figure 1.1**)[17,28]. The 5′ frameshifted polyprotein (ORF1a/ORF1b) is proteolytically cleaved by virus-encoded proteases (i.e., the papain-like protease (PL_{pro}) and the 3C-like cysteine protease ($3CL_{pro}$) or main protease

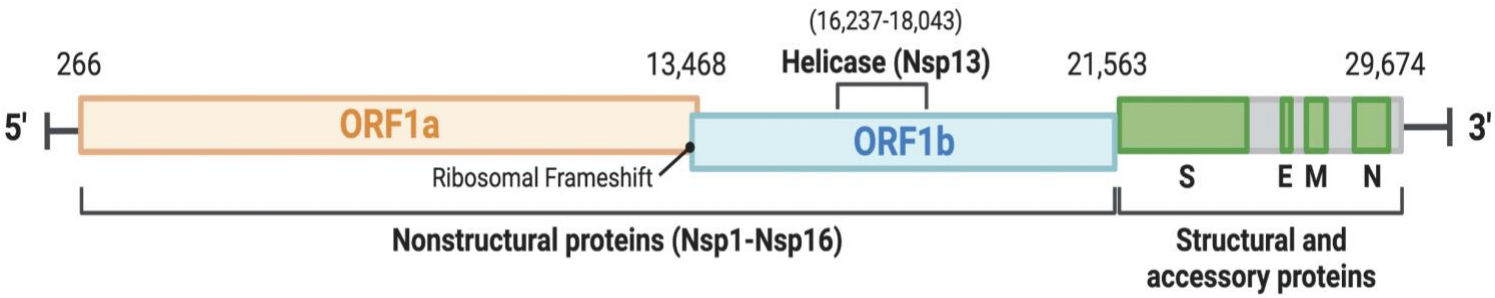

Figure 1.1 Organization of the SARS-CoV-2 Genome.

Structural organization of the SARS-CoV-2 genome, which encodes 16 non-structural proteins (Nsp1-Nsp16), 4 structural proteins (spike (S), envelope (E), membrane (M), nucleocapsid (N)) and several accessory proteins. Figure generated with BioRender.com.

(M_{pro})) into 16 non-structural proteins (Nsp1-Nsp16) that are involved in genome replication and transcription, four structural proteins (spike (S), envelope (E), membrane (M), nucleocapsid (N)), which are common to all coronaviruses, and several accessory proteins that may be important in the virus' pathogenicity[29,30]. Several of these Nsps assemble to form the replication-transcription complex (RTC), namely the RNA binding protein (Nsp9), the RNA-dependent RNA polymerase (RdRp; Nsp12) along with its cofactors Nsp7 and Nsp8 (a primase), and the viral helicase (Nsp13)[31,32]. This initiates viral replication and transcription of the genome that then assembles with the structural proteins to form the mature virion, which can subsequently be released through exocytosis to propel further infection[33].

1.3 Nsp13 Helicase

RNA viruses, such as SARS-CoV-2, often encode their own RNA helicase as they play important roles in viral replication[34,35]. The SARS-CoV-2 Nsp13 helicase (67.5 kDa) is a multi-

functional protein encoded by ORF1b. It possesses an N-terminal zinc-binding domain (ZBD) and C-terminal nucleoside triphosphatase (NTPase) domains[36–38] (**Figure 1.2 A**). It is a member of the superfamily 1 (SF1) helicases, sharing several conserved motifs and similar unwinding activity to other SF1 helicases[39–41]. Previous studies have shown that Nsp13 hydrolyzes nucleoside triphosphates (NTPs) to unwind double-stranded (ds) nucleic acids (both DNA and RNA) in a 5′ to 3′ direction[36,42–45]. This allows Nsp13 to preprocess the highly ordered structure of the viral genome before replication and unwind the dsRNA products generated during viral replication, making it an indispensable component in viral replication[46]. Additionally, there is growing evidence demonstrating that Nsp13 may play a pivotal role in the 5′-capping of viral messenger RNA (mRNA) through its RNA 5′-triphosphatase activity[38,44,47–50], as well as RdRp backtracking, which allows for template switching and proofreading of the viral genome[51,52].

Similar to other Nidovirus helicases, Nsp13 adopts a triangular pyramid architecture consisting of five domains[53,54]. This includes two "RecA-like" ATPase domains (1A and 2A) that possess residues involved in nucleotide (nt) binding and hydrolysis, an N-terminal ZBD, which coordinates three structural zinc ions, a helical stalk domain, and a beta-barrel domain (1B)[38,41,55] (**Figure 1.2 B**). The NTPase binding pocket of Nsp13 is located in a cleft between domains 1A and 2A and consists of six important residues (Lys288, Ser289, Asp374, Glu375, Gln404, Arg567)[38,41,56] (**Figure 1.2 C**). Recent studies have identified that the ZBD and stalk domain also play crucial roles in ATPase activity; however, their specific roles is still unclear[41,57]. The nucleic acid binding groove is formed with the 1A and 2A domains on one side, which makes contact with the 5′ end of the nucleic acid, and the 1B and stalk domains on the other, which makes contact with the 3′ end of the nucleic acid[32,38]. Four basic residues (Arg337, Arg339, Lys345, Lys347) are

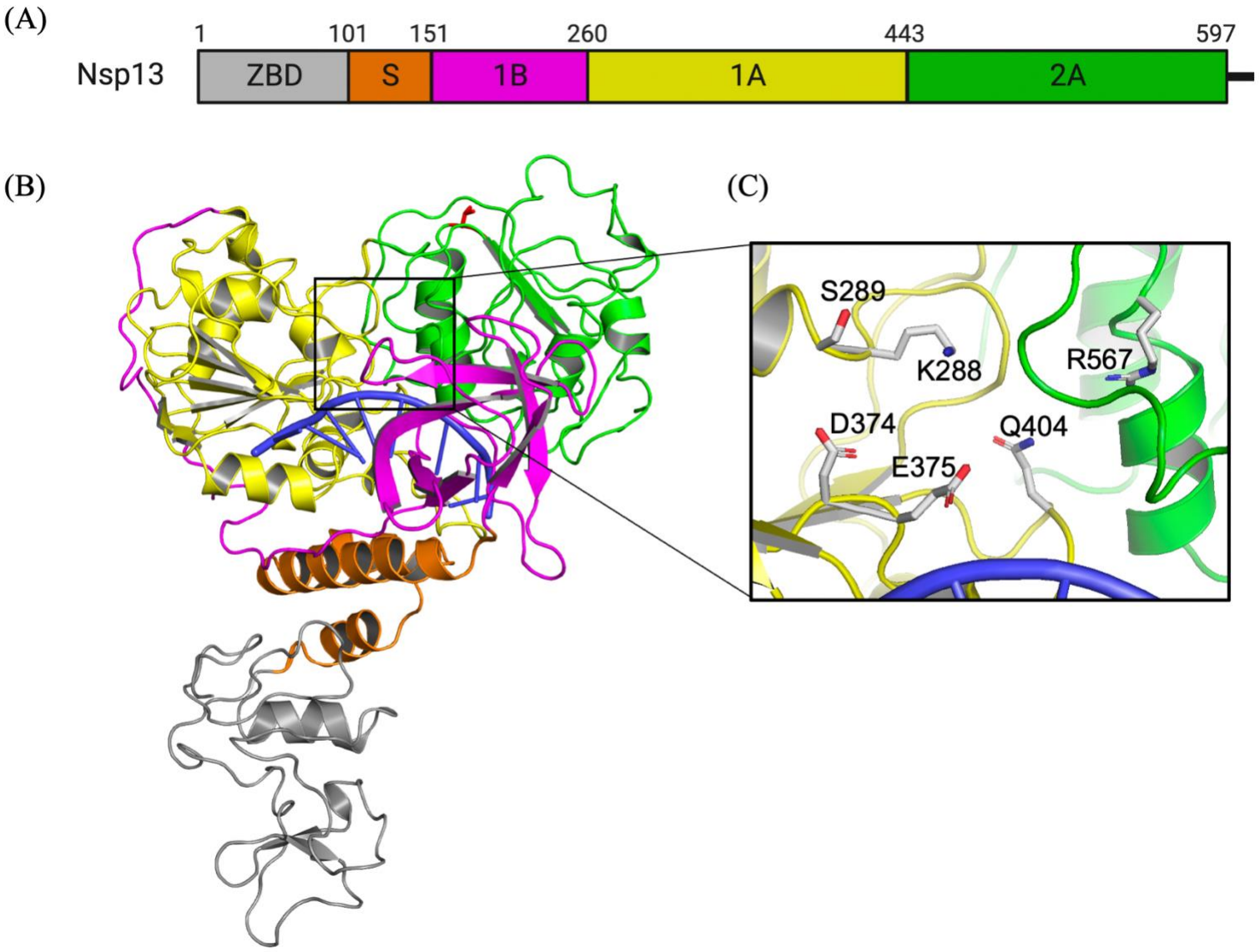

Figure 1.2 Sequence and Structure of SARS-CoV-2 Nsp13 Helicase.

(A) Nsp13 is a multi-functional protein that possesses an N-terminal zinc-binding domain (ZBD; grey), a helical stalk domain (S; orange), a beta-barrel domain (1B; magenta), and two "RecA-like" ATPase/helicase domains (1A; yellow, 2A; green). (B) A modelled Nsp13 with ADP and ssRNA (blue) was adapted from *Perez-Lemus et. al*[58] and shows a triangular pyramid architecture consisting of five domains. The single amino acid substitution between SARS-CoV and SARS-CoV-2 (I570V) is shown as sticks in red. (C) The putative ATP binding site residues are shown between domains 1A and 2A.

located at the entrance of the nucleic acid binding channel and have been found to be crucial for helicase unwinding activity[41]. Furthermore, recent cryo-electron microscopy studies have demonstrated that two Nsp13 molecules associate with the viral RTC[59]. It was identified that Nsp13 makes contact with the thumb domain of the RdRp and that the N-terminal domains of each Nsp13 interact with the N-terminal extension of each Nsp8. This places the nucleic acid-binding ATPase domains of the helicase directly in front of the replicating-transcribing RdRp, thereby facilitating genomic replication and potentially even the backtracking activity of the complex[59].

1.3.1 Nsp13 as a Therapeutic Target

Unlike the high level of variability observed in the structural proteins of SARS-CoV-2, such as the S protein that is commonly mutated in emerging COVID-19 variants[60], Nsp13 is one of the most conserved proteins in the SARS-CoV-2 genome[38,61]. More specifically, the SARS-CoV-2 Nsp13 remarkably shares a 99.8% and 72% sequence identity with the SARS-CoV and MERS-CoV Nsp13, respectively[62–64]. The single amino acid difference from I570 in SARS-CoV to V570 in SARS-CoV-2 (**Figure 1.2. B**) highlights how previous research, solved crystal structures, and drugs discovered against SARS-CoV Nsp13 were important resources early in the pandemic. Given that this viral helicase is both essential for viral replication and highly conserved, Nsp13 is often considered a promising therapeutic target against both SARS-CoV-2 and other HCoVs[38,65]. Unfortunately, while the targeting of viral helicases for drug discovery has been previously explored[66–69], it remains quite challenging in practice, with helicase research often lagging behind other therapeutic strategies such as inhibiting viral polymerases and proteases[10–13]. One major challenge for developing clinically effective helicase inhibitors is the need for highly specific therapeutics that can localize to their desired cellular compartment for targeting of the

viral helicase without inhibiting cellular proteins such as host helicases involved in nucleic acid metabolism and/or cellular homeostasis[70].

Two common methods for discovering Nsp13 helicase inhibitors include "virtual" *in silico* screening and docking studies of the ATP-binding pocket and *in vitro* characterization studies of the ATPase and unwinding activity[36,64,71–73]. Recently, a comprehensive review written by Halma et al. summarized the potential SARS-CoV-2 helicase inhibitors identified in the literature to date[65]. Some promising helicase inhibitors include Ranitidine Bismuth Citrate (a metallodrug commonly used against *Helicobacter pylori* infection)[72,74], SSYA10-001 (a synthetic pharmaceutical drug that inhibits the unwinding activity of a broad range of CoVs)[75–78], and natural flavonoids like myricetin and quercetin[63,77–79]. However, despite some of these helicase inhibitors having entered clinical trials, none have currently been approved for use against COVID-19[65]. As such, while vaccines remain imperative for preventing serious disease, more targeted therapeutics against conserved viral proteins like Nsp13 are also essential and relies on comprehensive understanding of the protein's mechanism of action and interactions with host signalling pathways.

1.4 The Innate Immune Response

Akin to other viruses, SARS-CoV-2 infection has been shown to activate innate immune responses, the host's first line of defence against invading pathogens[80,81]. Upon infection, viral RNA and surface glycoproteins can act as pathogen-associated molecular patterns (PAMPs) to activate host innate immune responses through recognition by host pattern recognition receptors (PRRs) such as retinoic acid-inducible gene I-like receptors (RLRs) and toll-like receptors (TLRs)[82–84]. The detection of dsRNA by the cytosolic RLRs retinoic acid-inducible gene I (RIG-

I) and melanoma differentiation-associated factor 5 (MDA5) activates the mitochondrial antiviral signalling protein (MAVS). In turn, this recruits the tumor necrosis factor receptor-associated factor 3 (TRAF3) to phosphorylate NF-κB activator (TANK)-binding kinase 1 (TBK1) and inhibitor of nuclear factor κB (IκB) kinase-ε (IKKε). This leads to the subsequent phosphorylation and dimerization of interferon (IFN) regulatory factor 3 (IRF3) and 7 (IRF7), which initiates the transcription of type I and type III IFNs[85,86]. These released IFNs can then bind to their receptors on neighbouring cells initiating the Janus kinase (JAK)/ signal transducer and activator of transcription (STAT) signalling pathway whereby phosphorylated STAT1 and STAT2 dimerize and associate with IRF9 to form a complex that localizes to the nucleus and facilitates the transcription of antiviral IFN-stimulated genes (ISGs)[87,88] (**Figure 1.3**).

Similarly, signalling through TLRs can also initiate the production of type I IFNs and proinflammatory cytokines to modulate inflammatory and immune responses[82,83]. In the context of infection by RNA viruses, intracellular TLRs (e.g., TLR3, TLR7, TLR8), that are localized in the endosome, recognize viral nucleic acids and initiate signalling cascades through the recruitment of various adapter proteins such as myeloid differentiation primary response protein 88 (MyD88) or TIR domain-containing adaptor-inducing IFN-β (TRIF)[84,89]. There are also cell surface TLRs, such as TLR4, which have previously been shown to recognize viral glycoproteins[90]. The association of TLRs (e.g., TLR4, TLR7, TLR8) with MyD88 recruits members of the interleukin-1 receptor-associated kinase (IRAK) family, which ultimately activate TNF receptor-associated factor 6 (TRAF6). This in turn results in downstream activation of the IKK complex (composed of NEMO, IKKα and IKKβ) that phosphorylates and subsequently degrades IκB, an inhibitory protein, resulting in the release of NF-κB (p65/p50) to the nucleus

where it can mediate the transcription of various pro-inflammatory genes[83,91–94]. When dsRNA is detected by TLR3, the adaptor protein TRIF is used to interact with TBK1 and mediate the phosphorylation of IRF3, leading to the transcription of IFNs[82,89]. TLR4 can also signal through TRIF leading to the activation of TRAF6 and its associated NF-κB activation as previously discussed[92] (**Figure 1.3**). NF-κB signalling pathways can be stimulated by a diverse array of external stimuli including inflammatory cytokines, growth factors, as well as bacterial and viral stressors[94]. In the context of COVID-19, there is accumulating evidence suggesting that the dysregulation of NF-κB signalling pathways, and its associated increase in cytokine and chemokine levels, plays a central role in acute disease severity[95].

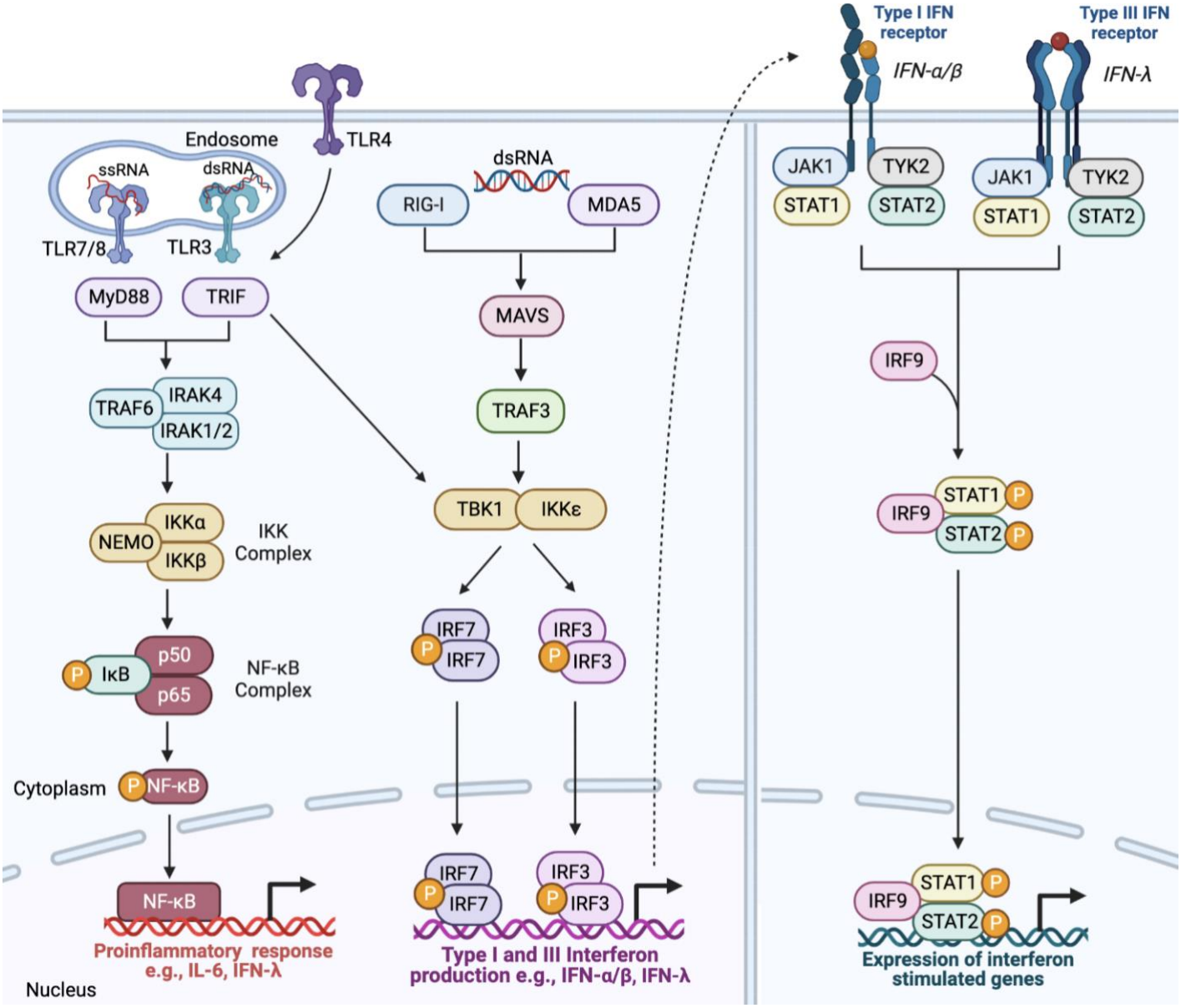

Figure 1.3 Innate Immune Responses.

Upon viral infection, various TLRs (TLR3, TLR4, TLR7, TLR8) and RLRs (RIG-I, MDA5) initiate signalling cascades leading to the activation of transcription factors such as NF-κB, IRF3 and IRF7. In turn, this stimulates the production of pro-inflammatory cytokines and type I and III IFNs, respectively. These IFNs are then secreted in an autocrine and/or paracrine fashion to induce the expression of ISGs through the JAK/STAT signalling pathway. Figure generated with BioRender.com.

1.4.1 Nsp13 Antagonizes Host Immune Responses

Coronaviruses, like SARS-CoV-2, have evolved several mechanisms to evade host innate immune responses. This includes strategies to minimize the detection of viral RNA by host cells, inhibit IFN signalling, and antagonize IFN production[96–100]. Several SARS-CoV-2 proteins, including but not limited to M[101,102], Nsp6[97], Nsp3[103,104], and ORF6[105], have been reported to antagonize type I IFN responses by targeting various effector proteins of the innate immune response. In particular, the SARS-CoV-2 Nsp13 has been identified as a potent immune antagonist that can act in multiple mechanisms for immune escape. To start, its role in the capping of viral RNA helps to enhance its translation by host cells and avoid detection by host PRRs[96,106]. In terms of modulating or blocking IFN signalling cascades, Nsp13 can reduce the expression of the IFN Alpha and Beta Receptor Subunit 1 (IFNAR1)[107] and even interact with STAT1 to prevent its phosphorylated-mediated activation[97,108]. Furthermore, the production of type I IFNs can also be hindered as Nsp13 has been shown to bind to TBK1, the kinase responsible for IRF3 activation, preventing its p62-dependent phosphorylation and degradation. As a result, nuclear localization of IRF3 is inhibited leading to a decrease in type I IFN transcription[97,105,109–111]. Nsp13 has also been suggested to downregulate NF-κB signalling, leading to the inhibition of proinflammatory responses[111]. Altogether, the conserved nature of Nsp13 and its extensive role in immune evasion highlight how further investigation into this viral helicase could offer new insight to facilitate the development of better pan-coronavirus therapeutics.

1.5 MicroRNAs

In addition to the interactions between SARS-CoV-2 proteins and host signalling pathways, such as immune responses, microRNAs (miRNAs) have also been shown to interact with various signalling pathways during viral infection[112]. miRNAs are small non-coding RNA

molecules, approximately 22 nts in length, that regulate gene expression, cell signalling, and host cell environment[113–115]. Acting as post-transcriptional gene regulators, miRNAs base-pair with the 3′ UTR of complementary mRNA sequences to induce translational repression, mRNA deadenylation, and decapping[116]. Non-canonical miRNA-mRNA interactions, such as those that interact with the 5′ UTR and coding region of target genes, have also been reported to be functional[117,118]. Research on miRNAs has implicated these molecules as important regulators of numerous biological functions including regulating cell growth and differentiation, inflammation, and immune responses[114,116,119–121]. As such, it is no surprise that there is growing evidence of their involvement in human diseases and cancer[122,123]. In the context of viral infection, miRNAs can serve as critical regulators of viral pathogenesis by acting through direct interactions with the viral genome[124–127]. Up- or down-regulation of various host miRNAs during viral infection can also induce either proviral responses to evade the host's immune system or antiviral responses that enable host cell defense mechanisms to fight against the infection [113,128,129]

1.6 The Expanded Genetic Code and Non-Canonical Amino Acids

As previously discussed, understanding the role Nsp13 plays in regulating host responses is important for developing therapeutics; however, comprehensive characterization of Nsp13's structure and function is also essential for developing potent helicase inhibitors. Current techniques to study the structure of a protein include crystallization, x-ray diffraction, and nuclear magnetic resonance analysis[130]. In contrast, the function of a protein can be examined through the analysis of proteins with similar sequences or through tracking its localization in cells using fluorescent tags[130]. Further investigations into a protein's interactions with other proteins or molecules, as determined through affinity chromatography or co-immunoprecipitation techniques, can also be

valuable for understanding the role of a protein in the cell[130]. While these are all important techniques for the characterization of both host and viral proteins, advances in the field of protein engineering, such as the rise of expanded genetic code techniques, have provided additional tools to study protein structure and function.

Advances in molecular biology have allowed for the site-specific substitution of any amino acid to another in a protein sequence. While this remains a common and useful practice to study protein structure and function to date, the potential applications of this technique are restricted by the 20 amino acids and 64 unique codons that synthesize all proteins in nature, with the exception of selenocysteine and pyrrolysine[131,132]. Fortunately, over the past few decades, there has been an emergence in the development and incorporation of unnatural or non-canonical amino acids (ncAAs) into proteins, which has provided chemical biologists and protein engineers alike, the potential to introduce novel functionalities and reactivities into proteins[131,133,134]. Importantly, these developed ncAAs are often metabolically stable in their cellular environment and well tolerated by the ribosome, making them valuable tools for studying biological systems[135,136]. To date, over 200 ncAAs have been developed, providing a diverse array of applications such as photo-crosslinking proteins to other biomolecules, serving as fluorescent probes, acting as bioorthogonal handles for click chemistry, and selectively introducing post-translational modifications and structural elements[137–141]. Methods to robustly introduce these ncAAs into proteins have also been well developed[135,136,142] (**Figure 1.4**). Briefly, these genetic code expansion techniques involve an evolved orthogonal tRNA/aminoacyl tRNA synthetase pair (tRNA/aaRS) that can site-specifically incorporate the specified ncAA into the protein of interest by recognizing "non-sense" stop codons in the mRNA sequence, as they are not recognized by endogenous

tRNAs[135]. The amber stop codon, UAG, is the most commonly used as it is found in only 9% of the *E.coli* genome and rarely terminates essential genes[135].

One commonly used ncAA is the tyrosine analogue *p*-azido-*L*-phenylalanine (AzF). It was first developed in 2002[143] and since then, AzF has been successfully incorporated into the tombusvirus' viral suppressor protein p19[144] and the human serotonin transporter (hSERT)[145] for its ultraviolet (UV) induced crosslinking capabilities. Moreover, the azide group on AzF can provide additional functionalities such as serving as a reactive bioorthogonal handle for different substrate conjugation through click chemistry[146–148]. Two commonly used azide-alkyne cycloaddition reactions include the copper(I)-catalyzed azide-alkyne cycloaddition (CuAAC) and strain-promoted alkyne-azide cycloaddition (SPAAC)[149–151]. While both are bioorthogonal and do not interfere with normal biological chemistries, SPAAC reactions have the added advantage of not needing a copper catalyst and therefore are less cytotoxic[151].

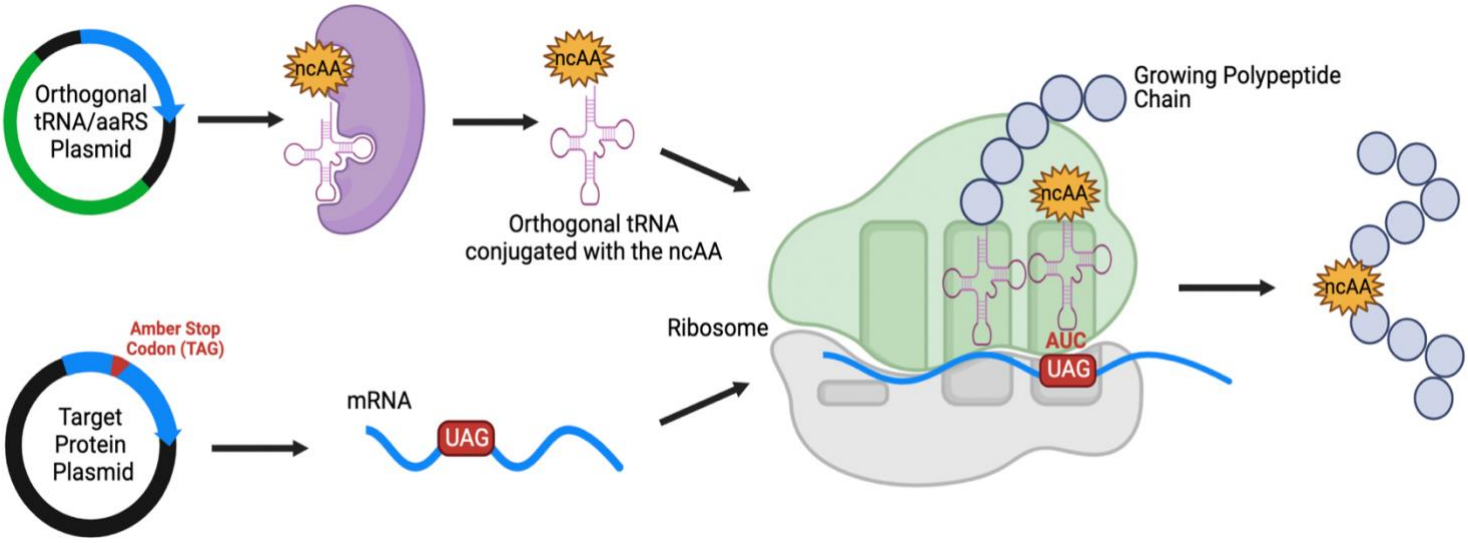

Figure 1.4 Incorporation of ncAAs into Proteins.

An orthogonal tRNA/aminoacyl tRNA synthetase (aaRS) is evolved to produce mature tRNA conjugated with the ncAA of interest. Site-directed mutagenesis is used to introduce the amber stop codon (TAG) into the coding sequence of the target protein. Co-expression of both plasmids will allow the orthogonal tRNA to recognize the amber stop codon and incorporate the ncAA into the growing polypeptide chain. Figure generated with BioRender.com.

1.6.1 Using ncAAs for FRET

Fluorescence (or Förster) resonance energy transfer (FRET) is a physical process that is commonly used in many biomedical and drug discovery applications[152,153]. It relies on the nonradiative concomitant transfer of energy between two suitable fluorophores only when there is a significant overlap of the emission spectrum of the donor with the absorption spectrum of the acceptor[154,155]. The strong distance dependence of FRET has warranted its use in investigating both inter- and intramolecular interactions[156]. This includes monitoring dynamic changes in protein structure and interactions both *in vivo* and *in vitro* [156–158]. As the utility of this method is contingent on the site-specific incorporation of these fluorophores on their target molecule, ncAAs have been widely used as bioorthogonal handles for FRET fluorophores to monitor changes in protein conformation[159,160], protein-protein interactions[161,162], as well as protein-nucleic acid interactions[144,148,163].

1.7 Outline of Work

The SARS-CoV-2 Nsp13 helicase is not only important for the life cycle of the virus, as evident by its nucleic acid unwinding activity that allows for genome replication, it also has important secondary roles in viral infectivity, as demonstrated by its interactions with host signalling pathways. Therefore, to better inform the development of Nsp13-based therapeutics against COVID-19, the objective of this work was to further characterize the enzymatic activities of the SARS-CoV-2 Nsp13 helicase and investigate its role in modulating host responses. First, we sought to examine the binding and unwinding activities of Nsp13 through the use of expanded genetic code techniques. The ncAA AzF was site-specifically incorporated into Nsp13 at five different sites to act as a bioorthogonal handle for the fluorescent labelling of the enzyme. To

identify the best Nsp13-AzF construct, we assessed these constructs for labelling efficiency and unaltered helicase unwinding activity. Next, FRET-based assays were conducted to monitor the binding of Nsp13 to a series of nucleic acid substrates in a distance-dependent manner. Moving forward, the successful Nsp13-AzF constructs can be implemented in single-molecule FRET (smFRET) studies to monitor the positioning and dynamics of Nsp13 binding with its nucleic acid substrates.

The second objective of this work was to investigate the potential role of Nsp13 in modulating cellular host processes. Using global transcriptomic analyses, we identified that Nsp13 modulates pathways involved in post-transcriptional gene silencing and translational repression by RNAs, such as miRNAs. To further explore potential miRNA-mediated signalling pathways influenced by Nsp13, we utilized bioinformatic techniques and identified miR-146a to be of interest. From the known role of miR-146a in inflammatory and innate immune responses, we conducted preliminary analyses to propose mechanisms by which Nsp13 may be modulating these cellular processes through miR-146a-mediated signalling.

1.8 References

1. Xu J, Zhao S, Teng T, et al. Systematic Comparison of Two Animal-to-Human Transmitted Human Coronaviruses: SARS-CoV-2 and SARS-CoV. *Viruses*. 2020;12(2):244. doi:10.3390/v12020244
2. Tang D, Comish P, Kang R. The hallmarks of COVID-19 disease. *PLoS Pathog*. 2020;16(5):e1008536. doi:10.1371/journal.ppat.1008536
3. Wu F, Zhao S, Yu B, et al. A new coronavirus associated with human respiratory disease in China *Nature*. 2020;579(7798):265-269. doi.org/10.1038/s41586-020-2008-3
4. Dong E, Du H, Gardner L. An interactive web-based dashboard to track COVID-19 in real time. Published online 2020. doi:10.1016/S1473-3099(20)30120-1
5. Mathieu E, Ritchie H, Rodés-Guirao L, et al. Coronavirus Pandemic (COVID-19). *Our World in Data*. Published online March 5, 2020. Accessed January 15, 2023. https://ourworldindata.org/coronavirus
6. Zhou F, Yu T, Du R, et al. Clinical course and risk factors for mortality of adult inpatients with COVID-19 in Wuhan, China: a retrospective cohort study. *The Lancet*. 2020;395(10229):1054-1062. doi:10.1016/S0140-6736(20)30566-3
7. Crook H, Raza S, Nowell J, Young M, Edison P. Long covid—mechanisms, risk factors, and management. *BMJ*. 2021;374. doi:10.1136/bmj.n1648
8. Mathieu E, Ritchie H, Ortiz-Ospina E, et al. Coronavirus Pandemic (COVID-19). *Our World in Data*. 2020;5(7):947-953. doi:10.1038/s41562-021-01122-8
9. Mathieu E, Ritchie H, Ortiz-Ospina E, et al. A global database of COVID-19 vaccinations. *Nat Hum Behav*. 2021;5(7):947-953. doi:10.1038/s41562-021-01122-8
10. Beigel JH, Tomashek KM, Dodd LE, et al. Remdesivir for the Treatment of Covid-19 — Final Report. *NEJM*. 2020;383(19):1813-1826. doi:10.1056/nejmoa2007764
11. Owen DR, Allerton CMN, Anderson AS, et al. An oral SARS-CoV-2 Mpro inhibitor clinical candidate for the treatment of COVID-19. *Science*. 2021;374(6575):1586-1593. doi:10.1126/science.abl4784
12. Eastman RT, Roth JS, Brimacombe KR, et al. Remdesivir: A Review of Its Discovery and Development Leading to Emergency Use Authorization for Treatment of COVID-19. *ACS Cent Sci*. 2020;6(5):672-683. doi:10.1021/acscentsci.0c00489
13. Painter WP, Holman W, Bush JA, et al. Human safety, tolerability, and pharmacokinetics of molnupiravir, a novel broad-spectrum oral antiviral agent with activity against SARS-CoV-2. *Antimicrob Agents Chemother*. 2021;65(5). doi:10.1128/aac.02428-20
14. Gordon DE, Jang GM, Bouhaddou M, et al. A SARS-CoV-2 protein interaction map reveals targets for drug repurposing. *Nature*. 2020;583(7816):459-468. doi:10.1038/s41586-020-2286-9

15. Zumla A, Chan JFW, Azhar EI, Hui DSC, Yuen KY. Coronaviruses — drug discovery and therapeutic options. *Nat Rev Drug Discov.* 2016;15(5):327-347. doi:10.1038/nrd.2015.37
16. Sharma A, Tiwari S, Deb MK, Marty JL. Severe acute respiratory syndrome coronavirus-2 (SARS-CoV-2): a global pandemic and treatment strategies. *Int J Antimicrob Agents*. 2020;56(2):106054. doi:10.1016/j.ijantimicag.2020.106054
17. Chen Y, Liu Q, Guo D. Emerging coronaviruses: Genome structure, replication, and pathogenesis. *J Med Virol*. 2020;92(4):418-423. doi:10.1002/jmv.25681
18. Cui J, Li F, Shi ZL. Origin and evolution of pathogenic coronaviruses. *Nat. Rev. Microbiol.* 2018;17(3):181-192. doi:10.1038/s41579-018-0118-9
19. Zhong NS, Zheng BJ, Li YM, et al. Epidemiology and cause of severe acute respiratory syndrome (SARS) in Guangdong, People's Republic of China, in February, 2003. *Lancet*. 2003;362(9393):1353-1358. doi:10.1016/S0140-6736(03)14630-2
20. Ksiazek TG, Erdman D, Goldsmith CS, et al. A Novel Coronavirus Associated with Severe Acute Respiratory Syndrome. *NEJM*. 2003;348(20):1953-1966. doi:10.1056/nejmoa030781
21. Zaki AM, van Boheemen S, Bestebroer TM, Osterhaus ADME, Fouchier RAM. Isolation of a Novel Coronavirus from a Man with Pneumonia in Saudi Arabia. *NEJM*. 2012;367(19):1814-1820. doi:10.1056/nejmoa1211721
22. Chan JFW, Kok KH, Zhu Z, et al. Genomic characterization of the 2019 novel human-pathogenic coronavirus isolated from a patient with atypical pneumonia after visiting Wuhan. *Emerg Microbes Infect*. 2020;9(1):221-236. doi:10.1080/22221751.2020.1719902
23. Qi F, Qian S, Zhang S, Zhang Z. Single cell RNA sequencing of 13 human tissues identify cell types and receptors of human coronaviruses. *Biochem Biophys Res Commun*. 2020;526(1):135-140. doi:10.1016/j.bbrc.2020.03.044
24. Hoffmann M, Kleine-Weber H, Schroeder S, et al. SARS-CoV-2 Cell Entry Depends on ACE2 and TMPRSS2 and Is Blocked by a Clinically Proven Protease Inhibitor. *Cell*. 2020;181(2):271-280.e8. doi:10.1016/j.cell.2020.02.052
25. V'kovski P, Kratzel A, Steiner S, Stalder H, Thiel V. Coronavirus biology and replication: implications for SARS-CoV-2. *Nat Rev Microbiol.* 2020;19(3):155-170. doi:10.1038/s41579-020-00468-6
26. Cantuti-Castelvetri L, Ojha R, Pedro LD, et al. Neuropilin-1 facilitates SARS-CoV-2 cell entry and infectivity. *Science*. Published online October 20, 2020. doi:10.1126/science.abd2985
27. Xu X, Chen P, Wang J, et al. Evolution of the novel coronavirus from the ongoing Wuhan outbreak and modeling of its spike protein for risk of human transmission. *Sci China Life Sci*. 2020;63(3):457-460. doi:10.1007/s11427-020-1637-5

28. Kim D, Lee JY, Yang JS, Kim JW, Kim VN, Chang H. The Architecture of SARS-CoV-2 Transcriptome. *Cell*. 2020;181(4):914-921.e10. doi:10.1016/j.cell.2020.04.011
29. Hartenian E, Nandakumar D, Lari A, Ly M, Tucker JM, Glaunsinger BA. The molecular virology of coronaviruses. *J Biol Chem*. 2020;295(37):12910-12934. doi:10.1074/jbc.rev120.013930
30. Astuti I, Ysrafil. Severe Acute Respiratory Syndrome Coronavirus 2 (SARS-CoV-2): An overview of viral structure and host response. *Diabetes Metab Syndr*. 2020;14(4):407-412. doi:10.1016/j.dsx.2020.04.020
31. Romano M, Ruggiero A, Squeglia F, Maga G, Berisio R. A Structural View of SARS-CoV-2 RNA Replication Machinery: RNA Synthesis, Proofreading and Final Capping. *Cells*. 2020;9(5). doi:10.3390/cells9051267
32. Yan L, Zhang Y, Ge J, et al. Architecture of a SARS-CoV-2 mini replication and transcription complex. *Nat Commun.* 2020;11(1):1-6. doi:10.1038/s41467-020-19770-1
33. Harrison AG, Lin T, Wang P. Mechanisms of SARS-CoV-2 Transmission and Pathogenesis. *Trends Immunol*. 2020;41(12):1100-1115. doi:10.1016/j.it.2020.10.004
34. Zhang R, Li Y, Cowley TJ, et al. The nsp1, nsp13, and M Proteins Contribute to the Hepatotropism of Murine Coronavirus JHM.WU. *J Virol*. 2015;89(7):3598-3609. doi:10.1128/jvi.03535-14
35. Lehmann KC, Snijder EJ, Posthuma CC, Gorbalenya AE. What we know but do not understand about nidovirus helicases. *Virus Res*. 2015;202:12-32. doi:10.1016/j.virusres.2014.12.001
36. Gurung AB. In silico structure modelling of SARS-CoV-2 Nsp13 helicase and Nsp14 and repurposing of FDA approved antiviral drugs as dual inhibitors. *Gene Rep*. 2020;21:100860. doi:10.1016/j.genrep.2020.100860
37. Jang KJ, Jeong S, Kang DY, Sp N, Yang YM, Kim DE. A high ATP concentration enhances the cooperative translocation of the SARS coronavirus helicase nsP13 in the unwinding of duplex RNA. *Sci Rep*. 2020;10(1). doi:10.1038/s41598-020-61432-1
38. Newman JA, Douangamath A, Yadzani S, et al. Structure, mechanism and crystallographic fragment screening of the SARS-CoV-2 NSP13 helicase. *Nat Commun.* 2021;12(1):1-11. doi:10.1038/s41467-021-25166-6
39. Gilhooly NS, Gwynn EJ, Dillingham MS. Superfamily 1 helicases. *Front Biosci (Schol Ed)*. 2013;5 S(1):206-216. doi:10.2741/s367
40. Fairman-Williams ME, Guenther UP, Jankowsky E. SF1 and SF2 helicases: family matters. *Curr Opin Struct Biol*. 2010;20(3):313-324. doi:10.1016/j.sbi.2010.03.011
41. Jia Z, Yan L, Ren Z, et al. Delicate structural coordination of the Severe Acute Respiratory Syndrome coronavirus Nsp13 upon ATP hydrolysis. *Nucleic Acids Res*. 2019;47(12):6538-6550. doi:10.1093/nar/gkz409

42. Mickolajczyk KJ, Shelton PMM, Grasso M, et al. Force-dependent stimulation of RNA unwinding by SARS-CoV-2 nsp13 helicase. *Biophys J*. 2021;120(6):1020-1030. doi:10.1016/j.bpj.2020.11.2276
43. Tanner JA, Watt RM, Chai YB, et al. The severe acute respiratory syndrome (SARS) coronavirus NTPasefhelicase belongs to a distinct class of 5′ to 3′ viral helicases. *J Biol Chem*. 2003;278(41):39578-39582. doi:10.1074/jbc.c300328200
44. Ivanov KA, Thiel V, Dobbe JC, van der Meer Y, Snijder EJ, Ziebuhr J. Multiple Enzymatic Activities Associated with Severe Acute Respiratory Syndrome Coronavirus Helicase. *J Virol*. 2004;78(11):5619-5632. doi:10.1128/jvi.78.11.5619-5632.2004
45. Adedeji AO, Marchand B, te Velthuis AJW, et al. Mechanism of Nucleic Acid Unwinding by SARS-CoV Helicase. *PLoS One*. 2012;7(5):e36521. doi:10.1371/journal.pone.0036521
46. Rangan R, Zheludev IN, Hagey RJ, et al. RNA genome conservation and secondary structure in SARS-CoV-2 and SARS-related viruses: a first look. *RNA*. 2020;26(8):937-959. doi:10.1261/rna.076141.120
47. Wilamowski M, Sherrell DA, Minasov G, et al. 2′-O methylation of RNA cap in SARS-CoV-2 captured by serial crystallography. *Proc Natl Acad Sci U S A*. 2021;118(21):e2100170118. doi:10.1073/pnas.2100170118
48. Rosas-Lemus M, Minasov G, Shuvalova L, et al. High-resolution structures of the SARS-CoV-2 2′-O-methyltransferase reveal strategies for structure-based inhibitor design. *Sci Signal*. 2020;13(651):1202. doi:10.1126/scisignal.abe1202
49. Park GJ, Osinski A, Hernandez G, et al. The mechanism of RNA capping by SARS-CoV-2. *Nature*. 2022;609(7928):793-800. doi:10.1038/s41586-022-05185-z
50. Viswanathan T, Arya S, Chan SH, et al. Structural basis of RNA cap modification by SARS-CoV-2. *Nat Commun*. 2020;11(1):1-7. doi:10.1038/s41467-020-17496-8
51. Yan W, Zheng Y, Zeng X, He B, Cheng W. Structural biology of SARS-CoV-2: open the door for novel therapies. *Signal Transduct Target Ther*. 2022;7(1):1-28. doi:10.1038/s41392-022-00884-5
52. Chen J, Malone B, Llewellyn E, et al. Structural Basis for Helicase-Polymerase Coupling in the SARS-CoV-2 Replication-Transcription Complex. *Cell*. 2020;182(6):1560-1573.e13. doi:10.1016/j.cell.2020.07.033
53. Deng Z, Lehmann KC, Li X, et al. Structural basis for the regulatory function of a complex zinc-binding domain in a replicative arterivirus helicase resembling a nonsense-mediated mRNA decay helicase. *Nucleic Acids Res*. 2014;42(5):3464-3477. doi:10.1093/nar/gkt1310
54. Tang C, Deng Z, Li X, et al. Helicase of Type 2 Porcine Reproductive and Respiratory Syndrome Virus Strain HV Reveals a Unique Structure. *Viruses*. 2020;12(2). doi:10.3390/v12020215

55. Mirza MU, Froeyen M. Structural elucidation of SARS-CoV-2 vital proteins: Computational methods reveal potential drug candidates against main protease, Nsp12 polymerase and Nsp13 helicase. *J Pharm Anal*. 2020;10(4):320-328. doi:10.1016/Jj.jpha.2020.04.008
56. Berta D, Badaoui M, Martino SA, et al. Modelling the active SARS-CoV-2 helicase complex as a basis for structure-based inhibitor design. *Chem Sci*. 2021;12(40):13492-13505. doi:10.1039/d1sc02775a
57. Yue K, Yao B, Shi Y, et al. The stalk domain of SARS-CoV-2 NSP13 is essential for its helicase activity. *Biochem Biophys Res Commun*. 2022;601:129. doi:10.1016/j.bbrc.2022.02.068
58. Perez-Lemus GR, Menéndez CA, Alvarado W, Byléhn F, de Pablo JJ. Toward wide-spectrum antivirals against coronaviruses: Molecular characterization of SARS-CoV-2 NSP13 helicase inhibitors. *Sci Adv*. 2022;8(1):4526. doi:10.1126/sciadv.abj4526
59. Malone B, Chen J, Wang Q, et al. Structural basis for backtracking by the SARS-CoV-2 replication-transcription complex. *Proc Natl Acad Sci U S A*. 2021;118(19):e2102516118. doi:10.1073/pnas.2102516118
60. Jian F, Yu Y, Song W, et al. Further humoral immunity evasion of emerging SARS-CoV-2 BA.4 and BA.5 subvariants. *Lancet Infect Dis*. 2022;22(11):1535-1537. doi:10.1016/s1473-3099(22)00642-9
61. Martin R, Li J, Parvangada A, et al. Genetic conservation of SARS-CoV-2 RNA replication complex in globally circulating isolates and recently emerged variants from humans and minks suggests minimal pre-existing resistance to remdesivir. *Antiviral Res*. 2021;188:105033. doi:10.1016/j.antiviral.2021.105033
62. Adedeji AO, Singh K, Calcaterra NE, et al. Severe Acute Respiratory Syndrome Coronavirus Replication Inhibitor That Interferes with the Nucleic Acid Unwinding of the Viral Helicase. *Antimicrob Agents Chemother*. 2012;56(9):4718-4728. doi:10.1128/aac.00957-12
63. Yu MS, Lee J, Lee JM, et al. Identification of myricetin and scutellarein as novel chemical inhibitors of the SARS coronavirus helicase, nsP13. *Bioorg Med Chem Lett*. 2012;22(12):4049-4054. doi:10.1016/j.bmcl.2012.04.081
64. White MA, Lin W, Cheng X. Discovery of COVID-19 Inhibitors Targeting the SARS-CoV-2 Nsp13 Helicase. *J Phys Chem Lett*. 2020;11(21):9144-9151. doi:10.1021/acs.jpclett.0c02421
65. Halma MTJ, Wever MJA, Abeln S, Roche D, Wuite GJL. Therapeutic potential of compounds targeting SARS-CoV-2 helicase. *Front Chem*. 2022;10:1531. doi:10.3389/fchem.2022.1062352
66. Shadrick WR, Ndjomou J, Kolli R, Mukherjee S, Hanson AM, Frick DN. Discovering New Medicines Targeting Helicases: Challenges and Recent Progress. *SLAS Discovery*. 2013;18(7):761-781. doi:10.1177/1087057113482586
67. Tyring S, Wald A, Zadeikis N, Dhadda S, Takenouchi K, Rorig R. ASP2151 for the Treatment of Genital Herpes: A Randomized, Double-Blind, Placebo- and Valacyclovir-Controlled, Dose-Finding Study. *J Infect Dis*. 2012;205(7):1100-1110. doi:10.1093/infdis/jis019

68. Kwong AD, Rao BG, Jeang KT. Viral and cellular RNA helicases as antiviral targets. *Nat Rev Drug Discov*. 2005;4(10):845. doi:10.1038/nrd1853
69. Chono K, Katsumata K, Kontani T, et al. ASP2151, a novel helicase-primase inhibitor, possesses antiviral activity against varicella-zoster virus and herpes simplex virus types 1 and 2. *J Antimicrob Chemother*. 2010;65(8):1733-1741. doi:10.1093/jac/dkq198
70. Datta A, Brosh RM. New insights into DNA helicases as druggable targets for cancer therapy. *Front Mol Biosci*. 2018;5(JUN). doi:10.3389/fmolb.2018.00059
71. Romeo I, Ambrosio FA, Costa G, et al. Targeting SARS-CoV-2 nsp13 Helicase and Assessment of Druggability Pockets: Identification of Two Potent Inhibitors by a Multi-Site In Silico Drug Repurposing Approach. *Molecules*. 2022;27(21):7522. doi:10.3390/molecules27217522/S1
72. Yuan S, Wang R, Chan JFW, et al. Metallodrug ranitidine bismuth citrate suppresses SARS-CoV-2 replication and relieves virus-associated pneumonia in Syrian hamsters. *Nat Microbiol*. 2020;5(11):1439-1448. doi:10.1038/s41564-020-00802-x
73. Adedeji AO, Singh K, Kassim A, et al. Evaluation of SSYA10-001 as a replication inhibitor of severe acute respiratory syndrome, mouse hepatitis, and Middle East respiratory syndrome coronaviruses. *Antimicrob Agents Chemother*. 2014;58(8):4894-4898. doi:10.1128/aac.02994-14
74. Yang N, Tanner JA, Wang Z, et al. Inhibition of SARS coronavirus helicase by bismuth complexes. *Chem Commun*. 2007;(42):4413-4415. doi:10.1039/b709515e
75. Adedeji AO, Singh K, Calcaterra NE, et al. Severe Acute Respiratory Syndrome Coronavirus Replication Inhibitor That Interferes with the Nucleic Acid Unwinding of the Viral Helicase. *Antimicrob Agents Chemother*. 2012;56(9):4718. doi:10.1128/aac.00957-12
76. Adedeji AO, Singh K, Kassim A, et al. Evaluation of SSYA10-001 as a replication inhibitor of severe acute respiratory syndrome, mouse hepatitis, and Middle East respiratory syndrome coronaviruses. *Antimicrob Agents Chemother*. 2014;58(8):4894-4898. doi:10.1128/aac.02994-14
77. Zeng J, Weissmann F, Bertolin AP, et al. Identifying SARS-CoV-2 antiviral compounds by screening for small molecule inhibitors of nsp13 helicase. *Biochem J*. 2021;478(13):2405-2423. doi:10.1042/bcj20210201
78. Corona A, Wycisk K, Talarico C, et al. Natural Compounds Inhibit SARS-CoV-2 nsp13 Unwinding and ATPase Enzyme Activities. *ACS Pharmacol Transl Sci*. 2022;5(4):226-239. doi:10.1021/acsptsci.1c00253
79. Lee C, Lee JM, Lee NR, Kim DE, Jeong YJ, Chong Y. Investigation of the pharmacophore space of Severe Acute Respiratory Syndrome coronavirus (SARS-CoV) NTPase/helicase by dihydroxychromone derivatives. *Bioorg Med Chem Lett*. 2009;19(16):4538-4541. doi:10.1016/j.bmcl.2009.07.009

80. Lowery SA, Sariol A, Perlman S. Innate immune and inflammatory responses to SARS-CoV-2: Implications for COVID-19. *Cell Host Microbe*. 2021;29(7):1052-1062. doi:10.1016/j.chom.2021.05.004
81. Diamond MS, Kanneganti TD. Innate immunity: the first line of defense against SARS-CoV-2. *Nat Immunol*. 2022;23(2):165-176. doi:10.1038/s41590-021-01091-0
82. Kawai T, Akira S. The roles of TLRs, RLRs and NLRs in pathogen recognition. *Int Immunol*. 2009;21(4):317. doi:10.1093/intimm/dxp017
83. Akira S, Uematsu S, Takeuchi O. Pathogen Recognition and Innate Immunity. *Cell*. 2006;124(4):783-801. doi:10.1016/j.cell.2006.02.015
84. Iwasaki A, Medzhitov R. Toll-like receptor control of the adaptive immune responses. *Nat Immunol*. 2004;5(10):987-995. doi:10.1038/ni1112
85. Liu GQ, Gack MU. Distinct and Orchestrated Functions of RNA Sensors in Innate Immunity. *Immunity*. 2020;53(1):26-42. doi:10.1016/j.immuni.2020.03.017
86. Liu S, Chen J, Cai X, et al. MAVS recruits multiple ubiquitin E3 ligases to activate antiviral signaling cascades. *Elife*. 2013;2013(2). doi:10.7554/elife.00785.001
87. Schneider WM, Chevillotte MD, Rice CM. Interferon-Stimulated Genes: A Complex Web of Host Defenses. 2014;32:513-545. doi:10.1146/annurev-immunol-032713-120231
88. Schneider WM, Chevillotte MD, Rice CM. Interferon-stimulated genes: A complex web of host defenses. *Annu Rev Immunol*. 2014;32:513-545. doi:10.1146/annurev-immunol-032713-120231
89. Akira S, Takeda K. Toll-like receptor signalling. *Nat Rev Immunol*. 2004;4(7):499-511. doi:10.1038/nri1391
90. Kurt-Jones EA, Popova L, Kwinn L, et al. Pattern recognition receptors TLR4 and CD14 mediate response to respiratory syncytial virus. *Nat Immunol*. 2000;1(5):398-401. doi:10.1038/80833
91. Karin M. How NF-κB is activated: the role of the IκB kinase (IKK) complex. *Oncogene*. 1999;18(49):6867-6874. doi:10.1038/sj.onc.1203219
92. Kawasaki T, Kawai T. Toll-like receptor signaling pathways. *Front Immunol*. 2014;5(SEP):461. doi:10.3389/fimmu.2014.00461
93. Liu T, Zhang L, Joo D, Sun SC. NF-κB signaling in inflammation. *Signal Transduct Target Ther*. 2017;2:17023. doi:10.1038/sigtrans.2017.23
94. Oeckinghaus A, Ghosh S. The NF-κB Family of Transcription Factors and Its Regulation. *Cold Spring Harb Perspect Biol*. 2009;1(4). doi:10.1101/cshperspect.a000034
95. Kircheis R, Haasbach E, Lueftenegger D, Heyken WT, Ocker M, Planz O. NF-κB Pathway as a Potential Target for Treatment of Critical Stage COVID-19 Patients. *Front Immunol*. 2020;11:3446. doi:10.3389/fimmu.2020.598444

96. Minkoff JM, tenOever B. Innate immune evasion strategies of SARS-CoV-2. *Nat Rev Microbiol*. 2023:1-17. doi:10.1038/s41579-022-00839-1
97. Xia H, Cao Z, Xie X, et al. Evasion of Type I Interferon by SARS-CoV-2. *Cell Rep*. 2020;33(1):108234. doi:10.1016/j.celrep.2020.108234
98. Beachboard DC, Horner SM. Innate immune evasion strategies of DNA and RNA viruses. *Curr Opin Microbiol*. 2016;32:113-119. doi:10.1016/j.mib.2016.05.015
99. Min YQ, Huang M, Sun X, Deng F, Wang H, Ning YJ. Immune evasion of SARS-CoV-2 from interferon antiviral system. *Comput Struct Biotechnol J*. 2021;19:4217-4225. doi:10.1016/j.csbj.2021.07.023
100. Beyer DK, Forero A. Mechanisms of Antiviral Immune Evasion of SARS-CoV-2. *J Mol Biol*. 2022;434(6):167265. doi:10.1016/j.jmb.2021.167265
101. Zheng Y, Zhuang MW, Han L, et al. Severe acute respiratory syndrome coronavirus 2 (SARS-CoV-2) membrane (M) protein inhibits type I and III interferon production by targeting RIG-I/MDA-5 signaling. *Signal Transduct Target Ther*. 2020;5(1):1-13. doi:10.1038/s41392-020-00438-7
102. Fu YZ, Wang SY, Zheng ZQ, et al. SARS-CoV-2 membrane glycoprotein M antagonizes the MAVS-mediated innate antiviral response. *Cell Mol Immunol*. 2020;18(3):613-620. doi:10.1038/s41423-020-00571-x
103. Moustaqil M, Ollivier E, Chiu HP, et al. SARS-CoV-2 proteases PLpro and 3CLpro cleave IRF3 and critical modulators of inflammatory pathways (NLRP12 and TAB1): implications for disease presentation across species. *Emerg Microbes Infect*. 2021;10(1):178-195. doi:10.1080/22221751.2020.1870414
104. Shin D, Mukherjee R, Grewe D, et al. Papain-like protease regulates SARS-CoV-2 viral spread and innate immunity. *Nature*. 2020;587(7835):657-662. doi:10.1038/s41586-020-2601-5
105. Yuen CK, Lam JY, Wong WM, et al. SARS-CoV-2 nsp13, nsp14, nsp15 and orf6 function as potent interferon antagonists. *Emerg Microbes Infect*. 2020;9(1):1418-1428. doi:10.1080/22221751.2020.1780953
106. Yan L, Ge J, Zheng L, et al. Cryo-EM Structure of an Extended SARS-CoV-2 Replication and Transcription Complex Reveals an Intermediate State in Cap Synthesis. *Cell*. 2021;184(1):184-193.e10. doi:10.1016/j.cell.2020.11.016
107. Hayn M, Hirschenberger M, Koepke L, et al. Systematic functional analysis of SARS-CoV-2 proteins uncovers viral innate immune antagonists and remaining vulnerabilities. *Cell Rep*. 2021;35(7):109126. doi:10.1016/j.celrep.2021.109126
108. Fung SY, Siu KL, Lin H, Chan CP, Yeung ML, Jin DY. SARS-CoV-2 NSP13 helicase suppresses interferon signaling by perturbing JAK1 phosphorylation of STAT1. *Cell Biosci*. 2022;12(1):1-12. doi:10.1186/s13578-022-00770-1

109. Sui C, Xiao T, Zhang S, et al. SARS-CoV-2 NSP13 Inhibits Type I IFN Production by Degradation of TBK1 via p62-Dependent Selective Autophagy. *J Immun*. 2022;208(3):753-761. doi:10.4049/jimmunol.2100684
110. Guo G, Gao M, Gao X, et al. SARS-CoV-2 non-structural protein 13 (nsp13) hijacks host deubiquitinase USP13 and counteracts host antiviral immune response. *Signal Transduct Target Ther*. 2021;6(1):1-3. doi:10.1038/s41392-021-00509-3
111. Vazquez C, Swanson SE, Negatu SG, et al. SARS-CoV-2 viral proteins NSP1 and NSP13 inhibit interferon activation through distinct mechanisms. *PLoS One*. 2021;16(6):e0253089. doi:10.1371/journal.pone.0253089
112. Barbu MG, Condrat CE, Thompson DC, et al. MicroRNA Involvement in Signaling Pathways During Viral Infection. *Front Cell Dev Biol*. 2020;8:143. doi:10.3389/fcell.2020.00143
113. Singaravelu R, Chen R, Lyn RK, et al. Hepatitis C virus induced up-regulation of microRNA-27: A novel mechanism for hepatic steatosis. *Hepatology*. 2014;59(1):98-108. doi:10.1002/hep.26634
114. Song L, Tuan RS. MicroRNAs and cell differentiation in mammalian development. *Birth Defects Res C Embryo Today*. 2006;78(2):140-149. doi:10.1002/bdrc.20070
115. Evers P, Pezacki JP. Unraveling Complex MicroRNA Signaling Pathways with Activity-Based Protein Profiling to Guide Therapeutic Discovery**. *Isr J Chem*. Published online 2023:e202200088. doi:10.1002/IJCH.202200088
116. Jonas S, Izaurralde E. Towards a molecular understanding of microRNA-mediated gene silencing. *Nat Rev Genet*. 2015;16(7):421-433. doi:10.1038/nrg3965
117. Broughton JP, Lovci MT, Huang JL, Yeo GW, Pasquinelli AE. Pairing beyond the Seed Supports MicroRNA Targeting Specificity. *Mol Cell*. 2016;64(2):320-333. doi:10.1016/j.molcel.2016.09.004
118. Reczko M, Maragkakis M, Alexiou P, Grosse I, Hatzigeorgiou AG. Functional microRNA targets in protein coding sequences. *Bioinformatics*. 2012;28(6):771-776. doi:10.1093/bioinformatics/bts043
119. Yang M, Liu W, Pellicane C, et al. Identification of miR-185 as a regulator of de novo cholesterol biosynthesis and low density lipoprotein uptake. *J Lipid Res*. 2014;55(2):226-238. doi:10.1194/jlr.m041335
120. Hayes J, Peruzzi PP, Lawler S. MicroRNAs in cancer: Biomarkers, functions and therapy. *Trends Mol Med*. 2014;20(8):460-469. doi:10.1016/j.molmed.2014.06.005
121. Gebert LFR, MacRae IJ. Regulation of microRNA function in animals. *Nat Rev Mol Cell Biol*. 2018;20(1):21-37. doi:10.1038/s41580-018-0045-7
122. Ardekani AM, Naeini MM. The Role of MicroRNAs in Human Diseases. *Avicenna J Med Biotechnol*. 2010;2(4):161. Accessed November 29, 2022. /pmc/articles/pmc3558168/

123. Li Y, Kowdley K v. MicroRNAs in Common Human Diseases. *Genomics Proteomics Bioinformatics*. 2012;10(5):246-253. doi:10.1016/j.gpb.2012.07.005
124. Pedersen IM, Cheng G, Wieland S, et al. Interferon modulation of cellular microRNAs as an antiviral mechanism. *Nature*. 2007;449(7164):919-922. doi:10.1038/nature06205
125. Girardi E, López P, Pfeffer S. On the importance of host MicroRNAs during viral infection. *Front Genet*. 2018;9(OCT):439. doi:10.3389/fgene.2018.00439
126. Scheel TKH, Luna JM, Liniger M, et al. A Broad RNA Virus Survey Reveals Both miRNA Dependence and Functional Sequestration. *Cell Host Microbe*. 2016;19(3):409-423. doi:10.1016/j.chom.2016.02.007
127. Luna JM, Scheel TKH, Danino T, et al. Hepatitis C virus RNA functionally sequesters miR-122. *Cell*. 2015;160(6):1099-1110. doi:10.1016/j.cell.2015.02.025
128. Singaravelu R, O'Hara S, Jones DM, et al. MicroRNAs regulate the immunometabolic response to viral infection in the liver. *Nat Chem Biol*. 2015;11(12):988-993. doi:10.1038/nchembio.1940
129. Motsch N, Pfuhl T, Mrazek J, Barth S, Grässer FA. Epstein-Barr Virus-Encoded Latent Membrane Protein 1 (LMP1) Induces the Expression of the Cellular MicroRNA miR-146a. *RNA Biol*. 2007;4(3):131-137. doi:10.4161/rna.4.3.5206
130. Alberts B, Johnson A, Lewis J, Raff M, Roberts K, Walter P. Analyzing protein structure and function. In: *In Molecular Biology of the Cell*. 4th ed. Garland Science; 2002.
131. Chin JW. Expanding and reprogramming the genetic code. *Nature*. 2017;550(7674):53-60. doi:10.1038/nature24031
132. Ambrogelly A, Palioura S, Söll D. Natural expansion of the genetic code. *Nat Chem Biol*. 2006;3(1):29-35. doi:10.1038/nchembio847
133. Liu CC, Schultz PG. Adding New Chemistries to the Genetic Code. *Annu Rev Biochem*. 2010;79:413-444. doi:10.1146/annurev.biochem.052308.105824
134. Young DD, Schultz PG. Playing with the Molecules of Life. *ACS Chem Biol*. 2018;13(4):854-870. doi:10.1021/acschembio.7b00974
135. Xie J, Schultz PG. An expanding genetic code. *Methods*. 2005;36(3):227-238. doi:10.1016/j.ymeth.2005.04.010
136. Lang K, Chin JW. Cellular incorporation of unnatural amino acids and bioorthogonal Labeling of Proteins. *Chem Rev*. 2014;114(9):4764-4806. doi:10.1021/cr400355w
137. Adhikari A, Bhattarai BR, Aryal A, et al. Reprogramming natural proteins using unnatural amino acids. *RSC Adv*. 2021;11(60):38126-38145. doi:10.1039/d1ra07028b
138. Xie J, Schultz PG. A chemical toolkit for proteins — an expanded genetic code. *Nat Rev Mol Cell Biol*. 2006;7(10):775-782. doi:10.1038/nrm2005

139. Sun SB, Schultz PG, Kim CH. Therapeutic applications of an expanded genetic code. *Chembiochem*. 2014;15(12):1721. doi:10.1002/cbic.201402154
140. Dougherty DA. Unnatural amino acids as probes of protein structure and function. *Curr Opin Chem Biol*. 2000;4(6):645-652. doi:10.1016/S1367-5931(00)00148-4
141. Pickens CJ, Johnson SN, Pressnall MM, Leon MA, Berkland CJ. Practical Considerations, Challenges, and Limitations of Bioconjugation via Azide-Alkyne Cycloaddition. *Bioconjug Chem*. 2018;29(3):686. doi:10.1021/acs.bioconjchem.7b00633
142. Noren CJ, Anthony-Cahill SJ, Griffith MC, Schultz PG. A General Method for Site-specific Incorporation of Unnatural Amino Acids into Proteins. *Science (1979)*. 1989;244(4901):182-188. doi:10.1126/science.2649980
143. Chin JW, Santoro SW, Martin AB, King DS, Wang L, Schultz PG. Addition of p-azido-L-phenylalanine to the genetic code of Escherichia coli. *J Am Chem Soc*. 2002;124(31):9026-9027. doi:10.1021/ja027007w
144. Ahmed N, Foss D v., Powdrill MH, Pezacki JP. Site-Specific Cross-Linking of a p19 Viral Suppressor of RNA Silencing Protein and Its RNA Targets Using an Expanded Genetic Code. *Biochemistry*. 2019;58(33):3520-3526. doi:10.1021/acs.biochem.9b00428
145. Rannversson H, Andersen J, Sørensen L, et al. Genetically encoded photocrosslinkers locate the high-affinity binding site of antidepressant drugs in the human serotonin transporter. *Nat Commun*. 2016;7. doi:10.1038/ncomms11261
146. Smits AH, Borrmann A, Roosjen M, van Hest JCM, Vermeulen M. Click-MS: Tagless Protein Enrichment Using Bioorthogonal Chemistry for Quantitative Proteomics. *ACS Chem Biol*. 2016;11(12):3245-3250. doi:10.1021/acschembio.6b00520
147. Koole C, Reynolds CA, Mobarec JC, Hick C, Sexton PM, Sakmar TP. Genetically encoded photocross-linkers determine the biological binding site of exendin-4 peptide in the N-terminal domain of the intact human glucagon-like peptide-1 receptor (GLP-1R). *J Biol Chem*. 2017;292(17):7131. doi:10.1074/jbc.m117.779496
148. Ablenas CJ, Gidi Y, Powdrill MH, et al. Hepatitis C Virus Helicase Binding Activity Monitored through Site-Specific Labeling Using an Expanded Genetic Code. *ACS Infect Dis*. 2019;5(12):2118-2126. doi:10.1021/acsinfecdis.9b00220
149. Tian H, Sakmar TP, Huber T. A simple method for enhancing the bioorthogonality of cyclooctyne reagent. *ChemComm*. 2016;52(31):5451-5454. doi:10.1039/c6cc01321j
150. Jewett JC, Sletten EM, Bertozzi CR. Rapid Cu-Free Click Chemistry with Readily Synthesized Biarylazacyclooctynones. *J Am Chem Soc*. 2010;132(11):3688. doi:10.1021/ja100014q

151. Agard NJ, Prescher JA, Bertozzi CR. A strain-promoted [3 + 2] azide-alkyne cycloaddition for covalent modification of biomolecules in living systems. *J Am Chem Soc*. 2004;126(46):15046-15047. doi:10.1021/ja044996f
152. Rodems SM, Hamman BD, Lin C, et al. A FRET-Based Assay Platform for Ultra-High Density Drug Screening of Protein Kinases and Phosphatases. *Assay and drug development technologies*. 2002;1(1):9-19. doi:10.1089/154065802761001266
153. Charron DM, Zheng G. Nanomedicine development guided by FRET imaging. *Nano Today*. 2018;18:124-136. doi:10.1016/j.nantod.2017.12.006
154. Sun Y, Wallrabe H, Seo SA, Periasamy A. FRET Microscopy in 2010: The Legacy of Theodor Fçrster on the 100th Anniversary of his Birth. *ChemPhysChem*. 2011;12:3. doi:10.1002/cphc.201000664
155. Piston DW, Kremers GJ. Fluorescent protein FRET: the good, the bad and the ugly. *Trends Biochem Sci*. 2007;32(9):407-414. doi:10.1016/j.tibs.2007.08.003
156. Truong K, Ikura M. The use of FRET imaging microscopy to detect protein–protein interactions and protein conformational changes in vivo. *Curr Opin Struct Biol*. 2001;11(5):573-578. doi:10.1016/s0959-440x(00)00249-9
157. Kopp MC, Nowak PR, Larburu N, Adams CJ, Ali MMU. In vitro FRET analysis of IRE1 and BiP association and dissociation upon endoplasmic reticulum stress. *Elife*. 2018;7. doi:10.7554/elife.30257
158. Wallrabe H, Periasamy A. Imaging protein molecules using FRET and FLIM microscopy. *Curr Opin Biotechnol*. 2005;16(1):19-27. doi:10.1016/j.copbio.2004.12.002
159. Wang K, Sachdeva A, Cox DJ, et al. Optimized orthogonal translation of unnatural amino acids enables spontaneous protein double-labelling and FRET. *Nat Chem*. 2014;6(5):393-403. doi:10.1038/nchem.1919
160. Mitchell AL, Addy PS, Chin MA, Chatterjee A. A Unique Genetically Encoded FRET Pair in Mammalian Cells. *ChemBioChem*. 2017;18(6):511-514. doi:10.1002/cbic.201600668
161. Park SH, Ko W, Lee HS, Shin I. Analysis of Protein-Protein Interaction in a Single Live Cell by Using a FRET System Based on Genetic Code Expansion Technology. *J Am Chem Soc*. 2019;141(10):4273-4281. doi:10.1021/jacs.8b10098
162. Willkomm S, Jakob L, Kramm K, et al. Single-molecule FRET uncovers hidden conformations and dynamics of human Argonaute 2. *Nat Commun*. 2022;13(1):1-13. doi:10.1038/s41467-022-31480-4
163. König SLB, Liyanage PS, Sigel RKO, Rueda D. Helicase-mediated changes in RNA structure at the single-molecule level. *RNA Biol*. 2013;10(1):133. doi:10.4161/rna.23507

Chapter 2

Monitoring SARS-CoV-2 Nsp13 Helicase Binding Activity Using Expanded Genetic Code Techniques

2.1 Abstract

The SARS-CoV-2 Nsp13 helicase is a multi-functional protein that can unwind dsDNA and dsRNA in an NTP-dependent manner. Given that this viral helicase is both essential for viral replication and highly conserved among coronaviruses, a thorough understanding of the helicase's unwinding and binding activity may allow for the development of more effective antiviral therapeutics against HCoV infections. Herein, we describe the use of genetic code expansion techniques to site-specifically incorporate the ncAA AzF into Nsp13 for fluorescent labelling of the enzyme with a conjugated Cy5 fluorophore. This Cy5-labelled Nsp13-AzF can then be used in FRET and smFRET experiments to investigate the dynamics of enzyme translocation during binding and unwinding. Five sites (F81, F90, Y205, Y246, and Y253) were identified for AzF incorporation in Nsp13 and assessed for fluorescent labelling efficiency. We then verified that the unwinding activity of the Nsp13-AzF constructs was not affected by the incorporation of AzF, before monitoring the binding activity between fluorescently labelled Nsp13-AzF and nucleic acids by FRET. Overall, this approach not only allows for the direct monitoring of Nsp13's binding activity on its substrate, it may also introduce a novel method to screen for compounds that can inhibit this essential enzymatic activity during viral replication.

2.2 Introduction

SARS-CoV-2 is the etiological agent responsible for the COVID-19 pandemic, which has caused extensive economic and health-related hardships worldwide[1–3]. Despite the rapid development of vaccines and antiviral therapeutics, SARS-CoV-2 remains a significant threat to human health as novel variants continue to emerge and evade developed therapeutics[4,5]. As a result, further investigations into the virus' pathogenic mechanisms remain essential in our quest to develop better pan-coronavirus therapeutics. In particular, the virally-encoded Nsp13 helicase has been identified to be essential for SARS-CoV-2 replication[6–8]. Since this helicase shares extremely high sequence conservation among coronaviruses[9,10], Nsp13 is often thought to be an ideal therapeutic target[11–13]. However, despite this therapeutic potential, its specific mechanism of binding and unwinding has yet to be fully characterized.

Many approaches have been used to study the catalytic mechanisms by which the Nsp13 helicase unwinds nucleic acids. For instance, recent cryo-electron microscopy studies uncovered that Nsp13 directly interacts with the RTC, acting together to facilitate the unwinding of the viral genome and allow for its replication[14,15]. This Nsp13-RTC interaction appears to go both ways as Nsp13 unwinding activity has been proposed to be force-dependent, requiring mechanoregulation by the RdRp[16,17]. High-resolution X-ray crystal structures and hydrogen-deuterium (H/D) exchange assays have also been used to monitor changes in the different conformational states of Nsp13[18,19]. From these studies, an inchworm-type model for Nsp13 translocation along ssRNA in the 5′ to 3′ direction was suggested, whereby ATP hydrolysis triggers a conformational change from the "closed" ATP-bound state to the more "open" product state by having the 1A domain slide 1 nt towards the 3′ end of the RNA[18,19]. Results from the H/D exchange assay also revealed

that the β19–β20 loop on the 1A domain may be involved in the unwinding process rather than binding[19].

In addition to these structural investigations, *in vitro* biochemical assays also account for a large portion of our mechanistic understanding of Nsp13. Previous studies have identified that SARS-CoV Nsp13 unwinding is enhanced with longer 5′-overhangs and that cooperative translocation of multiple Nsp13 molecules can enhance the processivity of DNA unwinding[20]. A later study found this cooperative translocation to be related to the amount of ATP present[21]. Interestingly, several of these biochemical assays showed robust enzymatic activity with DNA *in vitro*, despite Nsp13 often being thought to act on RNA *in vivo*[6,20,22]. This contrasts with another study which found that the SARS-CoV Nsp13 preferred dsRNA for its helicase activity rather than dsDNA at high ATP concentrations[21]. Recent analysis of the SARS-CoV-2 Nsp13 found that continuity of the helicase-translocating strand is essential for its unwinding activity[22]. Altogether, while these conventional biochemical methods provide enormous insight into Nsp13 binding and unwinding activities, they are limited by only reporting the average activities of a heterogenous population and cannot distinguish the activity of a single Nsp13 molecule. This poses a great limitation for multi-domain and multi-functional enzymes such as Nsp13, which cycles through different catalytic states during nucleotide binding and unwinding[18]. Therefore, to gain a detailed understanding of a single Nsp13's enzymatic activity, single-molecule experiments are warranted to capture the fast and transient dynamics involved in Nsp13 and nucleic acid binding and unwinding interactions.

Only a handful of single-molecule experiments have been done to explore the mechanistic

regulation of Nsp13 with its nucleic acid substrate. In one recent study, optical tweezer experiments uncovered that Nsp13 may be an intrinsically weak helicase that not only requires one ATP for every base pair unwound, but is also force-dependent, requiring a destabilizing force from external factors such as its substrate or complexed RdRp for unwinding[16]. Moreover, smFRET experiments have also been used to characterize a DNA unwinding step size of 4-9 base pairs for the MERS-CoV Nsp13[23]. While both studies provide useful characterizations of the unwinding dynamics of individual enzyme-substrate complexes, they remain limited in their ability to monitor the positioning of an enzyme bound to a nucleic acid substrate in real time. This is because previous smFRET experiments are often limited to tracking the hybridization state of the nucleic acid substrate as specific monitoring of the enzyme is often difficult. Since the ability to directly observe transient interactions and movements along a catalytic pathway is an invaluable method to gain a comprehensive understanding of an enzyme's activity, we sought to fluorescently label Nsp13 and observe its binding activity with fluorescently labelled nucleic acid substrates through FRET. Similar approaches have been successfully used for the characterization of other enzymes[24,25], including the hepatitis C virus helicase known as the non-structural protein 3[26].

In this work, we utilized genetic code expansion techniques to site-specifically incorporated the ncAA AzF into Nsp13 to act as a bioorthogonal handle for fluorescent labelling[27,28]. Next, we assessed the labelling efficiency of our Nsp13-AzF constructs with a Cy5-dibenzocyclooctyne (DBCO) conjugated dye and confirmed that helicase unwinding activity was not altered with the addition of AzF. After identifying suitable Nsp13-AzF constructs, these constructs were then used to characterize Nsp13 binding interactions with nucleic acids through

FRET. Ultimately, we aim to use our Nsp13-AzF constructs in smFRET experiments to monitor the positioning and dynamics of Nsp13 binding with its nucleic acid substrates.

2.3 Results

2.3.1 Identifying and Screening Potential Sites for the Incorporation of AzF into Nsp13

First, we sought to identify potential sites for AzF incorporation in Nsp13 that would be suitable to serve as a reactive site-specific bioorthogonal handle for fluorescent labelling. Using published crystal structures of the SARS-CoV-2 Nsp13 helicase, we first identified all the Tyr (Y) and Phe (F) residues in the structure as these two residues most closely resemble the structure of AzF. The goal here was to attempt to minimize any structural or functional changes to the enzyme. Structures of the SARS-CoV-2 RTC with Nsp13 bound (PDB: 6XEZ)[15], Nsp13 modelled with ADP and ssRNA[29], along with X-ray crystal structures of Nsp13 in APO form (PDB: 7NIO), phosphate-bound form (PDB: 6ZSL), and nucleotide-bound form using the ATP analog AMP-PNP (PDB: 7NN0)[18] were evaluated to visualize sidechain rotamers. To further narrow down potential candidates, we selected residues that were within FRET distance (10–100 Å) to the modelled RNA in the structure, were solvent or surface accessible for subsequent click chemistry reactions (e.g., had aromatic rings oriented towards the protein surface), and were not contained in any ordered secondary structures such as alpha helices and beta sheets. Furthermore, catalytic residues, such as those involved in ATP hydrolysis and nucleotide binding, were avoided to prevent altering the enzymatic activities of this helicase. In the end, residues F81, F90, Y205, Y246, and Y253 were selected for further analysis (**Figure 2.1 A and Supplemental Figure 2.1**).

To determine if AzF was successfully incorporated into Nsp13, we assessed for full-length wild type (WT) and Nsp13-AzF protein expression in bacterial cell lysates by western blot. In the absence of AzF in the growth media, the protein sequence was prematurely terminated at the mutated TAG site, as it is a canonical stop codon, and therefore no protein was detected by western blot probing against the C-terminal His-tag of the Nsp13 helicase. However, when AzF was supplemented to the growth media, AzF was incorporated at the mutated TAG site allowing for full-length protein expression (**Figure 2.1 B**). Full-length expression of all five Nsp13-AzF constructs was observed. No canonical amino acids were incorporated into our specified sites of interest in the absence of added AzF as no protein expression was observed (**Figure 2.1 C**).

2.3.2 Screening Nsp13-AzF Constructs for Site-specific Fluorescent Labelling with Cy5-DBCO

WT Nsp13 and Nsp13-AzF constructs were purified from bacterial cell lysates and labelled with a Cy5-DBCO conjugated dye through a SPAAC reaction (**Figure 2.2 A**). The labelling efficiencies of these Nsp13-AzF constructs were analyzed by western blot. Despite unequal Nsp13 protein abundance between samples, as observed when probing against the C-terminal His-tag on Nsp13, we observed minimal background Cy5 labelling of WT Nsp13. Normalizing the Cy5 fluorescence signal to the total protein abundance demonstrated that all Nsp13-AzF constructs yielded higher labelling efficiencies compared to WT ranging from 7-fold greater with Y205AzF; 15 to 16-fold greater with F90AzF, Y246AzF and Y253AzF; and 18-fold greater with F81AzF (**Figure 2.2 B, C**).

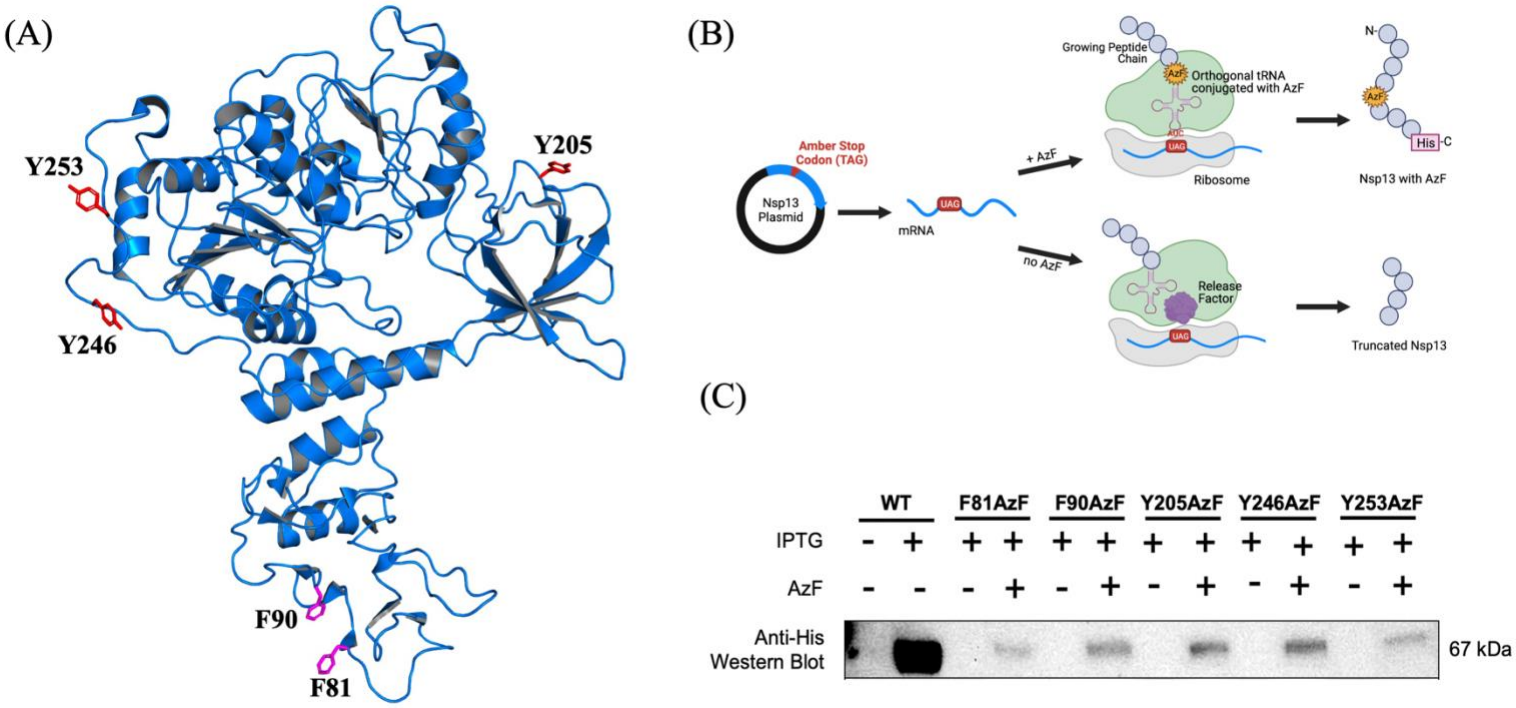

Figure 2.1 Site-specific Incorporation of AzF into Nsp13.

(A) Five sites were identified for AzF incorporation in SARS-CoV-2 Nsp13 (PDB: 6XEZ). Phe (F, purple) and Tyr (Y, red) residues that are within FRET distance to modelled RNA in the crystal structure, have their aromatic rings oriented towards the protein surface, and are not contained in ordered secondary structures were selected for AzF incorporation. (B) Schematic depicting the incorporation of AzF into C-terminal His-tag Nsp13 constructs. (C) Western blot showing full-length protein expression of Nsp13-AzF constructs in bacterial lysates in the presence of AzF in the growth media.

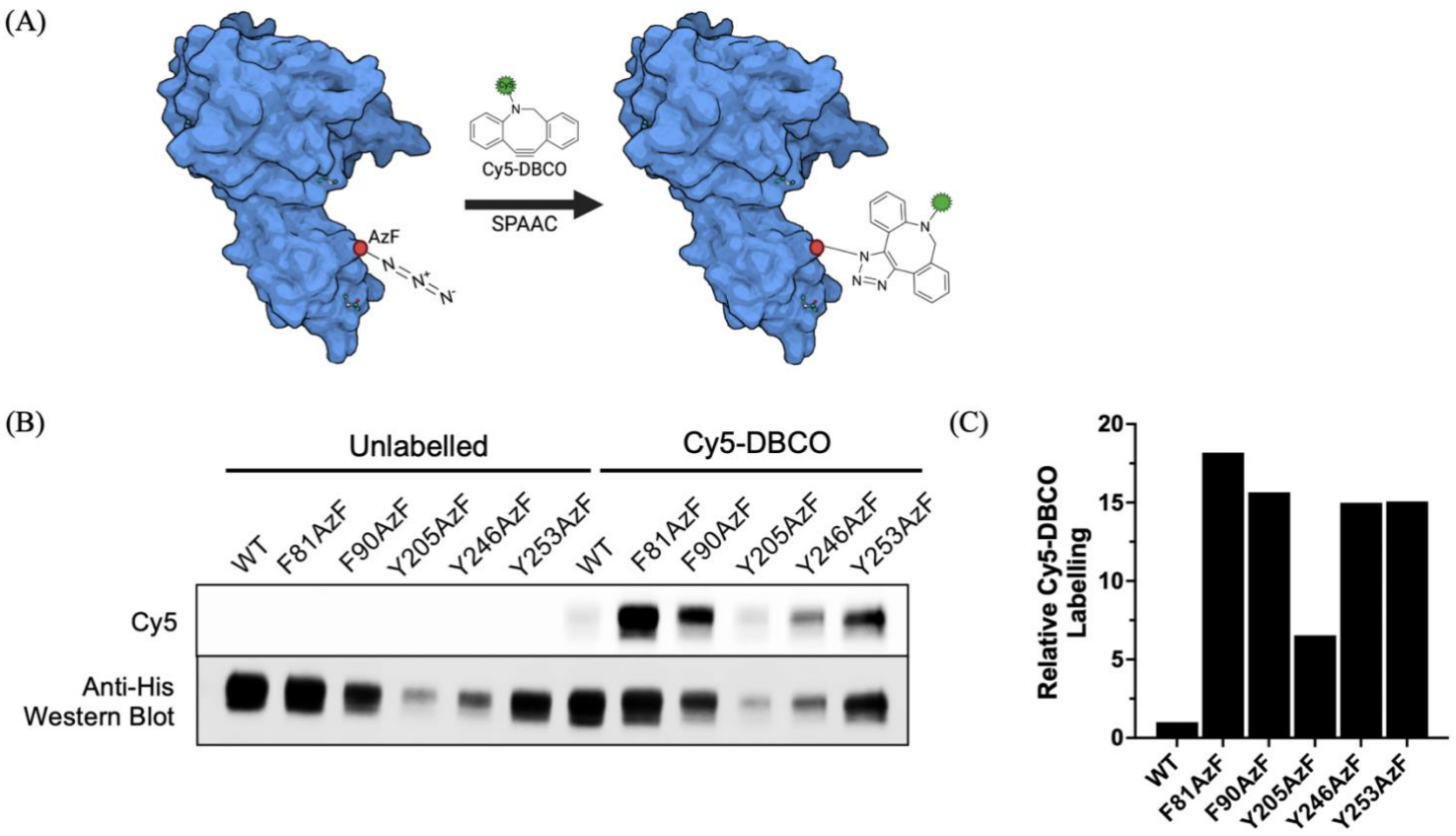

Figure 2.2 Site-specific Fluorescent Labelling of Nsp13-AzF Constructs with Cy5-DBCO.

(A) Schematic depicting the fluorescent labelling of Nsp13-AzF constructs through SPAAC reactions with a Cy5-DBCO conjugated dye. (B) Purified WT Nsp13 and Nsp13-AzF constructs were incubated with Cy5-DBCO at a molar ratio of 1:2 protein to dye in 1X PBS (pH 7.4). A Cy5 fluorescence scan was used to assess the labelling efficiency of the constructs. (C) Densitometry analysis was performed by normalizing the Cy5 intensity with the total protein abundance. The adjusted intensity is presented relative to the WT control.

2.3.3 The Unwinding Activity of F81AzF and Y253AzF were not affected by the Incorporation of AzF

After confirming that Nsp13-AzF constructs could be efficiently labelled with Cy5-DBCO, we wanted to ensure that the unwinding activity of these constructs was not affected by the incorporation of AzF. An unwinding assay was performed to monitor the rate each Nsp13-AzF construct unwinds a dsDNA substrate containing a black hole quencher and Cy3 fluorophore on opposite strands[30]. In this assay, as the dsDNA is unwound by Nsp13, the Cy3 strand is released generating a corresponding increase in Cy3 fluorescence (**Figure 2.3 A**). The unwinding activity of F81AzF, F90AzF, and Y253AzF were found to be the most similar to WT Nsp13, demonstrating unwinding rates of 0.42 ± 0.06 nM/min, 0.25 ± 0.03 nM/min, and 0.33 ± 0.05 nM/min, respectively, compared to the unwinding rate of 0.59 ± 0.14 nM/min observed with the WT (**Figure 2.3 B**). The other two Nsp13-AzF constructs, Y205AzF and Y246AzF, demonstrated a more gradual unwinding activity with rates of 0.04 ± 0.003 nM/min and 0.06 ± 0.005 nM/min, respectively (**Figure 2.3 B**). Altogether, F81AzF and Y253AzF were the two Nsp13-AzF constructs with the best labelling efficiency and unwinding rates most similar to WT Nsp13.

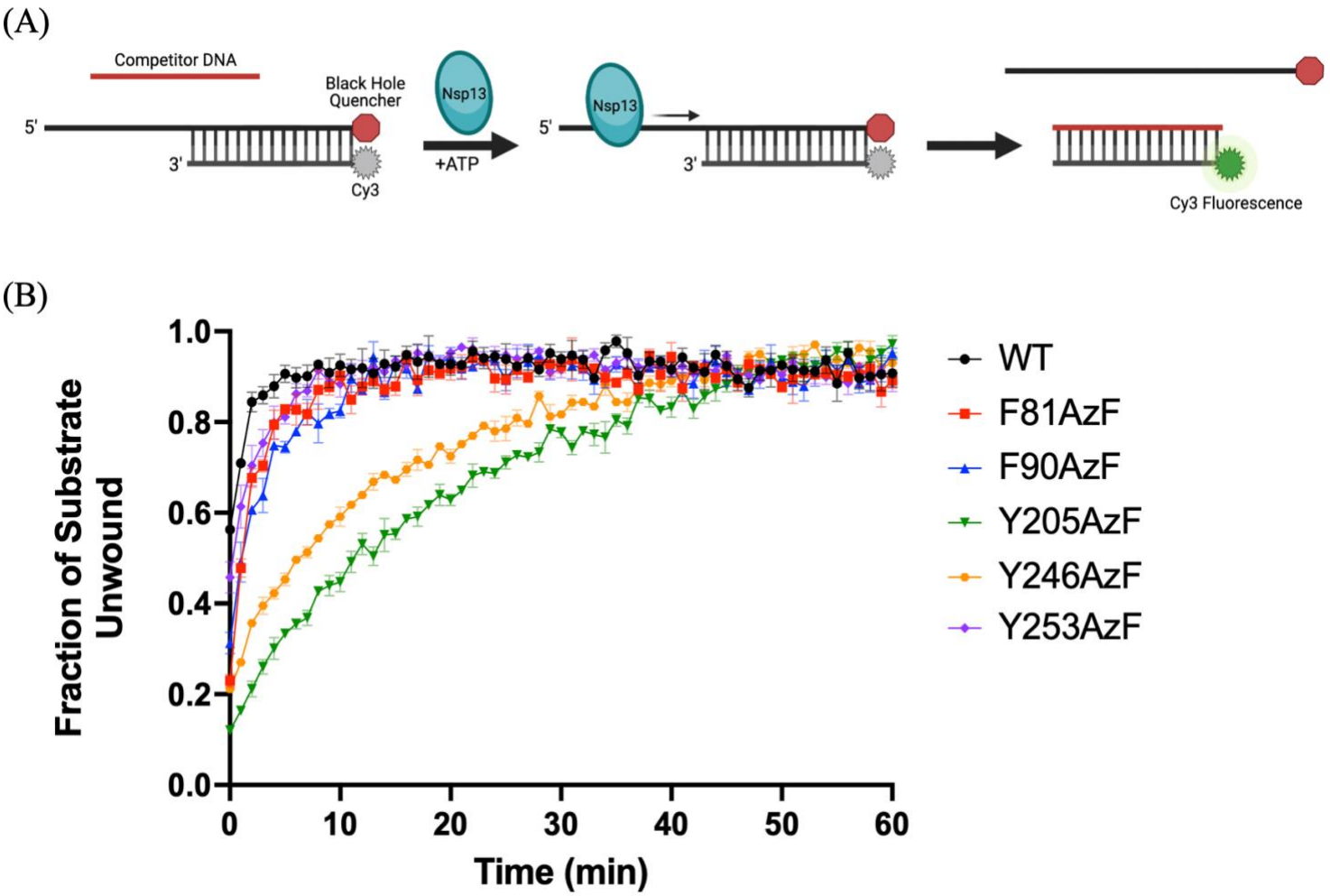

Figure 2.3 F81AzF and Y253AzF Demonstrate Similar Unwinding Rates to WT Nsp13.

(A) Schematic depicting the Nsp13 helicase unwinding assay. As Nsp13 unwinds a dsDNA substrate containing a black hole quencher and Cy3 fluorophore on opposite strands, the Cy3 strand is released generating a corresponding increase in Cy3 fluorescence. The competitor DNA captures the free Cy3 strand to prevent the substrate from re-annealing. (B) The unwinding activity of purified WT Nsp13 and Nsp13-AzF constructs was monitored. 5 nM of purified protein was incubated with 50 nM of dsDNA substrate and the reaction was initiated with the addition of 0.1 mM ATP. The graph is presented as the fraction of substrate unwound over time. Data is presented as mean ± SD (n=3). Fluorescence values were fitted using a one-phase association on PRISM-GraphPad (v9.4.1) to determine unwinding rates.

2.3.4 Monitoring the Binding of Nsp13-AzF to dsDNA Substrates by FRET

After determining that Nsp13 F81AzF and Y253AzF both showed efficient Cy5-labelling and similar unwinding rates to WT Nsp13, a FRET-based assay was conducted to monitor the binding of these constructs to Cy3-labelled substrates. While the Cy3 fluorophore (the donor) was placed on the nucleic acid substrates and the Cy5 fluorophore (the acceptor) was placed on Nsp13, we would expect to see similar FRET results if the fluorophores were reversed. This assay was done in the absence of ATP to observe Nsp13 substrate binding activity as opposed to helicase unwinding activity. A series of 20 nt long Cy3-labelled DNA substrates (S20-Cy3) with varying duplex lengths, denoted as "Xn" where "n" refers to the length of the duplex region, were designed to assess the distance-dependent relationship of FRET efficiency (S20-Cy3/X5, S20-Cy3/X8, S20-Cy3/X10, S20-Cy3/X12, S20-Cy3/X15, S20-Cy3/X17, S20-Cy3/X20) (**Supplemental Figure 2.2 A)**. As the length of the duplex region increases, the ss-overhang region shortens, and the distance between the bound Cy5-labelled Nsp13 and the Cy3 dye on the 3′ terminus of the substrate would also increase thereby reducing FRET efficiency (**Figure 2.4 A).**

First, we determined the ratiometric intensity-based FRET proximity ratio (E_{PR}), or FRET value, for the binding of Cy5-labelled WT Nsp13, F81AzF, and Y253AzF to a series of Cy3-labelled dsDNA substrates of varying duplex lengths. With the WT Nsp13, an E_{PR} value of ~0.08 was observed with the fully duplexed substrate (S20-Cy3/X20). The E_{PR} values for WT Nsp13 remained low and constant (~0.12-0.13) as the substrate's duplex length increased (X5-X17) (**Supplemental Figure 2.2 B**). The E_{PR} value of F81AzF and Y253AzF decreased in a distance-dependent manner as the length of the duplex region increased. With F81AzF, we determined a maximal E_{PR} value of ~0.35 with the S20-Cy3/X5 substrate as compared to the residual E_{PR} of

~0.14 with the fully duplexed substrate (S20-Cy3/X20) (**Supplemental Figure 2.2 B**). With Y253AzF, we determined a maximal E_{PR} value of ~0.28 with the S20-Cy3/X5 substrate as compared to the residual E_{PR} of ~0.12 with the fully duplexed substrate (S20-Cy3/X20) (**Supplemental Figure 2.2 B**).

Next, we evaluated how the FRET signal changes with varying protein concentrations. For all substrates, the E_{PR} value increased in a protein concentration-dependent manner for both F81AzF and Y253AzF, with a consistently higher E_{PR} value observed with F81AzF (**Figure 2.4. B**). The corresponding fluorescence emission spectra corroborate these findings and show that the F81AzF construct generates a protein concentration-dependent decrease in the Cy3 signal at 565 nm with a corresponding increase in the Cy5 signal at 670 nm, which is indicative of FRET (**Figure 2.4 C and Supplemental Figure 2.3**). Altogether, the F81AzF construct demonstrated the best distance-dependent FRET efficiency, making it a viable candidate for future smFRET experiments to monitor the direct binding and positioning of a Nsp13 molecule on its substrate.

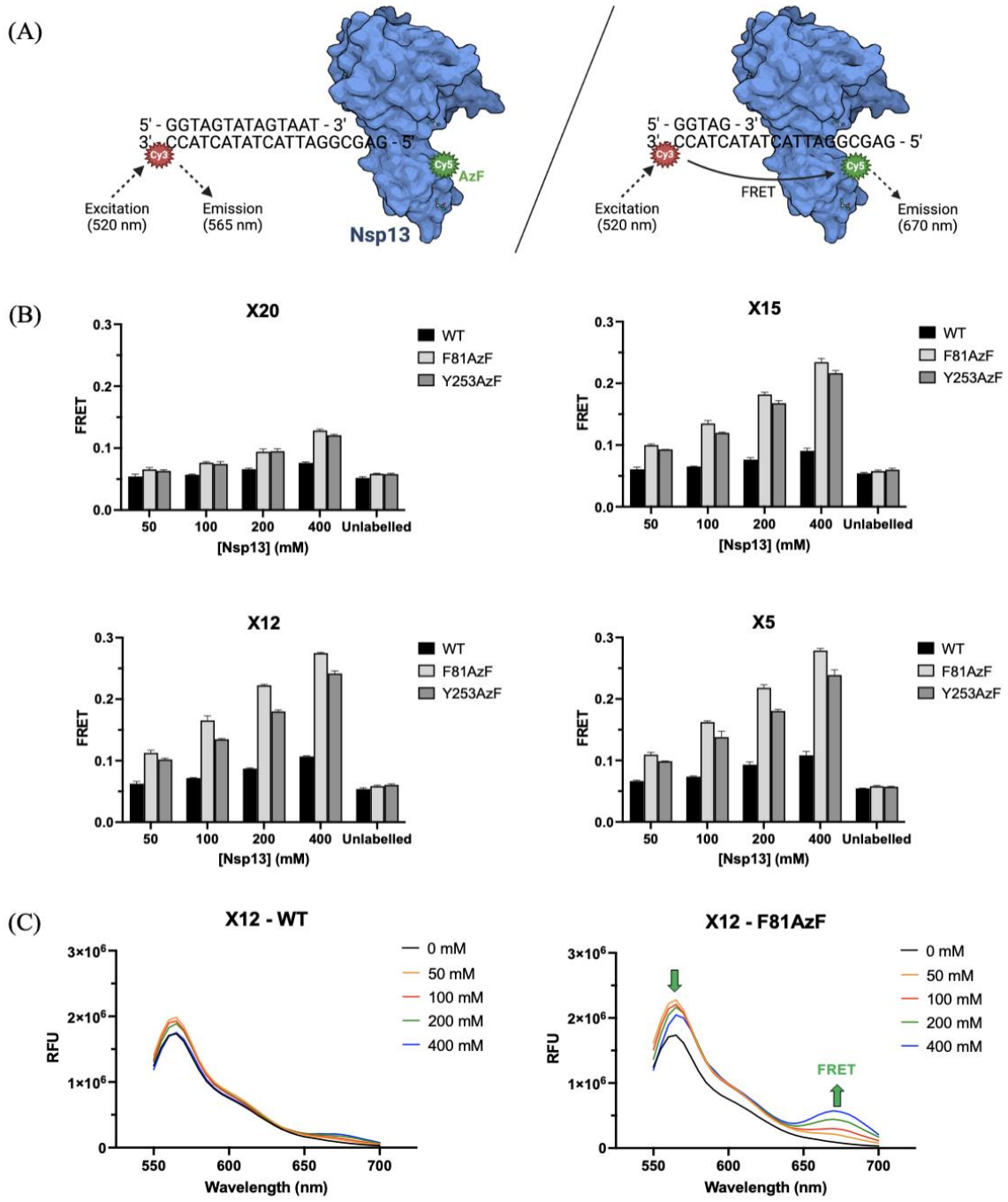

Figure 2.4 Monitoring the Binding of Cy5-labelled Nsp13 F81AzF and Y253AzF to Cy3-labelled dsDNA by FRET.

(A) Schematic representation of the binding of Cy5-labelled Nsp13-AzF to dsDNA substrates. Upon excitation at 520 nm, if Nsp13 is bound to the ss-overhang of the substrate at a close enough distance to the Cy3 dye on the dsDNA substrate, FRET will be observed through emission of the Cy5 signal at 670 nm. (B) The ratiometric intensity-based FRET proximity ratio (E_{PR}) for the binding of Cy5-labelled WT Nsp13,

F81AzF, and Y253AzF to dsDNA substrates with varying duplex lengths shows an increase in FRET with increasing protein concentration. Data are presented as mean ± SD (n=3). (C) The emission spectra for the binding of Cy-5 labelled WT Nsp13 and F81AzF to the S20-Cy3/X12 substrate shows a Cy3 peak at 565 nm and a Cy5 peak at 670 nm.

2.4 Discussion

The incorporation of ncAAs, such as AzF, into proteins requires some optimization; however, when successfully done, they can provide numerous potential applications. One of these highly useful applications includes the ability to serve as a site-specific bioorthogonal reactive handle for fluorescent labelling[31,32]. This is especially useful for studying the transient dynamics of enzyme and nucleic acid interactions as the site-specific labelling of each molecule with corresponding FRET-pair fluorophores allows for the direct monitoring of the enzyme along its bound substrate.

First, five potential sites for incorporating AzF into the SARS-CoV-2 Nsp13 helicase were investigated (F81, F90, Y205, Y246, and Y253) (**Figure 2.1 A and Supplemental Figure 2.1**). To minimize alterations to the structure and function of this highly conserved helicase, Tyr and Phe residues were selected as they most closely resemble the structure of AzF. The AzF handle was also selected to be solvent accessible and in an orientation and location suitable for generating FRET with nucleic substrates. Consequently, this resulted in residues within loops often being selected in order to not restrict the rotational freedom of the attached dye. Additionally, as the ultimate goal is to use these Nsp13-AzF constructs in functional enzymatic assays, we chose sites that were not involved in catalytic functions, such as nucleotide binding and unwinding. Two of the selected residues, F81 and F90, were located in the fairly flexible ZBD of SARS-CoV-2 and have been shown to be on the interface involved with interactions between Nsp13 and Nsp8a in

the RTC[15]. Y205 is found in the 1B domain and has been recently hypothesized to engage with residue W178 to form a platen that aids in the conformation-specific recognition of Z-RNA, the left-handed conformer of normal dsDNA[33]. Y246 and Y253 are both found on an exterior flexible loop in the 1B domain, next to the RecA-like 1A domain but away from conserved helicase motifs I, II, and III that make contact to bound nucleotides[18]. Full-length expression of all five Nsp13-AzF constructs was observed, but not to the same level as WT Nsp13 (**Figure 2.1 C**). This was to be expected since these evolved tRNAs conjugated with AzF may compete with release factors that facilitate the termination of protein synthesis at the amber stop codon, TAG[28,34]. Additionally, changes to the folding competency of these Nsp13-AzF constructs may account for some of the variability in protein abundance observed.

After confirming the recombinant protein expression of all five Nsp13-AzF constructs, we then assessed the reactivity of the azido group of AzF for a strained alkyne-conjugated dye, Cy5-DBCO. Since SPAAC click reactions have been shown to be slower and less selective compared to CuAAC[35], we needed to confirm both the efficiency and specificity of the fluorescent labelling of Nsp13-AzF constructs. When purified Nsp13-AzF was reacted with two-molar excess Cy5-DBCO, without the removal of unincorporated dye, we observed some background labelling of the unmodified WT Nsp13 (**Figure 2.2 B**). This unspecific labelling may be attributed to the fact that strained-alkynes can sometimes cross-react with nucleophiles, such as free thiols, via a Michael addition[36]. Therefore, as there are 26 cysteine residues in Nsp13, most of which are solvent accessible, these thiol side chains may react with the strained alkyne leading to some unspecific background labelling as the unreacted dye was not removed[37]. Further optimization of the labelling conditions (e.g., time, concentration etc.) and subsequent removal of unreacted dye

may help mitigate this concern. Additionally, we observed inconsistent protein concentrations between samples due to the instability of our purified proteins. During the protein purification process, reducing agents were avoided to prevent the reduction of the AzF azide group to an amine. While this was necessary for preserving the integrity of AzF, it became detrimental in Nsp13 protein stability and storage as the free cysteines may have formed artificial disulfide bonds, which can lead to aggregation of the protein[38]. This is why moving forward to *in vitro* helicase unwinding and binding assays, freshly purified protein was used. Despite this, it is evident that the Nsp13-AzF constructs can be efficiently and specifically labelled with Cy5-DBCO, with F81AzF showing the best labelling efficiency.

Another important aspect we needed to evaluate before using these Nsp13-AzF constructs for *in vitro* characterization studies was to ensure that the helicase unwinding activity of Nsp13-AzF constructs was not hindered. We found that F81AzF and Y253AzF, with unwinding rates of 0.42 ± 0.06 nM/min and 0.33 ± 0.05 nM/min respectively, were the only constructs to have unwinding rates within a two-fold difference compared to the WT (**Figure 2.3 B**). While F90AzF also demonstrated similar unwinding to the WT, we decided to not conduct FRET binding assays with this construct as the F81AzF mutation was located in the same region and had a more comparable unwinding rate to the WT. Interestingly, the Y246AzF showed a substantially lowered unwinding activity despite this mutation being located in the same region as Y253AzF. Both of these residues are not currently known to be directly involved in the unwinding process[18,19,39]; however, it may be interesting to further evaluate the kinetic implications of this Y246 residue on helicase activity in the future and see if the addition of AzF at this site changes the overall fold of the protein. Y205AzF demonstrated the lowest unwinding rate, which may correspond to its

hypothesized role in binding dsRNA[33]. Altogether, we showed that unwinding activity is not compromised with the incorporation of AzF at sites F81, F90 and Y253.

After screening for suitable Nsp13-AzF constructs, F81AzF and Y253AzF were selected for use in FRET-based binding assays. We were interested in evaluating FRET for both of these constructs as they were located in very different domains with F81 being in the ZBD and Y253 being in the catalytic Rec1A domain located relatively closer to the nucleic acid binding channel of Nsp13. When comparing the E_{PR} values of F81AzF and Y253AzF with varying substrate duplex lengths and protein concentrations, we found that F81AzF consistently showed higher FRET efficiency (**Figure 2.4 B and Supplemental Figure 2.2 B**). Despite the F81 site being further away from the nucleic acid binding site relative to Y253, this result was not entirely surprising as a previous study was able to measure FRET with more distant AzF sites as well[26]. In order to observe FRET, the donor and acceptor transition dipoles must be aligned[40–42]. As such, the higher E_{PR} values observed with F81AzF may suggest that the Cy5 fluorophore at this site is attached at a more suitable position/orientation for FRET with the Cy3 fluorophore located on the DNA substrate, as compared to Y253AzF. Overall, we found that as the length of the duplex increased, the E_{PR} value decreased, indicating that Nsp13 bound on average farther from the Cy3 fluorophore (**Figure 2.4 B and Supplemental Figure 2.2 B**). As expected, the greatest E_{PR} value for both Nsp13-AzF constructs was observed with the S20-Cy3/X5 substrate as it had the shortest duplex region. Previous studies have reported that the optimal footprint length of Nsp13 is 5 nt[43]; however, a 10 nt overhang is thought to allow one copy of Nsp13 to bind at a time[20]. This may explain why although we see a decrease in FRET efficiency with increasing duplex length, it is a relatively small change as we do not get enhanced cooperativity with multiple Nsp13 molecules binding the

substrate within this range. With the fully duplexed substrate (S20-Cy3/X20), the resulting E_{PR} was reduced to ~0.14 with F81AzF and ~0.12 with Y235AzF (**Supplemental Figure 2.2 B**). This residual E_{PR} may be due to the bleed-through of the Cy3 signal into the Cy5 channel, which is observed with the Cy3-labelled dsDNA substrate alone. Since the bleed-through for Cy3/Cy5 pairs has been reported to be between 8 and 15%[44], additional bandpass filters could be employed to correct for this signal. It is also important to note that this assay measures the average FRET of a heterogeneous population. Therefore, variations in the FRET efficiencies observed may reflect heterogeneity in the protein population (i.e., unlabelled or reduced Nsp13-AzF constructs in solution), as well as the dynamics and kinetics of the Nsp13 binding to its substrate. It is also possible that these FRET measurements reflect the presence of multiple protein binding modes and not solely the desired binding of Nsp13 at the ss/ds junction on the Cy3-labelled substrate. Since previous studies have demonstrated that some HCoV helicases can have basal ATPase activities stimulated by ss nucleic acids[45], our results may reflect the average FRET efficiency of Nsp13 as it slides along the ss-overhang of the substrates in the absence of ATP.

Another variable that may further convolute conclusions drawn from our ensemble FRET results is the presence of protein-induced fluorescence enhancement (PIFE) events. This photophysical effect refers to the enhancement in emission intensity of fluorescent dyes, including cyanine dyes like Cy3, when there is an increase in viscosity of their local molecular environment[46,47]. These events can be caused by the steric constraint of a protein binding near a Cy3 fluorophore, which reduces trans-cis photoisomerization of the dye[46–49]. In our FRET-based binding assay, we observed an increase in the baseline Cy3 signal at 565 nm when Cy5-labelled Nsp13-AzF is bound, which is not observed with the WT (**Figure 2.4 C and Supplemental Figure**

2.3). For the F81AzF construct specifically, as protein concentration increases, we observed an increase in the Cy5 signal at 670 nm by FRET, along with the expected concomitant decrease in the donor Cy3 signal at 565 nm. However, with the Y253AzF construct, we observed an increase in the Cy5 signal, with increasing protein concentration, but it was not anti-correlated with the donor Cy3 signal. This may be due to the fact that previous reports have indicated that PIFE can influence low FRET situations and cause the intensity of the dye on the protein (Cy5) to increase without the anti-correlated decrease exhibited by the other dye[46].

Collectively, these results show that we can fluorescently label Nsp13 through genetic code expansion techniques and use it to detect DNA binding by FRET. This approach in using ncAAs as a bioorthogonal handle for fluorescent labelling provides many advantages over other common methods of protein labelling, such as labelling through the cysteines or amine groups in the protein[50]. To start, this method enables the site-selective modification of a single residue, consequently minimizing alterations to the native protein structure and function. This starkly contrasts the relatively large size of many fluorescent proteins (typically ~25 kDa), such as the commonly used green fluorescent protein (GFP)[51], which can compromise the function of co-expressed biomolecules. Also, by attaching the fluorophore to a single position, we can improve the chances that the generated FRET observed in ensemble assays is specific to a given binding mode or conformation. The flexibility to label any residue on a protein is also imperative for ensuring that the fluorophore is in an agreeable position and orientation for FRET. However, despite this specific labelling of Nsp13, the FRET-based binding assays we have conducted here still report on the average of a heterogeneous population. Therefore, in order to delineate the specific mechanism by which this helicase interacts with its substrate, conducting further smFRET

experiments will help attribute the measured FRET efficiency to changes in the helicase position and/or orientation on the nucleic acid substrate during binding and unwinding.

2.5 Conclusion

Overall, we identified two Nsp13-AzF constructs, F81AzF and Y253AzF, that can be efficiently labelled with a Cy5-DBCO dye through SPAAC reactions. We confirmed that these mutations had little effect on its helicase unwinding activity and therefore were ideal candidates for FRET-based *in vitro* characterization of Nsp13 binding activity. Ultimately, F81AzF was identified to be the best Nsp13-AzF construct for use in future smFRET experiments to study the dynamics of Nsp13 translocation on its substrate during binding and unwinding.

2.6 Materials and Methods

2.6.1 Nucleic Acids

All subcloning and site-directed mutagenesis primers were purchased from Sigma-Aldrich (Darmstadt, Germany). All DNA oligonucleotides for the helicase unwinding assay and FRET assay were purchased from Integrated DNA Technologies (Coralville, IA, USA).

2.6.2 Subcloning and Site-directed Mutagenesis of Nsp13

The full-length coding sequence of the SARS-CoV-2 Nsp13 helicase was subcloned into the pET-21(a)+ vector for bacterial expression. Briefly, a bacterial codon-optimized sequence for SARS-CoV-2 Nsp13 helicase (Addgene, plasmid #159614) was subcloned by PCR into the pET21(a)+ bacterial expression vector using forward and reverse PCR primers (**Supplemental Table 2.1**). The PCR products were then digested with BamHI (New England Biolabs, Cat. #R0136S) and HindIII (New England Biolabs, Cat. #R0104S) and inserted into the multiple cloning site of pET21(a)+, keeping the C-terminal 6X-His-tag in frame. The resulting Nsp13 bacterial expression vector (pET21-Nsp13) was confirmed by sequencing performed at Genome Quebec (Montreal, QC).

Site-directed mutagenesis was performed to introduce an amber stop codon (TAG) mutation into pET21-Nsp13 at the following positions: F81, F90, Y205, Y246, and Y253. Reactions were carried out in PCR tubes consisting of 20 ng of pET21-Nsp13 plasmid DNA, 1X Xtremebuffer, 0.4 mM dNTPs, 0.3 µM each of the corresponding forward and reverse site-directed mutagenesis primers (**Supplemental Table 2.1**), and 0.02 U/µL KOD polymerase (Novagen, Cat. #71975-3) in a total reaction volume of 50 µL in water. Reactions were placed in a thermocycler

and run at 98ºC for 2 minutes, 95ºC for 30 seconds, 55ºC for 1 minute, 72ºC for 7 minutes (1 minute/KB), repeating steps 2-4 for a total of 18 cycles before a final extension at 72ºC for 5 minutes. The resulting Nsp13-AzF plasmid sequences were confirmed by sequencing performed at Genome Quebec (Montreal, QC).

2.6.3 Small-scale Bacterial Expression and Screening of AzF Incorporation

To assess the bacterial expression of Nsp13-AzF constructs, *E. coli* strain BL21 (DE3) (Thermofisher Scientific) cells were transformed with Nsp13-AzF plasmids along with an orthogonal tRNA/aminoacyl tRNA synthetase pair (tRNA/aaRS) gifted from the lab of Dr. Peter Schultz[52]. The transformed cells were then grown in 2 mL cultures of LB media supplemented with 100 µg/mL ampicillin and 50 µL/mL spectinomycin at 37ºC to an OD of 0.5-0.6. Expression of the Nsp13-AzF constructs was induced with the addition of 1 mM isopropyl β-D-1-thiogalactopyranoside (IPTG) (Teknova, Cat. #I3325) and 1 mM AzF (MedChemExpress LLC, #HY-16714) to the media. Cultures were then allowed to grow at 18ºC overnight. The cells were pelleted by centrifugation, resuspended in 100 µL of 2X Laemmli Buffer (Biorad, Cat. #1610737EDU), and heated at 95ºC for 15 minutes. The samples were resolved on a 10% stain-free SDS-PAGE gel (Bio-Rad, Cat. #1610183) and scanned on a ChemiDoc MP imager (Bio-Rad) before the proteins were transferred to a PDVF membrane and probed for Nsp13-AzF expression using a 6X-His Tag monoclonal antibody (Thermofisher Scientific, Cat. #MA1-21315-HRP).

2.6.4 WT Nsp13 and Nsp13-AzF Protein Purification

Large-scale bacterial expression of WT and Nsp13-AzF were prepared as described under "Small-scale Bacterial Expression and Screening of AzF Incorporation". Briefly, transformed *E.*

coli strain BL21 (DE3) cells containing the Nsp13-AzF plasmids were grown in 600 mL of LB supplemented with 100 µg/mL ampicillin and 50 µL/mL spectinomycin at 37ºC to an OD of 0.5-0.6. Protein expression was induced with the addition of 1 mM IPTG (Teknova, Cat. #I3325) and 1 mM AzF (MedChemExpress LLC, #HY-16714) to the media before allowing the cultures to grow at 18ºC overnight. Cells were harvested by centrifugation at 5000 x g for 5 minutes. The pellet was resuspended in lysis buffer (50 mM Tris (pH 8.0), 300 mM NaCl, 10 mM imidazole (pH 8.0)) supplemented with cOmplete™ Protease Inhibitor Cocktail (Roche, Cat. #11697498001) and subsequently lysed by sonication (50% amplitude) for 2 minutes cycling between 1 second off and 1 second on ice. The cells were then centrifuged at 20,000 x g for 20 minutes at 4ºC to obtain the soluble fraction. WT Nsp13 and Nsp13-AzF constructs were purified using HisTrap HP columns (Sigma, Cat. #GE17-5319-01) and washed with wash buffer (500 mM Tris (pH 8.0), 600 mM NaCl, 60 mM imidazole (pH 8.0)). Purified protein was eluted using elution buffer (50 mM Tris (pH 8.0), 300 mM NaCl, 300 mM imidazole (pH 8.0)) and concentrated using 30 kDa MWCO ultra-centrifugation tubes (Amicon, Cat. #UFC903024) before buffer-exchanged into a buffer containing 50 mM Tris (pH 8.0), and 100 mM NaCl. Size-exclusion fast protein liquid chromatography (FPLC) was then performed using a S75 column (GE Healthcare Life Sciences). Purified protein concentrations were determined both by the absorbance at 280 nm on a NanoDrop 2000 (Thermo Scientific) and using the calculated extinction coefficient of 68,785 $M^{-1}cm^{-1}$ [11].

2.6.5 Fluorescent Labelling of Nsp13-AzF with Cy5-DBCO

5 µM of purified WT Nsp13 or Nsp13-AzF constructs were allowed to react with 10 µM Cy5-DBCO (Sigma Aldrich, Cat. #777374) in 1X PBS (pH 7.4) at room temperature for 30 minutes. To remove excess dye, the labelled proteins were run through a P30 gel microspin column

(Bio-Rad, Cat. #7326250) according to the manufacturer's protocol. SDS-PAGE loading buffer was added to the samples and heated at 95ºC for 10 minutes before being resolved on a 10% stain-free SDS-PAGE gel (Bio-Rad, Cat. #1610183). The gel was scanned for Cy5 fluorescence and stain-free protein visualization on a ChemiDoc MP imager (Bio-Rad). The labelled proteins were then transferred to a PDVF membrane and probed for Nsp13-AzF expression using a 6X-His Tag monoclonal antibody (Thermofisher Scientific, Cat. #MA1-21315-HRP).

2.6.6 Helicase Unwinding Assay

The helicase unwinding assay was adapted from a previous publication with some modifications[30]. Briefly, the Cy3-DNA strand and Black Hole Quencher-2 (BHQ-2) (**Supplemental Table 2.2)** were annealed at a 1:1.1 ratio with concentrations of 20 µM:22 µM, respectively, in a thermocycler by heating to 75ºC for 5 minutes followed by a gradual cooling to 4ºC over 50 minutes. In a 96-well black bottom plate, a 2X enzyme solution containing 5 nM of purified WT Nsp13 or Nsp13-AzF in reaction buffer (20 mM HEPES (pH 7.6), 20 mM NaCl, 5 mM $MgCl_2$, and 0.1 mg/mL BSA) was added in triplicate. To start the reaction, a 2X solution containing 50 nM duplex substrate, 250 nM competitor strand DNA, and 100 µM ATP in reaction buffer was added to the enzyme solution in the plate. Samples were excited at 530 nm (9 nm slit width) and emission was recorded at 570 nm (15 nm slit width) using a SpectraMax i3 plate reader (Molecular Devices) every minute for 60 minutes. Fluorescence values were fitted using a one-phase association on PRISM-GraphPad (v9.4.1) to determine unwinding rates.

2.6.7 Fluorescent Resonance Energy Transfer Assay

A 20 nt long DNA strand was ordered with a Cy3 dye attached to the 3′ terminus (S20-Cy3). A series of complementary DNA sequences were designed to form partial duplexes of varying lengths with the S20-Cy3 strand. These sequences are denoted as "Xn", where "n" refers to the length of the duplex region (**Supplemental Table 2.3**). For the FRET assay, the substrates were prepared by annealing the S20-Cy3 strand with the Xn strands at a 1:2 ratio with concentrations of 20 µM:40 µM, respectively, by heating to 75ºC for 5 minutes followed by gradual cooling to 4ºC over 50 minutes in a thermocycler.

The FRET assay was performed in a total volume of 40 µL in 96-well black bottom plates. Purified and Cy5-DBCO labelled WT Nsp13, F81AzF and Y253AzF Nsp13 constructs (50-400 nM) were serially diluted in FRET reaction buffer (25 mM MOPS (pH 6.0), 10 mM NaCl, 3 mM $MgCl_2$, and 0.1% Tween-20) and incubated with 100 nM of corresponding Cy3-DNA substrate (S20-Cy3/X20, S20-Cy3/X17, S20-Cy3/X15, S20-Cy3/X12, S20-Cy3/X10, S20-Cy3/X8, S20-Cy3/X5) for 30 minutes at room temperature. Samples were excited at 520 nm and the fluorescence spectra were recorded from 555 to 700 nm using a SpectraMax i3 plate reader (Molecular Devices). The ratiometric intensity-based FRET proximity ratio (E_{PR}) was defined as $I_A/(I_A + I_D)$, where I_A and I_D are the emission maximum intensities of the Cy5 acceptor at 670 nm and the Cy3 donor at 565 nm, respectively[53].

2.7 References

1. Wu F, Zhao S, Yu B, et al. A new coronavirus associated with human respiratory disease in China *Nature*. 2020;579(7798):265-269. doi.org/10.1038/s41586-020-2008-3
2. Pak A, Adegboye OA, Adekunle AI, Rahman KM, McBryde ES, Eisen DP. Economic Consequences of the COVID-19 Outbreak: the Need for Epidemic Preparedness. *Front Public Health*. 2020;8:241. doi:10.3389/fpubh.2020.00241
3. Tang D, Comish P, Kang R. The hallmarks of COVID-19 disease. *PLoS Pathog*. 2020;16(5):e1008536. doi:10.1371/journal.ppat.1008536
4. Zhou F, Yu T, Du R, et al. Clinical course and risk factors for mortality of adult inpatients with COVID-19 in Wuhan, China: a retrospective cohort study. *The Lancet*. 2020;395(10229):1054-1062. doi:10.1016/S0140-6736(20)30566-3
5. Mathieu E, Ritchie H, Ortiz-Ospina E, et al. A global database of COVID-19 vaccinations. *Nat Hum Behav*. 2021;5(7):947-953. doi:10.1038/s41562-021-01122-8
6. Mickolajczyk KJ, Shelton PMM, Grasso M, et al. Force-dependent stimulation of RNA unwinding by SARS-CoV-2 nsp13 helicase. *Biophys J*. 2021;120(6):1020-1030. doi:10.1016/j.bpj.2020.11.2276
7. Tanner JA, Watt RM, Chai YB, et al. The severe acute respiratory syndrome (SARS) coronavirus NTPasefhelicase belongs to a distinct class of 5′ to 3′ viral helicases. *J Biol Chem*. 2003;278(41):39578-39582. doi:10.1074/jbc.c300328200
8. Ivanov KA, Thiel V, Dobbe JC, van der Meer Y, Snijder EJ, Ziebuhr J. Multiple Enzymatic Activities Associated with Severe Acute Respiratory Syndrome Coronavirus Helicase. *J Virol*. 2004;78(11):5619-5632. doi:10.1128/jvi.78.11.5619-5632.2004
9. Frick DN, Virdi RS, Vuksanovic N, Dahal N, Silvaggi NR. Molecular Basis for ADP-Ribose Binding to the Mac1 Domain of SARS-CoV-2 nsp3. *Biochemistry*. 2020;59(28):2608-2615. doi:10.1021/acs.biochem.0C00309
10. White MA, Lin W, Cheng X. Discovery of COVID-19 Inhibitors Targeting the SARS-CoV-2 Nsp13 Helicase. *J Phys Chem Lett*. 2020;11(21):9144-9151. doi:10.1021/acs.jpclett.0c02421
11. Gurung AB. In silico structure modelling of SARS-CoV-2 Nsp13 helicase and Nsp14 and repurposing of FDA approved antiviral drugs as dual inhibitors. *Gene Rep*. 2020;21:100860. doi:10.1016/j.genrep.2020.100860
12. Adedeji AO, Singh K, Calcaterra NE, et al. Severe Acute Respiratory Syndrome Coronavirus Replication Inhibitor That Interferes with the Nucleic Acid Unwinding of the Viral Helicase. *Antimicrob Agents Chemother*. 2012;56(9):4718-4728. doi:10.1128/aac.00957-12

13. Yu MS, Lee J, Lee JM, et al. Identification of myricetin and scutellarein as novel chemical inhibitors of the SARS coronavirus helicase, nsP13. *Bioorg Med Chem Lett*. 2012;22(12):4049-4054. doi:10.1016/j.bmcl.2012.04.081
14. Yan L, Zhang Y, Ge J, et al. Architecture of a SARS-CoV-2 mini replication and transcription complex. *Nat Commun*. 2020;11(1):1-6. doi:10.1038/s41467-020-19770-1
15. Chen J, Malone B, Llewellyn E, et al. Structural Basis for Helicase-Polymerase Coupling in the SARS-CoV-2 Replication-Transcription Complex. *Cell*. 2020;182(6):1560-1573.e13. doi:10.1016/j.cell.2020.07.033
16. Mickolajczyk KJ, Shelton PMM, Grasso M, et al. Force-dependent stimulation of RNA unwinding by SARS-CoV-2 nsp13 helicase. *Biophys J*. 2021;120(6):1020-1030. doi:10.1016/j.bpj.2020.11.2276
17. Jia Z, Yan L, Ren Z, et al. Delicate structural coordination of the Severe Acute Respiratory Syndrome coronavirus Nsp13 upon ATP hydrolysis. *Nucleic Acids Res*. 2019;47(12):6538-6550. doi:10.1093/nar/gkz409
18. Newman JA, Douangamath A, Yadzani S, et al. Structure, mechanism and crystallographic fragment screening of the SARS-CoV-2 NSP13 helicase. *Nat Commun*. 2021;12(1):1-11. doi:10.1038/s41467-021-25166-6
19. Jia Z, Yan L, Ren Z, et al. Delicate structural coordination of the Severe Acute Respiratory Syndrome coronavirus Nsp13 upon ATP hydrolysis. *Nucleic Acids Res*. 2019;47(12):6538-6550. doi:10.1093/nar/gkz409
20. Lee NR, Kwon HM, Park K, Oh S, Jeong YJ, Kim DE. Cooperative translocation enhances the unwinding of duplex DNA by SARS coronavirus helicase nsP13. *Nucleic Acids Res*. 2010;38(21):7626-7636. doi:10.1093/nar/gkq647
21. Jang KJ, Jeong S, Kang DY, Sp N, Yang YM, Kim DE. A high ATP concentration enhances the cooperative translocation of the SARS coronavirus helicase nsP13 in the unwinding of duplex RNA. *Sci Rep*. 2020;10(1):1-13. doi:10.1038/s41598-020-61432-1
22. Sommers JA, Loftus LN, Jones MP, et al. Biochemical analysis of SARS-CoV-2 Nsp13 helicase implicated in COVID-19 and factors that regulate its catalytic functions. *JBC*. 2023;299(3):102980. doi:10.1016/j.jbc.2023.102980
23. Hu X, Hao W, Qin B, et al. Mechanism of duplex unwinding by coronavirus nsp13 helicases. *bioRxiv*. Published online August 3, 2020. doi:10.1101/2020.08.02.233510
24. Zander A, Holzmeister P, Klose D, Tinnefeld P, Grohmann D. Single-molecule FRET supports the two-state model of Argonaute action. *RNA Biol*. 2014;11(1):45. doi:10.4161/RNA.27446

25. Jakob L, Gust A, Grohmann D. Evaluation and optimisation of unnatural amino acid incorporation and bioorthogonal bioconjugation for site-specific fluorescent labelling of proteins expressed in mammalian cells. *Biochem Biophys Rep*. 2019;17:1. doi:10.1016/j.bbrep.2018.10.011
26. Ablenas CJ, Gidi Y, Powdrill MH, et al. Hepatitis C Virus Helicase Binding Activity Monitored through Site-Specific Labeling Using an Expanded Genetic Code. *ACS Infect Dis*. 2019;5(12):2118-2126. doi:10.1021/acsinfecdis.9b00220
27. Chin JW, Santoro SW, Martin AB, King DS, Wang L, Schultz PG. Addition of p-azido-L-phenylalanine to the genetic code of Escherichia coli. *J Am Chem Soc*. 2002;124(31):9026-9027. doi:10.1021/ja027007w
28. Lang K, Chin JW. Cellular incorporation of unnatural amino acids and bioorthogonal Labeling of Proteins. *Chem Rev*. 2014;114(9):4764-4806. doi:10.1021/cr400355w
29. Perez-Lemus GR, Menéndez CA, Alvarado W, Byléhn F, de Pablo JJ. Toward wide-spectrum antivirals against coronaviruses: Molecular characterization of SARS-CoV-2 NSP13 helicase inhibitors. *Sci Adv*. 2022;8(1):4526. doi:10.1126/sciadv.abj4526
30. Zeng J, Weissmann F, Bertolin AP, et al. Identifying SARS-CoV-2 antiviral compounds by screening for small molecule inhibitors of nsp13 helicase. *Biochem J*. 2021;478(13):2405-2423. doi:10.1042/bcj20210201
31. Sun SB, Schultz PG, Kim CH. Therapeutic applications of an expanded genetic code. *Chembiochem*. 2014;15(12):1721. doi:10.1002/cbic.201402154
32. Wang K, Sachdeva A, Cox DJ, et al. Optimized orthogonal translation of unnatural amino acids enables spontaneous protein double-labelling and FRET. *Nat Chem*. 2014;6(5):393-403. doi:10.1038/nchem.1919
33. Herbert A, Poptsova M. Z-RNA and the Flipside of the SARS Nsp13 Helicase: Is There a Role for Flipons in Coronavirus-Induced Pathology? *Front Immunol*. 2022;13:2814. doi:10.3389/fimmu.2022.912717
34. Chin JW. Expanding and Reprogramming the Genetic Code of Cells and Animals. *Annu Rev Biochem*. 2014;83:379-408. doi:10.1146/annurev-biochem-060713-035737
35. Spicer CD, Davis BG. Selective chemical protein modification. *Nat Commun*. 2014;5(1):1-4. doi:10.1038/ncomms5740
36. McKay CS, Finn MG. Click Chemistry in Complex Mixtures: Bioorthogonal Bioconjugation. *Chem Biol*. 2014;21(9):1075-1101. doi:10.1016/j.chembiol.2014.09.002
37. Hoogenboom R. Thiol–Yne Chemistry: A Powerful Tool for Creating Highly Functional Materials. *Angewandte Chemie International Edition*. 2010;49(20):3415-3417. doi:10.1002/anie.201000401

38. Remans K, Lebendiker M, Abreu C, et al. Protein purification strategies must consider downstream applications and individual biological characteristics. *Microb Cell Fact*. 2022;21(1). doi:10.1186/s12934-022-01778-5
39. Berta D, Badaoui M, Martino SA, et al. Modelling the active SARS-CoV-2 helicase complex as a basis for structure-based inhibitor design. *Chem Sci*. 2021;12(40):13492-13505. doi:10.1039/disc02775A
40. Ha T. Single-molecule fluorescence methods for the study of nucleic acids. *Curr Opin Struct Biol*. 2001;11(3):287-292. doi:10.1016/s0959-440x(00)00204-9
41. Iqbal A, Wang L, Thompson KC, Lilley DMJ, Norman DG. The structure of cyanine 5 terminally attached to double-stranded DNA: Implications for FRET studies. *Biochemistry*. 2008;47(30):7857-7862. doi:10.1021/bi800773f
42. Vogel SS, Thaler C, Koushik S v. Fanciful FRET. *Sci STKE*. 2006;2006(331). doi:10.1126/stke.3312006re2
43. Adedeji AO, Marchand B, te Velthuis AJW, et al. Mechanism of Nucleic Acid Unwinding by SARS-CoV Helicase. *PLoS One*. 2012;7(5):e36521. doi:10.1371/journal.pone.0036521
44. Ha T. Single-molecule fluorescence resonance energy transfer. *Methods*. 2001;25(1):78-86. doi:10.1006/meth.2001.1217
45. Seybert A, Hegyi A, Siddell SG, Ziebuhr J. The human coronavirus 229E superfamily 1 helicase has RNA and DNA duplex-unwinding activities with 5′-to-3′ polarity. *RNA*. 2000;6(7):1056-1068. doi:10.1017/s1355838200000728
46. Hwang H, Myong S. Protein induced fluorescence enhancement (PIFE) for probing protein–nucleic acid interactions. *Chem Soc Rev*. 2014;43(4):1221-1229. doi:10.1039/c3cs60201j
47. Stennett EMS, Ciuba MA, Lin S, Levitus M. Demystifying PIFE: The Photophysics behind the Protein-Induced Fluorescence Enhancement Phenomenon in Cy3. *J Phys Chem Lett*. 2015;6(10):1819-1823. doi:10.1021/acs.jpclett.5b00613
48. Hwang H, Kim H, Myong S. Protein induced fluorescence enhancement as a single molecule assay with short distance sensitivity. *Proc Natl Acad Sci U S A*. 2011;108(18):7414-7418. doi:10.1073/pnas.1017672108
49. Lerner E, Ploetz E, Hohlbein J, Cordes T, Weiss S. A Quantitative Theoretical Framework for Protein-Induced Fluorescence Enhancement-Förster-Type Resonance Energy Transfer (PIFE-FRET). *J Phys Chem B*. 2016;120(26):6401-6410. doi:10.1021/acs.jpcb.6b03692
50. Toseland CP. Fluorescent labeling and modification of proteins. *J Chem Biol*. 2013;6(3):85. doi:10.1007/s12154-013-0094-5
51. Chudakov DM, Lukyanov S, Lukyanov KA. Fluorescent proteins as a toolkit for in vivo imaging. *Trends Biotechnol*. 2005;23(12):605-613. doi:10.1016/j.tibtech.2005.10.005

52. Chin JW, Santoro SW, Martin AB, King DS, Wang L, Schultz PG. Addition of p-azido-L-phenylalanine to the genetic code of Escherichia coli. *J Am Chem Soc*. 2002;124(31):9026-9027. doi:10.1021/ja027007w

53. Roy R, Hohng S, Ha T. A practical guide to single-molecule FRET. *Nat Methods*. 2008;5(6):507-516. doi:10.1038/nmeth.1208

Chapter 3

Investigations into the Role of the SARS-CoV-2 Nsp13 Helicase in Modulating Cellular Host Processes

3.1 Abstract

SARS-CoV-2 has caused millions of deaths worldwide and has been the subject of considerable global research efforts in recent years. Despite the successful development of vaccines and antiviral therapeutics against this virus, its tendency to mutate rapidly has emphasized the need for continued research to better understand this virus' mechanism of pathogenesis and interactions with host signalling pathways. In this study, we sought to explore how the SARS-CoV-2 Nsp13 helicase, a highly conserved coronavirus protein that is essential for viral replication, influences host biological and cellular processes. Global transcriptomic analyses of Nsp13-transfected A549 cells identified changes in pathways involved in post-transcriptional gene silencing and translational repression by RNA, such as miRNA. Upon further bioinformatic analyses, we identified miR-146a-mediated signalling pathways to be of interest as this miRNA has been previously linked to the regulation of host inflammation and innate immune responses, similar to Nsp13. We found that miR-146a was induced in Nsp13-transfected cells and observed a corresponding decrease in the gene expression of two miR-146a targets, TRAF6 and IRAK1, which are important upstream regulators of NF-kB activation and IFN signalling. From these results, we propose that a more in-depth evaluation of potential Nsp13-induced miR-146a signalling cascades, namely NF-kB activation and SMAD4 signalling, may provide valuable insight for the development of novel therapeutics against COVID-19.

3.2 Introduction

Despite the successful development of COVID-19 vaccines, the continued emergence of more infectious SARS-CoV-2 variants has left individuals susceptible to re-infection. As a result, there is a need for more effective broad coronavirus antivirals and inhibitors to combat serious disease[1]. Many viral proteins are considered potential therapeutic targets; however, the Nsps encoded by the SARS-CoV-2 genome are of particular interest as they are generally highly conserved among coronaviruses and have been shown to interact with host processes and pathways[2]. Oftentimes, these viral Nsps can antagonize host interferon production and signalling cascades to allow the virus to evade host immune responses, which leads to more serious disease [3–5].

To develop more effective therapeutic approaches against COVID-19, a good understanding of the molecular mechanisms behind SARS-CoV-2 pathogenesis and host-virus interactions is required. Previous proteomic studies have characterized the direct interactions between SARS-CoV-2 viral proteins and host proteins by affinity purification coupled with mass spectrometry to identify druggable host protein targets[2,6,7]. Proximity-dependent biotin labelling (BioID) coupled with mass spectrometry methods have also been implemented to further expand our knowledge of host-virus interactions and reveal potential pathogenic strategies of the virus[8–12]. While both these interaction mapping methods are useful for identifying biologically meaningful interactions[13], there is oftentimes little overlap between these results[8,14]. As well, their reliance on direct or nearby protein interactions may limit the ability to capture downstream targets influenced by these Nsps. To assemble a complete picture of how these Nsps modify and influence host signalling pathways and environments, a more global, genome-wide approach is needed.

The SARS-CoV-2 Nsp13 helicase is one of the most highly conserved proteins among coronaviruses and has been reported to antagonize host innate immune responses[3,5,15,16]. It is a viral protein that can be both nuclear and cytoplasmic meaning that Nsp13 can interact with both nucleic acids and host proteins to modulate host responses to infection[17]. As a result of its important implications in infection, Nsp13 is often considered a promising therapeutic target[16,18–20]. Previous studies have identified that Nsp13 interacts with TBK1 to disrupt IRF3 phosphorylation, as well as suppress STAT1 and STAT2 phosphorylation to impede IFN production[21–24]. However, aside from its role in immune responses, other interactions between Nsp13 and host cellular processes are not well known.

In this study, we use genome-wide transcriptomic profiling techniques to investigate the role of Nsp13 in modifying host cellular processes. Polyinosinic: polycytidylic acid (poly(I:C)), a commonly used synthetic dsRNA analog, was used as an immunostimulant to study inflammatory and immune responses to infection[25]. We uncovered that, in addition to influencing immune responses, Nsp13 may also modulate host miRNA expression and signalling pathways. As Nsp13 is an RNA-binding protein that is essential for unwinding the viral genome during replication, we hypothesized that Nsp13 may influence host immune responses and other pathways through the regulation of miRNA expression. In particular, we explore how in A549 cells, Nsp13 overexpression led to an increase in miR-146a, a known inflammatory regulator[26–29]. We investigated how this miRNA may impact inflammation and other immune responses through the repression of key miR-146a targets such as TRAF6, IRAK1, and SMAD4. Collectively, we propose that further investigation into the relationship between Nsp13 and miRNA regulation may present an alternative strategy for developing better pan-coronavirus therapeutics.

3.3 Results

3.3.1 Identifying Host Biological and Cellular Processes Modified by Nsp13

To gain insight into the global effects of Nsp13 on host biological and cellular processes, we performed microarray gene expression analyses to assess for changes in the transcriptomic profiles of Nsp13-transfected A549 lung adenocarcinoma cells. These experiments were conducted both with naive non-treated cells and cells treated with poly (I:C) to simulate immune responses to viral infection. After confirming the overexpression of Nsp13 in A549 cells (**Figure 3.1 A**), microarray analysis was performed. Profiling results revealed over 1400 differentially-expressed genes ($\leq$ -1.5 or $\geq$ 1.5 fold change between the mock- and Nsp13-transfected sample) in each of the two conditions, with 181 genes in common (**Figure 3.1 B)** (microarray results will be deposited online). To identify pathways that may be modulated by Nsp13, we performed candidate gene prioritization or gene ontology enrichment analyses of these differentially-expressed genes. From this, we found that pathways involved in post-transcriptional gene silencing and translational repression by RNA, namely miRNA, were affected by Nsp13 overexpression, both with and without poly (I:C) stimulation (**Table 3.1**). Additionally, the detection of stimuli involved in sensory perception (e.g., olfactory) along with immunity (innate and adaptive) and other host defense response pathways were also altered with Nsp13 overexpression (**Table 3.1**). When the cells were treated with poly (I:C), antigen and receptor binding, phagocytosis (recognition and engulfment), and membrane invagination processes were found to be down-regulated with Nsp13 overexpression (**Table 3.1**). A complete list of the molecular functions and biological processes

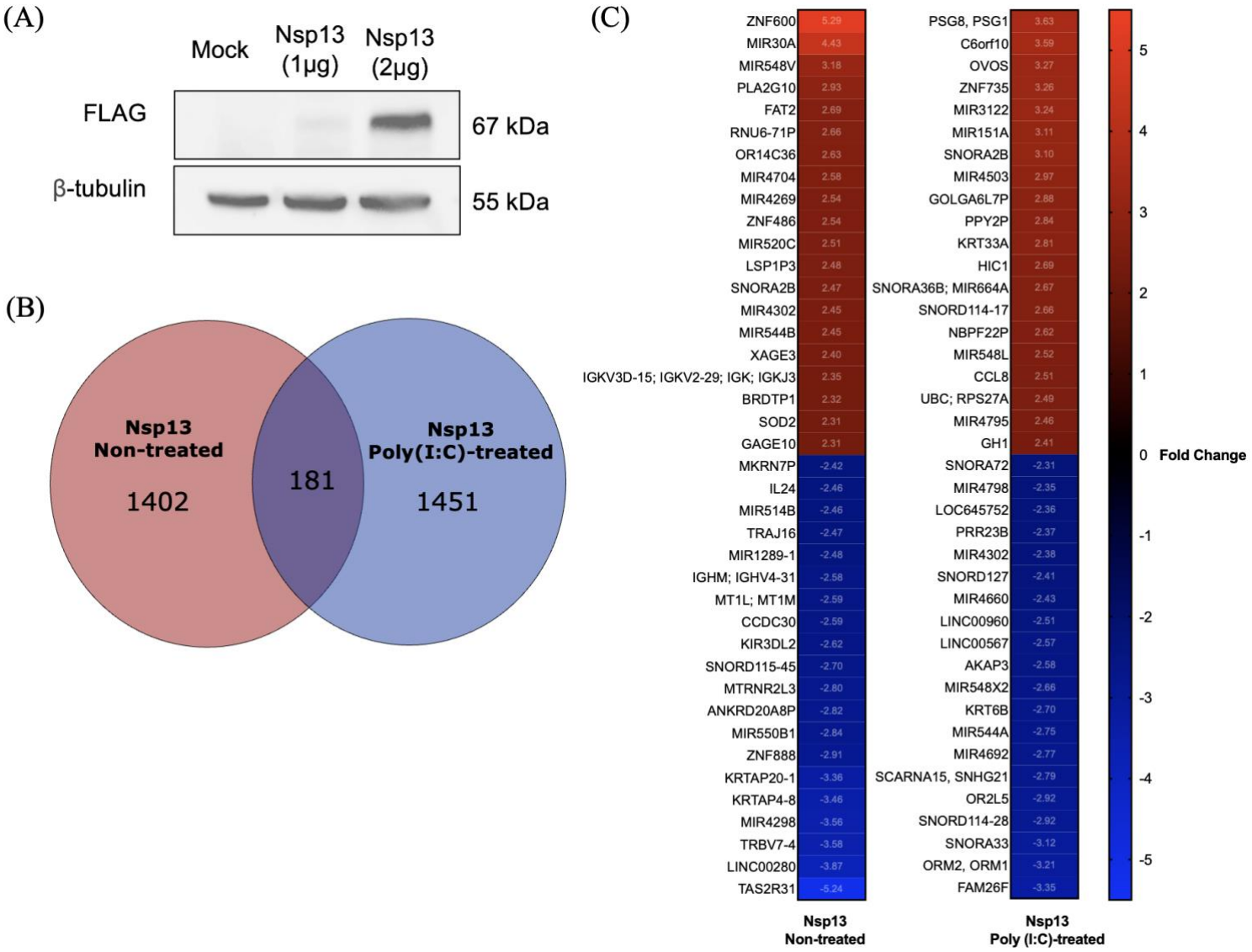

Figure 3.1 Nsp13 Overexpression Modulates Cellular Processes in A549 Cells.

(A) A549 cells were transfected with either a mock or Nsp13 plasmid and protein expression was confirmed by western blot analysis. (B) Microarray analysis identified differentially-expressed genes (≤ -1.5 or ≥ 1.5 fold change) between mock- and Nsp13-transfected A549 cells in two conditions: with and without poly (I:C) treatment. The number of gene hits is presented in a Venn Diagram. (C) Heat map showing the top 20 up- and down-regulated microarray hits from each experimental condition.

modified by Nsp13 expression can be found in **Supplemental Tables 3.1 and 3.2**. When looking at the highest fold change hits in each condition, numerous miRNAs were identified to be highly dysregulated (**Figure 3.1 C**), further confirming this trend in altered miRNA expression and signalling pathways. From these results, we hypothesized that a novel mechanism by which Nsp13 alters host pathways and processes may be through the modulation of miRNA expression and signalling.

Table 3.1 Gene Ontology Analysis of Nsp13 Overexpression in A549 Cells.

Gene ontology (GO) analysis of the differentially-expressed genes (≤ -1.5 or ≥ 1.5 fold change) was performed using ToppGene[30] to show the molecular functions and biological processes that were up- or down-regulated with Nsp13 overexpression. A summary of the altered GO molecular functions and biological processes are presented here and the full results can be found in **Supplemental Tables 3.1 and 3.2**.

Sample	Regulation	Altered GO: Molecular Function and Biological Process
Nsp13 (Non-treated)	↑	• N/A
	↓	• Post-transcriptional gene silencing and translational repression by RNA (e.g., miRNA) • Detection of stimulus in sensory perception and receptor activity • Adaptive immune response
Nsp13 (Poly (I:C) treated)	↑	• Post-transcriptional gene silencing and translational repression by RNA (e.g., miRNA) • Detection of stimulus in sensory perception and receptor activity
	↓	• Immunity and other host defense responses (innate and adaptive) • Antigen and receptor binding • Phagocytosis, recognition and engulfment • Membrane invagination

3.3.2 Investigating Nsp13's Potential Role in Modulating miRNA Expression and Signalling

To address our hypothesis that host pathways and processes altered by Nsp13 may be mediated through the action of miRNAs, we first needed to identify specific miRNA signalling pathways that may be potentially modulated by Nsp13 overexpression. To do this, we first identified all the differentially-expressed miRNAs in our microarray ($\leq$ -1.5 or $\geq$ 1.5 fold change). Next, we generated a list of their predicted targets using online software (TargetScan[31] and microRNA.org[32]). We then assessed for any overlap between this list of predicted targets and all the differentially-expressed genes found in our microarray (**Figure 3.2**). Since miRNA binding leads to repression of its target gene, we further filtered our results for negatively-correlated miRNA-gene pairs (e.g., increased miRNA expression and decreased expression of its predicted target genes) using miRTarVis[33]. Ultimately, we identified 27 and 26 miRNAs in the non-treated and poly (I:C) treated samples, respectively, to have corresponding negatively-correlated predicted gene targets in our dataset (**Table 3.2 and Supplemental Tables 3.3 and 3.4**). Through extensive review of the literature, we noticed that several of these miRNAs (e.g., miR-21, miR-196a, let-7 family) have been previously implicated in viral infection[26,34,35]. This includes miR-146a whose expression has been reported to be upregulated during many viral infections to modulate inflammatory and innate immune responses[36–39]. As Nsp13 has also been suggested to modulate several effector proteins in innate immune signalling pathways[21–23], we wanted to further evaluate if Nsp13 could be influencing these inflammatory and immune responses through miR-146a-mediated signalling.

Table 3.2 **Summary of Potentially Altered miRNA Signalling Pathways with Nsp13 Overexpression.**

Sample	Correlation	miRNA
Nsp13 (Non-treated)	Up miRNA-Down Gene	miR-23a, miR-23b, miR-30a, miR-133b, miR-141, miR-191, miR-200c, miR-378i, miR-494, miR-4295, miR-4500
	Down miRNA-Up Gene	let-7f-2, miR-21, miR-23c, miR-30d, miR-33b, miR-130a, miR-135b, miR-152, miR-196a-1, miR-320d-1, miR-370, miR-376a-2, miR-381, miR-495, miR-3529, miR-4306
Nsp13 (Poly (I:C) treated)	Up miRNA-Down Gene	let-7a-1, miR-7-2, miR-16-2, miR-29c, miR-34a, miR-141, miR-146a, miR-196a-1, miR-197, miR-300, miR-329-1, miR-429, miR-448, miR-495, miR-758
	Down miRNA-Up Gene	miR-23c, miR-30c-1, miR-31, miR-96, miR-181b-1, miR-194-2hg, miR-200a, miR-329-2, miR-374a, miR-874, miR-4500

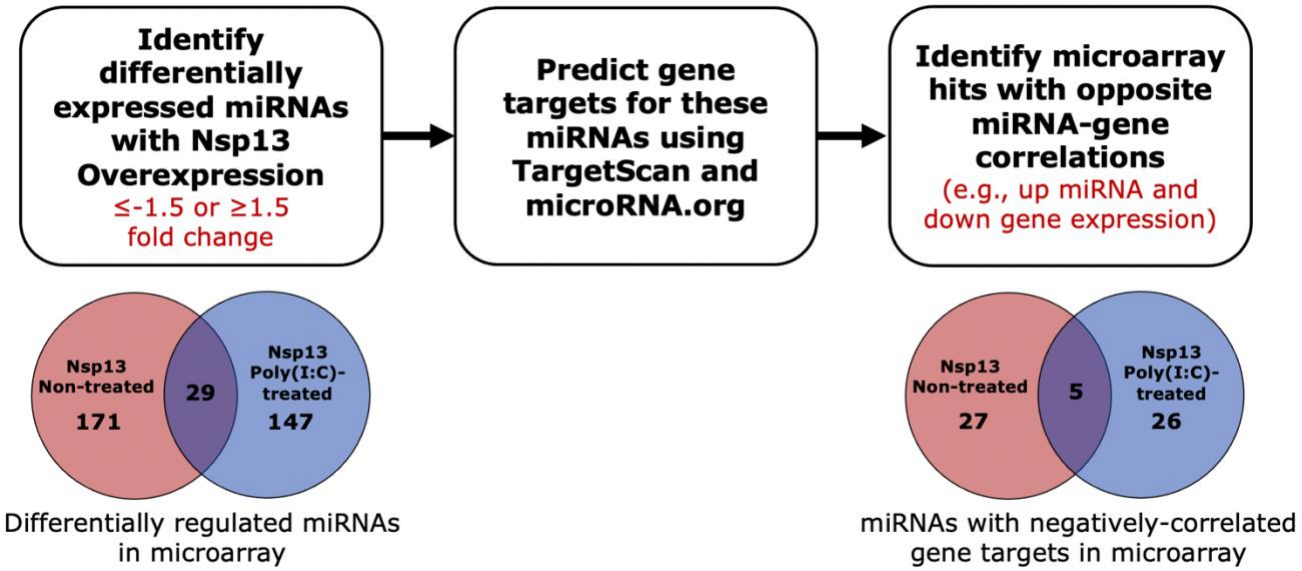

Figure 3.2 Identification of Potentially Altered miRNA Signalling Pathways with Nsp13 Overexpression.

From the microarray results, 171 and 147 differentially-expressed miRNAs (≤ -1.5 or ≥ 1.5 fold change) were identified in the non-treated and poly (I:C) treated samples, respectively. Next, online software (TargetScan and microRNA.org) was used to predict targets for these miRNAs before we assessed the overlap between this list of predicted targets and all the differentially-expressed genes found in our microarray. The results were further filtered to identify negatively-correlated miRNA-gene hits (e.g., up-regulated miRNA expression and down-regulated expression of its corresponding predicted target genes).

3.3.3 Nsp13-induced miR-146a Potentially Regulates Host Inflammatory and Immune Responses

To investigate the relationship between Nsp13 and miR-146a, we first evaluated the levels of miR-146a expression in our cells. We observed that both with and without poly (I:C) treatment, there was an approximately 3-fold increase in miR-146a levels when Nsp13 is overexpressed (**Figure 3.3 A**). Next, given that miR-146a is a known inflammatory regulator, we sought to investigate how miR-146a targets involved in host innate immune responses were influenced by Nsp13 overexpression. Using RT-qPCR, we assessed the mRNA expression of two miR-146a targets, TRAF6 and IRAK1. TRAF6 was observed to be down-regulated in both non-treated and poly (I:C) treated A549 cells while IRAK1 expression was only found to be down-regulated in poly (I:C) treated cells (**Figure 3.3 B**). The downstream effects on NF-κB activation by TRAF6 and IRAK1 were then assessed by western blot where a decrease in the level of phosphorylated NF-κB was observed in Nsp13-transfected cells. No significant changes in NF-κB protein level was observed with Nsp13 overexpression (**Figure 3.3 C and Supplemental Figure 3.1**). We also explored other potential host pathways mediated by miR-146a and found that SMAD4 gene expression was down-regulated in Nsp13 overexpressed cells (**Figure 3.4**).

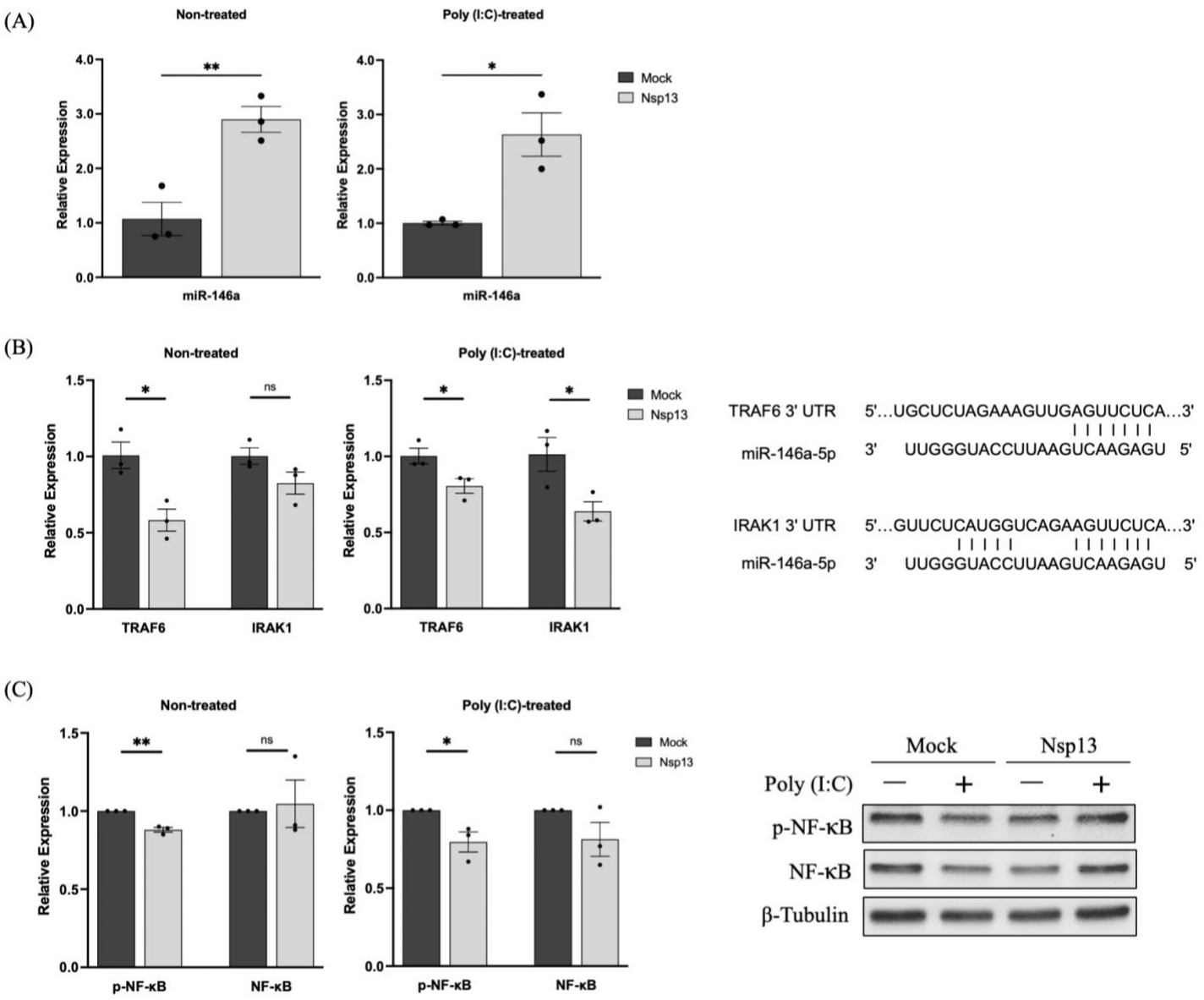

Figure 3.3 Nsp13 may Regulate NF-κB Activation through miR-146a-mediated Signalling.

(A) A549 cells were transfected with either a mock or Nsp13 plasmid under two conditions, with and without poly (I:C) treatment for 24 hours. Forty-eight hours post-transfection, cells were lysed and the level of miR-146a was evaluated by TaqMan miRNA assay. (B) RT-qPCR analysis of these Nsp13 overexpressed samples showed a decrease in relative TRAF6 and IRAK1 gene expression. On the right, the sequence complementary between the 3′ UTR of TRAF6 and IRAK1 with the miR-146a seed site (nt 2-7) are shown. (C) A representative western blot and densitometric analysis of the level of phosphorylated NF-κB and NF-κB is shown. β-tubulin was used as a loading control. Data is presented as mean ± SEM of three independent biological replicates. *P < 0.05, **P < 0.01.

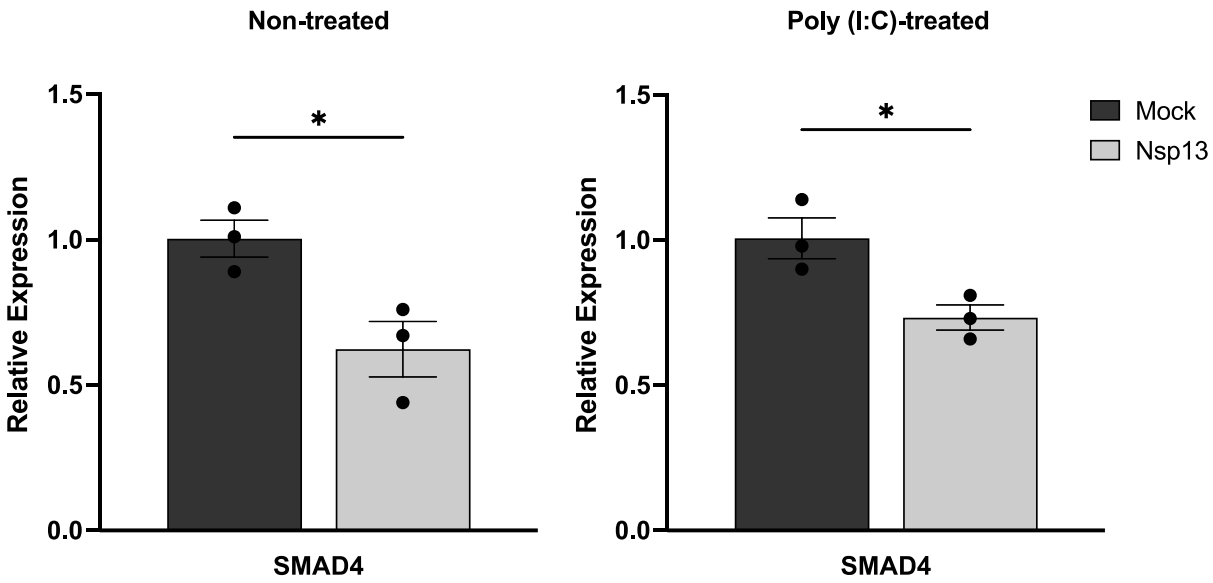

Figure 3.4 Nsp13 may Modulate SMAD4-related Signalling Pathways.

A549 cells were transfected with either a mock or Nsp13 plasmid under two conditions, with and without poly (I:C) treatment for 24 hours. Forty-eight hours post-transfection, cells were lysed and RT-qPCR analysis showed a decrease in relative SMAD4 gene expression with Nsp13 overexpression. Data is presented as mean ± SEM of three independent biological replicates. *P < 0.05, **P < 0.01.

3.4 Discussion

As we surpass the third year since the emergence of SARS-CoV-2, immense global efforts have generated a wealth of knowledge on the molecular mechanisms behind SARS-CoV-2 infection and pathogenesis[40]. Despite this, the rapid emergence of more infectious variants continues to pose a significant global threat, highlighting the need for continued research on this virus for the development of better pan-coronavirus therapeutics[1]. Notably, Nsp13 is often considered a promising pan-coronavirus therapeutic target[16,19,20,41,42]. In this study, we sought to investigate the interactions between the SARS-CoV-2 Nsp13 helicase and host cellular processes and pathways. Previous reports have found that Nsp13 plays a role in regulating innate immune responses[21–23], but beyond this, the role of Nsp13 in other host processes is not well-known. As such, we reasoned that further exploration of Nsp13's influence on host pathways and processes may provide insight into novel mechanisms that can be exploited in the development of drugs and antivirals against this virus.

To begin investigating the global effect of Nsp13 on host biological and cellular processes, we conducted microarray gene expression analyses of A549 lung cells transfected with Nsp13 (**Figure 3.1 B**). We examined the transcriptomic profiles of these cells with and without the treatment of poly (I:C) to assess for changes in host processes when immune responses are stimulated. From gene ontology analyses of these transcriptomic profiles, we detected a down-regulation of innate and adaptive immune responses with Nsp13 overexpression, something that has been previously reported[21–23], as well as alterations to post-transcriptional gene silencing and translational repression pathways by RNA, namely miRNAs (**Table 3.1 and Supplemental Tables 3.1 and 3.2**). While direct interactions between miRNAs and Nsp13 have not been

previously explored, it has been suggested that the SARS-CoV Nsp13 can interact directly with DDX5, a host helicase involved in RNA metabolism including miRNA biogenesis[43–45], to enhance viral genome transcription and proliferation[46,47]. Despite needing further experimental validation to determine the mechanism of this interaction, we began to consider if the SARS-CoV-2 Nsp13 may be influencing miRNA biogenesis through interactions with this host helicase during infection. Alternatively, with Nsp13 being a helicase that can unwind dsRNA, it is also plausible that Nsp13 may be post-transcriptionally regulating miRNA processing. Recently, several factors have been identified to regulate miRNA processing post-transcriptionally including adenosine deaminase acting on RNA (ADAR)[35]. It was found that the expression of ADAR is upregulated during inflammation leading to the regulation of primary miRNA (pri-miRNA) processing through mutations to the miRNA stem sequence[48]. Therefore, in the same vein, we hypothesized that Nsp13 may selectively unwind various dsRNA structures in both pri-miRNA and pre-miRNA resulting in alterations to mature miRNA production and targeted signalling. To the best of our knowledge, the specific regulation of miRNA transcription and processing by Nsp13 has not yet been studied; however, we propose this to be a fascinating area for future research as its implications could be important for understanding SARS-CoV-2 infection.

While the mechanistic characterization of how Nsp13 influences miRNA expression is beyond the scope of this work, we did elect to investigate how Nsp13 may modulate miRNA signalling pathways to alter cellular host processes. To address this hypothesis, we first needed to identify miRNA signalling pathways that may be altered by Nsp13 expression and could be of interest for future investigations. To start, we generated a list of predicted gene targets for all the differentially-expressed miRNAs and then assessed the overlap between these predicted targets

and the genes identified in the microarray. As miRNA binding is typically associated with repression of the target gene[49,50], we further filtered our results to isolate negatively-correlated miRNA-gene hits (**Figure 3.2 and Supplemental Tables 3.3 and 3.4**). This approach, however, is not without its limitations as firstly, some miRNAs, like those that bind the 5' UTR, can lead to the activation and translation of its mRNA target[51–53]. In looking solely at negatively-correlated miRNA-gene associations, we may miss these miRNA-mediated pathways. Additionally, the complexity of miRNA regulation and signalling makes identifying specific miRNA-mediated effects difficult. For instance, miRNAs can have one or several direct targets, but they can also have even more indirect and downstream effects that may not be captured in our analysis looking at direct miRNA-gene targeting[50]. Moreover, a single mRNA may be targeted by multiple different miRNAs making it hard to identify which miRNA is regulating each gene using microarray analysis alone[54]. Collectively, these microarray analyses provide valuable insight into global cellular changes and patterns; however, more poignant experimental investigations still need to be conducted to identify specific relationships.

From our miRNA-gene analyses (**Table 3.2**), we identified miR-146a to be of interest as this miRNA has been previously implicated in viral infections and is involved in the regulation of innate immune responses[26–29,35,55]. Since Nsp13 is also a well-known modulator of host innate immune responses[21–23], we thought it would be interesting to explore if Nsp13 may be mediating these inflammatory responses through miR-146a regulation and targeting. In our study, we showed an upregulation of miR-146a expression in A549 cells when Nsp13 is overexpressed (**Figure 3.3 A**), corroborating the known induction of this miRNA in response to cytokines (e.g., TNF-α and IL-1β), bacterial components (e.g., lipopolysaccharide; LPS), and viral infections[27,36,56–58]. The

fact that the relative induction of miR-146a in non-treated and poly (I:C) treated cells were similar may reflect how activation of TLR3, an intracellular receptor localized on the endosome that detects dsRNA, such as poly (I:C)), often has little effect on miR-146a expression[27,59]. Instead, miR-146a is often considered an endotoxin-responsive gene whose induction is triggered by cell surface receptors such as TLR4 and TLR5[60–62]. This may suggest that Nsp13, without viral infection, may be enough to induce miR-146a expression, but the mechanism by which this occurs still needs to be further explored. Altogether, these results demonstrate that Nsp13 in host cells can induce miR-146a expression; however, the subsequent signalling and targeting of miR-146a still needs to be further investigated.

As miR-146a is known to modulate host inflammatory and innate immune responses in response to viral infection[29,37,39,63,64], we sought to explore how these pathways may be influenced by Nsp13. Previous reports have established that miR-146a directly targets and represses TRAF6 and IRAK1, two key adaptor proteins involved in inflammatory-related TLR and NF-κB signalling, resulting in the inhibition of NF-κB activation[27,36,57,65–67]. This is particularly interesting as NF-κB plays an essential role in many aspects of innate and adaptive immune signalling[68,69]. Through RT-qPCR, we observed a downregulation of TRAF6 and IRAK1 expression in Nsp13-transfected cells (**Figure 3.3 B**). Despite demonstrating that miR-146a is induced in these A549 cells, these results do not definitively show whether this decrease is mediated by direct miR-146a binding or by other unknown Nsp13-mediated effects. Therefore, performing additional experiments whereby cellular miR-146a levels are inhibited or using miR-146a mimics may help to elucidate this mechanism of action and delineate Nsp13 protein-mediated effects against miR-146a-mediated effects. Moreover, western blot analysis will also need to be done to assess and

validate if we see a corresponding decrease in the protein expression levels of these targets. Next, we wanted to explore if this potential miR-146a-mediated repression of TRAF6 and IRAK1 resulted in the known downstream inhibition of NF-κB activation and inflammatory responses. From preliminary western blot results, we observed a slight decrease in the level of phosphorylated NF-κB with no significant changes in overall NF-κB levels between the mock and Nsp13-transfected samples (**Figure 3.3 C**); however, additional experiments are still needed to evaluate if this corresponds to a decrease in NF-κB nuclear localization and activation. Another potential approach to assessing changes to NF-κB activation could involve the assessment of proinflammatory cytokine and chemokine expression. With less phosphorylation of NF-κB, a decrease in the transcription of key proinflammatory genes such as IL-1, IL-6 and TNF-α would be expected[65,69,70]. In addition to repressing upstream signalling molecules of NF-κB activation, miR146a has also been shown to be transcriptionally induced by NF-κB in response to activation of innate immune responses[27]. This suggests that Nsp13 may be acting pro-virally to modulate this miR-146a negative feedback loop, consequently enhancing the observed effect in the cell[71]. Collectively, these results start to suggest a mechanism of action by which Nsp13 may induce the expression of miR-146a to repress TRAF6 and IRAK1 expression in order to impede NF-κB activation and consequently, the production of proinflammatory cytokines and type I IFNs to facilitate viral infection.

Moreover, from our microarray results, we noticed that several type I IFNs (e.g., IFNA4, IFNA13, IFNA16) were downregulated in Nsp13-transfected A549 cells treated with poly (I:C) (data not shown; microarray results will be deposited online). While additional experiments will need to be conducted to verify these observations, this parallels previous studies in which

enterovirus 71 (EV71) and vesicular stomatitis virus (VSV)-induced miR-146a expression was found to be pro-viral by suppressing type I IFN production[36,72]. Coupling this with the fact that miR-146a dysregulation is involved with several human diseases[73–76], we believe that a more complete understanding of this miRNA signalling pathway during SARS-CoV-2 infection could aid in the development of novel therapeutic interventions.

In addition to the potential effects on innate immune responses, miR-146a has also been reported to mediate other cellular processes including cell differentiation and adaptive immune responses[29,55,77–79]. Since adaptive immune responses were found to be downregulated in the Nsp13-transfected cells (**Table 3.1**), further investigations on how miR-146a could modulate these pathways may be warranted. Another interesting miR-146a target is SMAD4, a member of the SMAD family, which is important in the TGF-β signalling pathway[80–82]. For both non-treated and poly (I:C) treated samples, a decrease in SMAD4 gene expression was observed with Nsp13-overexpression (**Figure 3.4**). SMAD4 is an important co-mediator SMAD that complexes with various receptor-activated SMADs to regulate the transcription of many types of cell signals[83] and is frequently mutated in cancer[84–87]. While additional experiments will need to be carried out, such as assessing SMAD4 protein expression levels, this dysregulation of SMAD4 could allude to alterations in proliferation, cell differentiation, and fibrosis pathways[82]. Previous reports have demonstrated that the SARS-CoV N protein associates with SMAD3 to interfere with SMAD3/SMAD4 complex formation and consequently modulates TGF-β signalling, blocks apoptosis, and promotes tissue fibrosis[88]. Therefore, the idea that Nsp13 directly, or through its induction of miR-146a expression, may contribute to COVID-19-related fibrosis and other associated pathology is yet another interesting avenue to investigate.

3.5 Conclusions

In summary, the SARS-CoV-2 Nsp13 was identified to potentially modulate miRNA expression and signalling pathways to regulate inflammatory and immune responses, a mechanism of action that has not been previously proposed. In particular, it was identified that Nsp13 induces miR-146a expression in A549 cells leading to the repression of its direct targets TRAF6 and IRAK1, which are involved in NF-κB activation and IFN production. We propose that further investigation into these miR-146a-mediated signalling pathways may present novel avenues for antiviral therapeutic development; however, acknowledge that future work with infectious models and *in vivo* studies is still required.

3.6 Methods

3.6.1 Cell Culture and Transfection

Adherent A549 lung adenocarcinoma epithelial cancer cells (CCL-185) were purchased from ATCC. The SARS-CoV-2 mammalian expression vector pTwist-CMV-Nsp13-3xFlag (pGBW-m4133197; plasmid #152383) was purchased from Addgene. The empty pTwist-CMV control vector was generated by restriction digest of the coding sequence of the pTwist-CMV-Nsp2-3xFlag (pGBW-m4134143; plasmid #152022) expression vector followed by subsequent re-ligation. The plasmid was verified by sequencing at Genome Quebec (Montreal, QC). Low-molecular-weight (LMW) poly (I:C) complexed with LyoVec was purchased from Invivogen.

A549 cells were cultured in Dulbecco's Modification Eagle's Medium (DMEM; Wisent Inc.) supplemented with 10% fetal bovine serum (FBS; Wisent Inc.) and maintained at 37ºC and 5% CO_2. For western blot and RT-qPCR analysis, plasmid DNA was transfected into A549 cells using Lipofectamine 2000 (Life Technologies, Carlsbad, CA) according to the manufacturer's protocol. Briefly, 750,000 cells per well were reversed-transfected into six-well plates with either 2 µg of pTwist-CMV control vector or Nsp13 plasmid DNA. After 24 hours, cells were treated with 500 ng/mL poly (I:C) and lysed 48 hours post-transfection for downstream analysis. Cells were lysed with 1X sodium dodecyl sulfate (SDS) lysis buffer (50 mM Tris−HCl (pH 6.8), 2% SDS, and 10% glycerol) for western blot analysis and RLT Plus lysis buffer (RNeasy Plus kit, Qiagen, Mississauga, ON) for RT-qPCR analysis.

3.6.2 Microarray Analysis

A549 cells were cultured and transfected as previously described under "Cell Culture and Transfection". Forty-eight hours post-transfection, RNA isolation from pTwist-CMV mock- and Nsp13-transfected samples, both with and without poly (I:C) treatment, was performed using the RNeasy RNA isolation kit (Qiagen, Mississauga, ON) according to the manufacturer's protocol. Microarray gene profiling was performed using the Affymetrix Human Gene ST.2.0 array by The Centre for Applied Genomics (TCAG) (The Hospital for Sick Children, Toronto, ON). The results were analyzed and normalized using the Affymetrix Expression Console (Thermo Fisher Scientific) and the Transcriptome Analysis Console (v4.0) (Thermo Fisher Scientific). Pathway enrichment and gene ontology analysis were conducted using ToppGene Suite[30]. Bonferroni correction was utilized to adjust P-values with $P < 0.05$ deemed significant.

3.6.3 TaqMan and Quantitative Real-Time PCR

Relative miR-146a levels were quantified using TaqMan miRNA Assay (Thermo Fisher Scientific; Assay ID: 000468). miRNA cDNA was synthesized using the TaqMan MicroRNA Reverse Transcription Kit (Thermo Fisher Scientific), according to the manufacturer's protocol, with 10 ng of total RNA. RT-qPCR was performed with 1X TaqMan Universal PCR Master Mix No AmpErase UNG (Thermo Fisher Scientific), 1X TaqMan Small RNA Assay for miR-146a (Thermo Fisher Scientific; Assay ID: 000468) and RNU6B (Thermo Fisher Scientific; Assay ID: 001093) in a reaction volume of 20 µL. The reactions were run on a CFX Connect Real-Time PCR Detection System (Bio-Rad) and analyzed using the $2^{-\Delta\Delta Ct}$ method[89]. miRNA expression levels were reported relative to pTwist-CMV mock control with RNU6B levels being used for normalization.

For RT-qPCR analyses, total RNA isolation was performed using RNeasy Plus Kits (Qiagen, Mississauga, ON) according to the manufacturer's protocol. The isolated RNA was quantified on a NanoDrop 2000 (Thermo Scientific) and reverse transcribed (250 ng) using the iScript Reverse Transcription Supermix (Bio-Rad) according to the manufacturer's protocol. RT-qPCR was performed using the SSOAdvanced Universal SYBR Green Supermix (Bio-Rad), according to the manufacturer's protocol with a final concentration of 500 nM of each primer in a reaction volume of 20 µL. A list of the qPCR primers used in this study can be found in **Supplemental Table 3.5**. The reactions were run on a CFX Connect Real-Time PCR Detection System (Bio-Rad) and analyzed using the $2^{-\Delta\Delta Ct}$ method[89]. mRNA expression levels were reported relative to pTwist-CMV mock control with 18S rRNA levels being used for normalization.

3.6.4 Immunoblotting

Transfected A549 samples were lysed in 1X SDS lysis buffer with cOmplete™ Protease Inhibitor Cocktail (Roche, Cat. #11697498001) and sheared using a 21 G needle (BD Biosciences). The protein concentration of each sample was determined by DC assay (Bio-Rad) according to the manufacturer's protocol. SDS-PAGE was performed with 30 µg of protein loaded onto a 10% stain-free SDS-PAGE gel (Bio-Rad, Cat. #1610183). Protein bands were visualized on a ChemiDoc MP imager (Bio-Rad) before being transferred to a PVDF membrane by using a Trans-Blot turbo transfer system (Bio-Rad). Membranes were blocked with 3% BSA in TBS-Tween-20 (pH 7.4, 0.05%) and subsequently incubated with the appropriate primary antibody (**Supplemental Table 3.6**) overnight at 4ºC with agitation. Afterward, donkey anti-rabbit or goat anti-mouse secondary antibodies conjugated with horseradish peroxidase (1:20,000; Jackson ImmunoResearch Laboratories, Inc.) was added to the blot and incubated for an hour at room

temperature, with agitation, before blots were visualized with Clarity Western ECL Substrate solution (Bio-Rad) on a ChemiDoc MP imager (Bio-Rad). Image Lab (Bio-Rad) was used to perform densitometry analysis with β-tubulin levels used as the loading control.

3.6.5 Statistical Analysis

Data are presented as the mean with error bars representing the standard error of the mean. Statistical significance was assessed using a two-tailed, unpaired student's t-test where P-values less than 0.05 are deemed significant.

3.7 References

1. Hacisuleyman E, Hale C, Saito Y, et al. Vaccine Breakthrough Infections with SARS-CoV-2 Variants. *NEJM*. 2021;384(23):2212-2218. doi:10.1056/nejmoa2105000
2. Gordon DE, Jang GM, Bouhaddou M, et al. A SARS-CoV-2 protein interaction map reveals targets for drug repurposing. *Nature*. 2020;583(7816):459-468. doi:10.1038/s41586-020-2286-9
3. Low ZY, Zabidi NZ, Yip AJW, Puniyamurti A, Chow VTK, Lal SK. SARS-CoV-2 Non-Structural Proteins and Their Roles in Host Immune Evasion. *Viruses*. 2022;14(9):1991. doi:10.3390/v14091991
4. Min YQ, Huang M, Sun X, Deng F, Wang H, Ning YJ. Immune evasion of SARS-CoV-2 from interferon antiviral system. *Comput Struct Biotechnol J*. 2021;19:4217-4225. doi:10.1016/j.csbj.2021.07.023
5. Lei X, Dong X, Ma R, et al. Activation and evasion of type I interferon responses by SARS-CoV-2. *Nat Commun*. 2020;11(1). doi:10.1038/s41467-020-17665-9
6. Stukalov A, Girault V, Grass V, et al. Multilevel proteomics reveals host perturbations by SARS-CoV-2 and SARS-CoV. *Nature*. 2021;594(7862):246-252. doi:10.1038/s41586-021-03493-4
7. Davies JP, Almasy KM, McDonald EF, Plate L. Comparative Multiplexed Interactomics of SARS-CoV-2 and Homologous Coronavirus Nonstructural Proteins Identifies Unique and Shared Host-Cell Dependencies. *ACS Infect Dis*. 2020;6(12):3174-3189. doi:10.1021/acsinfecdis.0c00500
8. Zhang Y, Shang L, Zhang J, et al. An antibody-based proximity labeling map reveals mechanisms of SARS-CoV-2 inhibition of antiviral immunity. *Cell Chem Biol*. 2022;29(1):5-18.e6. doi:10.1016/j.chembiol.2021.10.008
9. St-Germain JR, Astori A, Samavarchi-Tehrani P, et al. A SARS-CoV-2 BioID-based virus-host membrane protein interactome and virus peptide compendium: new proteomics resources for COVID-19 research. *bioRxiv*. Published online August 28, 2020. doi:10.1101/2020.08.28.269175
10. Samavarchi-Tehrani P, Abdouni H, Knight JDR, et al. A SARS-CoV-2 – host proximity interactome. *bioRxiv*. Published online September 4, 2020. doi:10.1101/2020.09.03.282103
11. Laurent EMN, Sofianatos Y, Komarova A, et al. Global BioID-based SARS-CoV-2 proteins proximal interactome unveils novel ties between viral polypeptides and host factors involved in multiple COVID19-associated mechanisms. *bioRxiv*. Published online August 29, 2020. doi:10.1101/2020.08.28.272955
12. Liu X, Huuskonen S, Laitinen T, et al. SARS-CoV-2–host proteome interactions for antiviral drug discovery. *Mol Syst Biol*. 2021;17(11):e10396. doi:10.15252/msb.202110396
13. Liu X, Salokas K, Tamene F, et al. An AP-MS- and BioID-compatible MAC-tag enables comprehensive mapping of protein interactions and subcellular localizations. *Nat Commun*. 2018;9(1):1-16. doi:10.1038/s41467-018-03523-2

14. Terracciano R, Preianò M, Fregola A, Pelaia C, Montalcini T, Savino R. Mapping the SARS-CoV-2–Host Protein–Protein Interactome by Affinity Purification Mass Spectrometry and Proximity-Dependent Biotin Labeling: A Rational and Straightforward Route to Discover Host-Directed Anti-SARS-CoV-2 Therapeutics. *Int J Mol Sci*. 2021;22(2):1-38. doi:10.3390/ijms22020532
15. Beyer DK, Forero A. Mechanisms of Antiviral Immune Evasion of SARS-CoV-2. *J Mol Biol*. 2022;434(6):167265. doi:10.1016/j.jmb.2021.167265
16. White MA, Lin W, Cheng X. Discovery of COVID-19 Inhibitors Targeting the SARS-CoV-2 Nsp13 Helicase. *J Phys Chem Lett*. 2020;11(21):9144-9151. doi:10.1021/acs.jpclett.0c02421
17. Zhang J, Cruz-cosme R, Zhuang MW, et al. A systemic and molecular study of subcellular localization of SARS-CoV-2 proteins. *Signal Transduct Target Ther*. 2020;5(1):1-3. doi:10.1038/s41392-020-00372-8
18. Gurung AB. In silico structure modelling of SARS-CoV-2 Nsp13 helicase and Nsp14 and repurposing of FDA approved antiviral drugs as dual inhibitors. *Gene Rep*. 2020;21:100860. doi:10.1016/j.genrep.2020.100860
19. Zeng J, Weissmann F, Bertolin AP, et al. Identifying SARS-CoV-2 antiviral compounds by screening for small molecule inhibitors of nsp13 helicase. *Biochem J*. 2021;478(13):2405-2423. doi:10.1042/bcj20210201
20. Perez-Lemus GR, Menéndez CA, Alvarado W, Byléhn F, de Pablo JJ. Toward wide-spectrum antivirals against coronaviruses: Molecular characterization of SARS-CoV-2 NSP13 helicase inhibitors. *Sci Adv*. 2022;8(1):4526. doi:10.1126/aciadv.ABJ4526
21. Guo G, Gao M, Gao X, et al. SARS-CoV-2 non-structural protein 13 (nsp13) hijacks host deubiquitinase USP13 and counteracts host antiviral immune response. *Signal Transduct Target Ther*. 2021;6(1):1-3. doi:10.1038/s41392-021-00509-3
22. Yuen CK, Lam JY, Wong WM, et al. SARS-CoV-2 nsp13, nsp14, nsp15 and orf6 function as potent interferon antagonists. *Emerg Microbes Infect*. 2020;9(1):1418-1428. doi:10.1080/22221751.2020.1780953
23. Xia H, Cao Z, Xie X, et al. Evasion of Type I Interferon by SARS-CoV-2. *Cell Rep*. 2020;33(1):108234. doi:10.1016/j.celrep.2020.108234
24. Sui C, Xiao T, Zhang S, et al. SARS-CoV-2 NSP13 Inhibits Type I IFN Production by Degradation of TBK1 via p62-Dependent Selective Autophagy. *J Immunol*. 2022;208(3):753-761. doi:10.4049/jimmunol.2100684
25. Field AK, Tytell AA, Lampson GP, Hilleman MR. Inducers of interferon and host resistance. II. Multistranded synthetic polynucleotide complexes. *Proc Natl Acad Sci U S A*. 1967;58(3):1004-1010. doi:10.1073/PNAS.58.3.1004

26. Lindsay MA. microRNAs and the immune response. *Trends Immunol*. 2008;29(7):343-351. doi:10.1016/j.it.2008.04.004
27. Taganov KD, Boldin MP, Chang KJ, Baltimore D. NF-κB-dependent induction of microRNA miR-146, an inhibitor targeted to signaling proteins of innate immune responses. *Proc Natl Acad Sci U S A*. 2006;103(33):12481. doi:10.1073/pnas.0605298103
28. Perry MM, Moschos SA, Williams AE, Shepherd NJ, Larner-Svensson HM, Lindsay MA. Rapid changes in microRNA-146a expression negatively regulate the interleukin-1β induced inflammatory response in human lung alveolar epithelial cells. *J Immunol*. 2008;180(8):5689. doi:10.4049/jimmunol.180.8.5689
29. Labbaye C, Testa U. The emerging role of MIR-146A in the control of hematopoiesis, immune function and cancer. *J Hematol Oncol*. 2012;5(1):1-10. doi:10.1186/1756-8722-5-13
30. Chen J, Bardes EE, Aronow BJ, Jegga AG. ToppGene Suite for gene list enrichment analysis and candidate gene prioritization. *Nucleic Acids Res*. 2009;37:W305. doi:10.1093/nar/gkp427
31. McGeary SE, Lin KS, Shi CY, et al. The biochemical basis of microRNA targeting efficacy. *Science (1979)*. 2019;366(6472). doi:10.1126/science.aav1741
32. Betel D, Wilson M, Gabow A, Marks DS, Sander C. The microRNA.org resource: targets and expression. *Nucleic Acids Res*. 2008;36. doi:10.1093/nar/gkm995
33. Jung D, Kim B, Freishtat RJ, Giri M, Hoffman E, Seo J. MiRTarVis: An interactive visual analysis tool for microRNA-mRNA expression profile data. *BMC Proc*. 2015;9(6):1-16. doi:10.1186/1753-6561-9-s6-s2
34. Barbu MG, Condrat CE, Thompson DC, et al. MicroRNA Involvement in Signaling Pathways During Viral Infection. *Front Cell Dev Biol*. 2020;8:143. doi:10.3389/fcell.2020.00143
35. O'Connell RM, Rao DS, Chaudhuri AA, Baltimore D. Physiological and pathological roles for microRNAs in the immune system. *Nat Rev Immunol*. 2010;10(2):111-122. doi:10.1038/nri2708
36. Hou J, Wang P, Lin L, et al. MicroRNA-146a Feedback Inhibits RIG-I-Dependent Type I IFN Production in Macrophages by Targeting TRAF6, IRAK1, and IRAK2. *J Immunol*. 2009;183(3):2150-2158. doi:10.4049/jimmunol.0900707
37. Wu S, He L, Li Y, et al. MiR-146a facilitates replication of dengue virus by dampening interferon induction by targeting TRAF6. *J Infect*. 2013;67(4):329-341. doi:10.1016/j.jinf.2013.05.003
38. Nahand JS, Karimzadeh MR, Nezamnia M, et al. The role of miR-146a in viral infection. *IUBMB Life*. 2020;72(3):343-360. doi:10.1002/iub.2222
39. Zhang F, Sun X, Zhu Y, Qin W. Downregulation of miR-146a inhibits influenza A virus replication by enhancing the type I interferon response in vitro and in vivo. *Biomed Pharmacother*. 2019;111:740-750. doi:10.1016/j.biopha.2018.12.103

40. Lamers MM, Haagmans BL. SARS-CoV-2 pathogenesis. *Nat Rev Microbiol*. 2022;20(5):270-284. doi:10.1038/s41579-022-00713-0
41. Adedeji AO, Singh K, Calcaterra NE, et al. Severe Acute Respiratory Syndrome Coronavirus Replication Inhibitor That Interferes with the Nucleic Acid Unwinding of the Viral Helicase. *Antimicrob Agents Chemother*. 2012;56(9):4718. doi:10.1128/aac.00957-12
42. Gurung AB. In silico structure modelling of SARS-CoV-2 Nsp13 helicase and Nsp14 and repurposing of FDA approved antiviral drugs as dual inhibitors. *Gene Rep*. 2020;21:100860. doi:10.1016/j.genrep.2020.100860
43. Wilson BJ, Bates GJ, Nicol SM, Gregory DJ, Perkins ND, Fuller-Pace F v. The p68 and p72 DEAD box RNA helicases interact with HDAC1 and repress transcription in a promoter-specific manner. *BMC Mol Biol*. 2004;5(1):1-15. doi:10.1186/1471-2199-5-11
44. Dardenne E, PolayEspinoza M, Fattet L, et al. RNA Helicases DDX5 and DDX17 Dynamically Orchestrate Transcription, miRNA, and Splicing Programs in Cell Differentiation. *Cell Rep*. 2014;7(6):1900-1913. doi:10.1016/j.celrep.2014.05.010
45. Cheng W, Chen G, Jia H, He X, Jing Z. DDX5 RNA Helicases: Emerging Roles in Viral Infection. *Int J Mol Sci.* 2018;19(4):1122. doi:10.3390/ijms19041122
46. Chen JY, Chen WN, Poon KMV, et al. Interaction between SARS-CoV helicase and a multifunctional cellular protein (Ddx5) revealed by yeast and mammalian cell two-hybrid systems. *Arch Virol*. 2009;154(3):507-512. doi:10.1007/s00705-009-0323-y
47. Squeglia F, Romano M, Ruggiero A, Maga G, Berisio R. Host DDX Helicases as Possible SARS-CoV-2 Proviral Factors: A Structural Overview of Their Hijacking Through Multiple Viral Proteins. *Front Chem*. 2020;8:1150. doi:10.3389/fchem.2020.602162
48. Yang W, Chendrimada TP, Wang Q, et al. Modulation of microRNA processing and expression through RNA editing by ADAR deaminases. *Nat Struct Mol Biol*. 2005;13(1):13-21. doi:10.1038/nsmb1041
49. Iwakawa H oki, Tomari Y. Life of RISC: Formation, action, and degradation of RNA-induced silencing complex. *Mol Cell*. 2022;82(1):30-43. doi:10.1016/j.molcel.2021.11.026
50. Bartel DP. Metazoan MicroRNAs. *Cell*. 2018;173(1):20-51. doi:10.1016/j.cell.2018.03.006
51. O'Brien J, Hayder H, Zayed Y, Peng C. Overview of microRNA biogenesis, mechanisms of actions, and circulation. *Front Endocrinol (Lausanne)*. 2018;9(AUG):402. doi:10.3389/fendo.2018.00402
52. Garzon R, Marcucci G, Croce CM. Targeting MicroRNAs in Cancer: Rationale, Strategies and Challenges. *Nat Rev Drug Discov*. 2010;9(10):775. doi:10.1038/nrd3179
53. Henke JI, Goergen D, Zheng J, et al. microRNA-122 stimulates translation of hepatitis C virus RNA. *EMBO J*. 2008;27(24):3300-3310. doi:10.1038/emboj.2008.244

54. Peter ME. Targeting of mRNAs by multiple miRNAs: the next step. *Oncogene*. 2010;29(15):2161-2164. doi:10.1038/onc.2010.59
55. Rusca N, Monticelli S. MiR-146a in Immunity and Disease. *Mol Biol Int*. 2011;2011:1-7. doi:10.4061/2011/437301
56. Zhang F, Sun X, Zhu Y, Qin W. Downregulation of miR-146a inhibits influenza A virus replication by enhancing the type I interferon response in vitro and in vivo. *Biomed Pharmacother*. 2019;111:740-750. doi:10.1016/j.biopha.2018.12.103
57. Luly FR, Lévêque M, Licursi V, et al. MiR-146a is over-expressed and controls IL-6 production in cystic fibrosis macrophages. *Sci Rep*. 2019;9(1):1-10. doi:10.1038/s41598-019-52770-w
58. Cameron JE, Yin Q, Fewell C, et al. Epstein-Barr Virus Latent Membrane Protein 1 Induces Cellular MicroRNA miR-146a, a Modulator of Lymphocyte Signaling Pathways. *J Virol*. 2008;82(4):1946. doi:10.1128/jvi.02136-07
59. Fei Y, Chaulagain A, Wang T, et al. MiR-146a down-regulates inflammatory response by targeting TLR3 and TRAF6 in Coxsackievirus B infection. *RNA*. 2020;26(1):91-100. doi:10.1261/rna.071985.119/-/dc1
60. Akira S, Uematsu S, Takeuchi O. Pathogen Recognition and Innate Immunity. *Cell*. 2006;124(4):783-801. doi:10.1016/j.cell.2006.02.015
61. Iwasaki A, Medzhitov R. Toll-like receptor control of the adaptive immune responses. *Nat Immunol*. 2004;5(10):987-995. doi:10.1038/ni1112
62. Nahid MA, Pauley KM, Satoh M, Chan EKL. miR-146a Is Critical for Endotoxin-induced Tolerance. *J Biol Chem*. 2009;284(50):34590-34599. doi:10.1074/jbc.m109.056317
63. Selvamani SP, Mishra R, Singh SK. Chikungunya Virus Exploits miR-146a to Regulate NF-κB Pathway in Human Synovial Fibroblasts. *PLoS One*. 2014;9(8):e103624. doi:10.1371/journal.pone.0103624
64. Teng Y, Luo M, Yu T, et al. CRISPR/Cas9-mediated deletion of miR-146a enhances antiviral response in HIV-1 infected cells. *Genes Immun*. 2019;20(4):327-337. doi:10.1038/s41435-018-0036-x
65. Park H, Huang X, Lu C, Cairo MS, Zhou X. MicroRNA-146a and MicroRNA-146b Regulate Human Dendritic Cell Apoptosis and Cytokine Production by Targeting TRAF6 and IRAK1 Proteins. *J Biol Chem*. 2015;290(5):2831. doi:10.1074/jbc.m114.591420
66. Ma X, Becker Buscaglia LE, Barker JR, Li Y. MicroRNAs in NF-κB signaling. *J Mol Cell Biol*. 2011;3(3):159-166. doi:10.1093/jmcb/mjr007
67. Bhaumik D, Scott GK, Schokrpur S, Patil CK, Campisi J, Benz CC. Expression of microRNA-146 suppresses NF-κB activity with reduction of metastatic potential in breast cancer cells. *Oncogene*. 2008;27(42):5643-5647. doi:10.1038/onc.2008.171
68. Liu T, Zhang L, Joo D, Sun SC. NF-κB signaling in inflammation. *Signal Transduct Target Ther*. 2017;2:17023. doi:10.1038/sigtrans.2017.23

69. Hoesel B, Schmid JA. The complexity of NF-κB signaling in inflammation and cancer. *Molecular Cancer*. 2013;12(1):1-15. doi:10.1186/1476-4598-12-86
70. Tak PP, Firestein GS. NF-κB: a key role in inflammatory diseases. *J Clin Invest*. 2001;107(1):7-11. doi:10.1172/jcI11830
71. Xiang M, Birkbak NJ, Vafaizadeh V, et al. STAT3 induction of miR-146b forms a feedback loop to inhibit the NF-κB to IL-6 signaling axis and STAT3-driven cancer phenotypes. *Sci Signal*. 2014;7(310). doi:10.1126/scisignal.2004497
72. Ho BC, Yu IS, Lu LF, et al. Inhibition of miR-146a prevents enterovirus-induced death by restoring the production of type I interferon. *Nat Commun*. 2014;5:3344-3344. doi:10.1038/ncomms4344
73. Pauley KM, Stewart CM, Gauna AE, et al. Altered miR-146a expression in Sjögren's syndrome and its functional role in innate immunity. *Eur J Immunol*. 2011;41(7):2029-2039. doi:10.1002/eji.201040757
74. Tang Y, Luo X, Cui H, et al. MicroRNA-146a contributes to abnormal activation of the type I interferon pathway in human lupus by targeting the key signaling proteins. *Arthritis Rheum*. 2009;60(4):1065-1075. doi:10.1002/art.24436
75. He H, Jazdzewski K, Li W, et al. The role of microRNA genes in papillary thyroid carcinoma. *Proc Natl Acad Sci U S A*. 2005;102(52):19075. doi:10.1073/pnas.0509603102
76. Paterson MR, Kriegel AJ. MiR-146a/b: A family with shared seeds and different roots. *Physiol Genomics*. 2017;49(4):243-252. doi:10.1152/physiolgenomics.00133.2016
77. Monticelli S, Ansel KM, Xiao C, et al. MicroRNA profiling of the murine hematopoietic system. *Genome Biol*. 2005;6(8):R71. doi:10.1186/gb-2005-6-8-r71
78. Nguyen LS, Fregeac J, Bole-Feysot C, et al. Role of miR-146a in neural stem cell differentiation and neural lineage determination: Relevance for neurodevelopmental disorders. *Mol Autism*. 2018;9(1):1-12. doi:10.1186/S13229-018-0219-3
79. Nunes ADC, Weigl M, Schneider A, et al. miR-146a-5p modulates cellular senescence and apoptosis in visceral adipose tissue of long-lived Ames dwarf mice and in cultured pre-adipocytes. *Geroscience*. 2022;44(1):503. doi:10.1007/s11357-021-00490-3
80. Kuang W, Zheng L, Xu X, et al. Dysregulation of the miR-146a-Smad4 axis impairs osteogenesis of bone mesenchymal stem cells under inflammation. *Bone Res*. 2017;5:17037. doi:10.1038/boneres.2017.37
81. Zhong H, Wang HR, Yang S, et al. Targeting Smad4 links microRNA-146a to the TGF-β pathway during retinoid acid induction in acute promyelocytic leukemia cell line. *Int J Hematol*. 2010;92(1):129-135. doi:10.1007/S12185-010-0626-5
82. Zhao M, Mishra L, Deng CX. The role of TGF-β/SMAD4 signaling in cancer. *Int J Biol Sci*. 2018;14(2):111. doi:10.7150/ijbs.23230

83. Lai LYS, Gracie NP, Gowripalan A, Howell LM, Newsome TP. SMAD proteins: Mediators of diverse outcomes during infection. *Eur J Cell Biol*. 2022;101(2):151204. doi:10.1016/j.ejcb.2022.151204
84. de Bosscher K, Hill CS, Nicolás FJ. Molecular and functional consequences of Smad4 C-terminal missense mutations in colorectal tumour cells. *Biochem J*. 2004;379(Pt 1):209. doi:10.1042/bj20031886
85. Imai Y, Kurokawa M, Izutsu K, et al. Mutations of the Smad4 gene in acute myelogeneous leukemia and their functional implications in leukemogenesis. *Oncogene*. 2001;20(1):88-96. doi:10.1038/sj.onc.1204057
86. Wan R, Feng J, Tang L. Consequences of Mutations and Abnormal Expression of SMAD4 in Tumors and T Cells. *Onco Targets Ther*. 2021;14:2531. doi:10.2147/ott.s297855
87. Tan X, Tong L, Li L, et al. Loss of Smad4 promotes aggressive lung cancer metastasis by de-repression of PAK3 via miRNA regulation. *Nat Commun*. 2021;12(1). doi:10.1038/s41467-021-24898-9
88. Zhao X, Nicholls JM, Chen YG. Severe Acute Respiratory Syndrome-associated Coronavirus Nucleocapsid Protein Interacts with Smad3 and Modulates Transforming Growth Factor-β Signaling. *J Biol Chem*. 2008;283(6):3272. doi:10.1074/jbc.m708033200
89. Livak KJ, Schmittgen TD. Analysis of Relative Gene Expression Data Using Real-Time Quantitative PCR and the 2−ΔΔCT Method. *Methods*. 2001;25(4):402-408. doi:10.1006/meth.2001.1262

Chapter 4

Future Directions

The SARS-CoV-2 Nsp13 helicase is an attractive therapeutic target for COVID-19. Its high conservation rate among coronaviruses and SARS-CoV-2 variants, along with its indispensable role in viral replication and host cell immune evasion emphasize why a more comprehensive characterization of this viral helicase may be important for developing therapeutic interventions against COVID-19. In this work, two different approaches were used to study Nsp13. First, we sought to gain a greater understanding of the mechanisms by which Nsp13 unwinds and binds nucleic acids through the use of genetic code expansion techniques. Secondly, we employed various bioinformatics techniques to identify potential host processes modulated by Nsp13 as an alternative method to inform therapeutic strategies.

In chapter 2, we used genetic code expansion techniques to site-specifically incorporate the ncAA AzF into Nsp13 for fluorescent labelling. We demonstrated that the Nsp13 F81AzF construct maintained its helicase unwinding activity and that its DNA binding activity could be detected by ensemble FRET experiments in a distance-dependent manner. Moving forward, we believe that this fluorescently labelled construct could be a powerful tool for monitoring the dynamics of enzyme translocation during ATP-fueled unwinding and nucleic acid binding by smFRET. We propose that by delivering Cy5-labelled Nsp13 F81AzF to surface-anchored Cy3-labelled DNA substrates in smFRET experiments, the transient binding of the Nsp13 to the substrate can be recorded through an increase in Cy5 signal with the concomitant decrease in Cy3 signal. By testing substrates with different overhang lengths and/or locations of the Cy3 fluorophore, we may be able to uncover the kinetics of this enzymatic activity along with different

binding conformations. These single-molecule investigations will not only provide enormous insight into Nsp13's mechanistic properties at all stages of its catalytic cycle, but can also be used to explore how external factors, such as its association with the RTC or the RdRp in particular, influences this activity. Altogether, these detailed characterizations of Nsp13 may contribute to the development of clinically relevant helicase inhibitors, an area of research that is trailing behind other COVID-19 drug discoveries. Currently, molecular docking investigations are a common practice for identifying helicase inhibitors; however, experimental validation is often still required. As such, our developed fluorescent-based unwinding and binding assays may also present convenient methods to screen and characterize these potential helicase inhibitors *in vitro*.

In chapter 3, we highlight the important role of Nsp13 in regulating host responses to infection. Through transcriptomic profiling analyses, we proposed the novel role of Nsp13 in modulating miRNA expression and signalling as a mechanism to facilitate inflammatory and innate immune responses. More specifically, our findings suggest that Nsp13 induces miR-146a expression to downregulate upstream activators of NF-κB signalling. However, further work is still required to validate this proposed inhibition of NF-κB activation, as well as the resulting regulation of IFN signalling. Like many mammalian miRNAs, miR-146a can target a wide array of genes involved in the regulation of multiple cellular processes. In this work we introduce the role of miR-146a in innate immune responses, adaptive immune responses, and SMAD4 signalling; however, further evaluation of these pathways is needed to identify viable therapeutic targets. Alternatively, the use of miR-146a mimics and inhibitors is yet another plausible therapeutic strategy. With the growing interest in investigating miRNAs that modulate host-virus interactions and the recent advancements in RNA-based therapeutics, we believe that a more

exhaustive interrogation of these miR-146a-mediated pathways may be instrumental to introduce novel avenues for antiviral therapies against COVID-19.

Appendix A

Supplemental Figures and Tables for Chapter 2

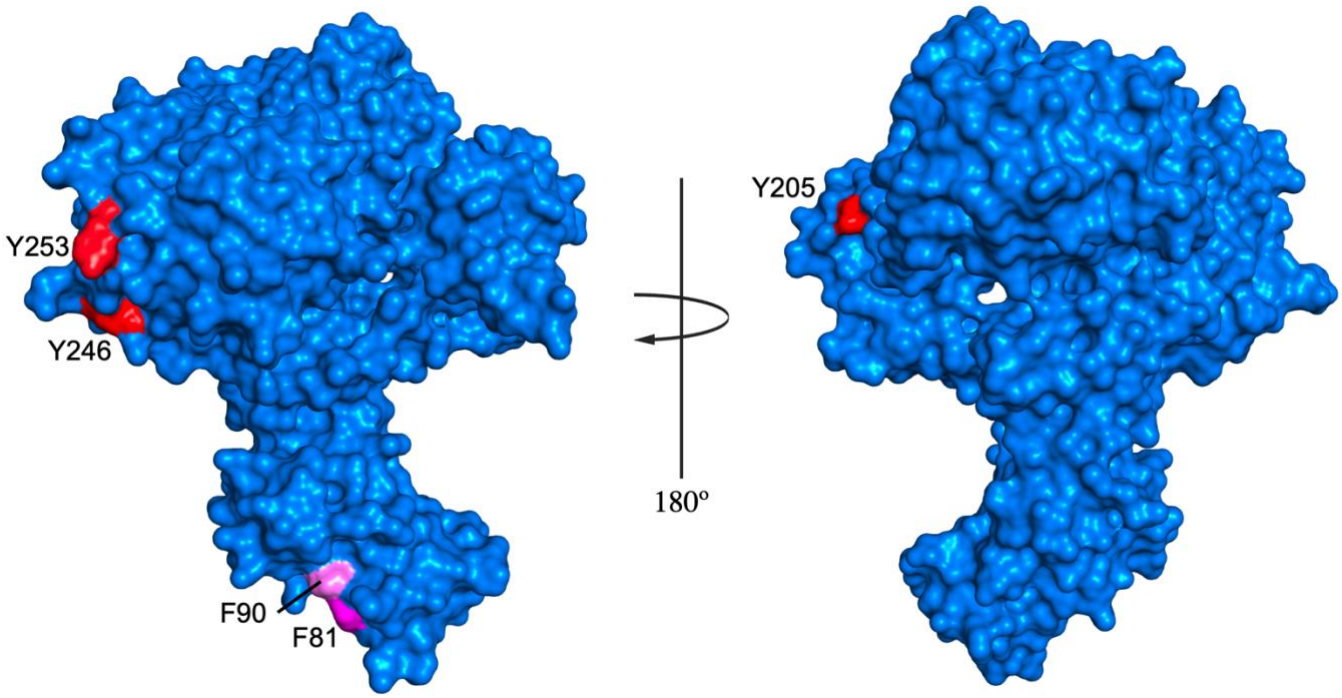

Supplemental Figure 2. 1 Surface Accessible Sites for AzF Incorporation in the SARS-CoV-2 Nsp13.

Surface representation of the crystal structure of Nsp13 (PDB: 6ZSL) where the selected sites for AzF incorporation, shown in red (Y205, Y246, Y253) and pink/purple (F81, F90), were observed to be surface accessible.

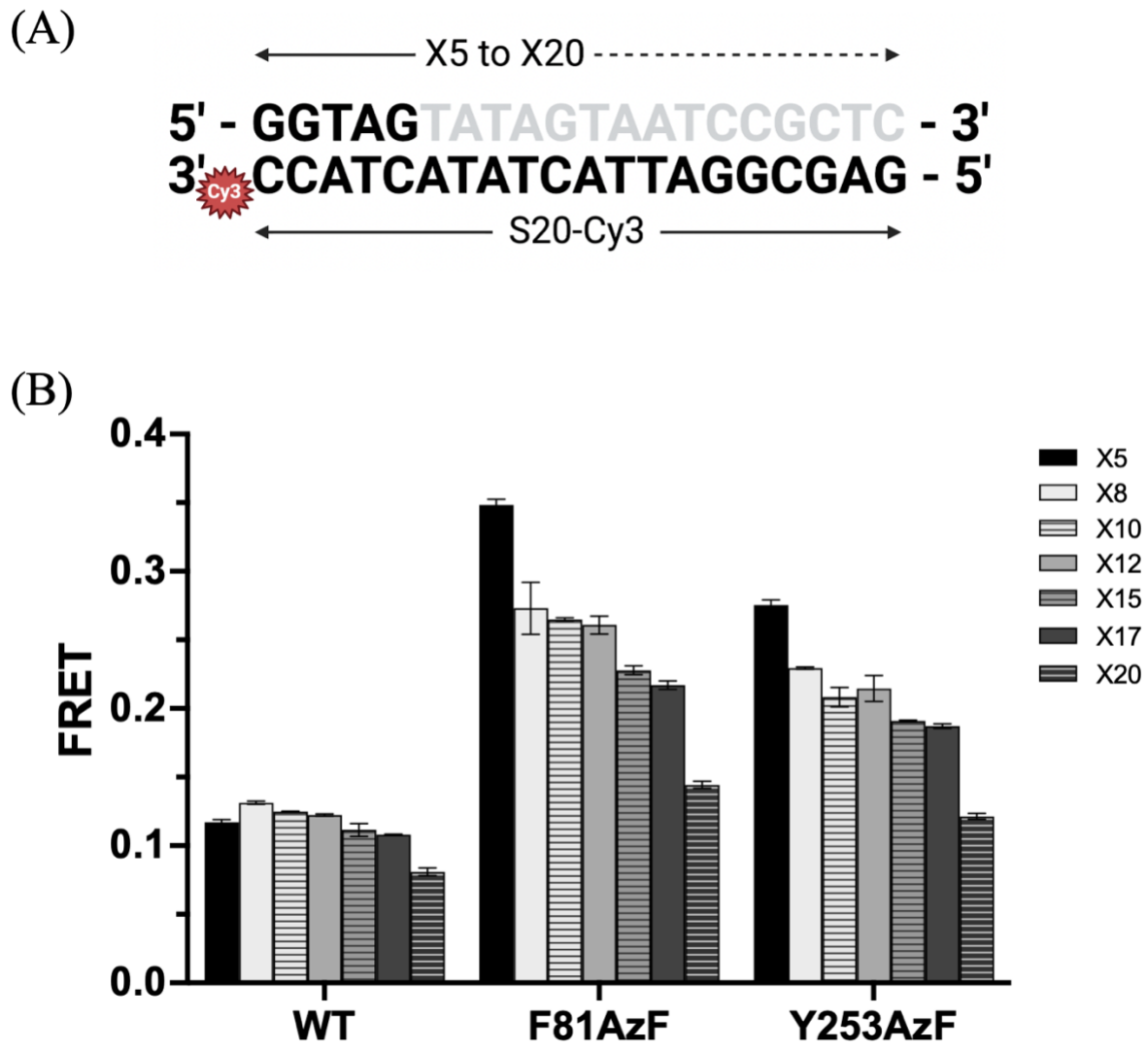

Supplemental Figure 2.2 Monitoring the Binding of Nsp13-AzF Constructs to dsDNA Substrates with Varying Duplex Lengths by FRET.

(A) A series of DNA substrates with duplex lengths varying from 5 to 20 nt were used in FRET-based binding assays. (B) The ratiometric intensity-based FRET proximity ratio (E_{PR}) was calculated to assess the binding of Cy5-labelled WT Nsp13 and Nsp13-AzF to a series of dsDNA substrates. Data is presented as mean ± SD (n=3).

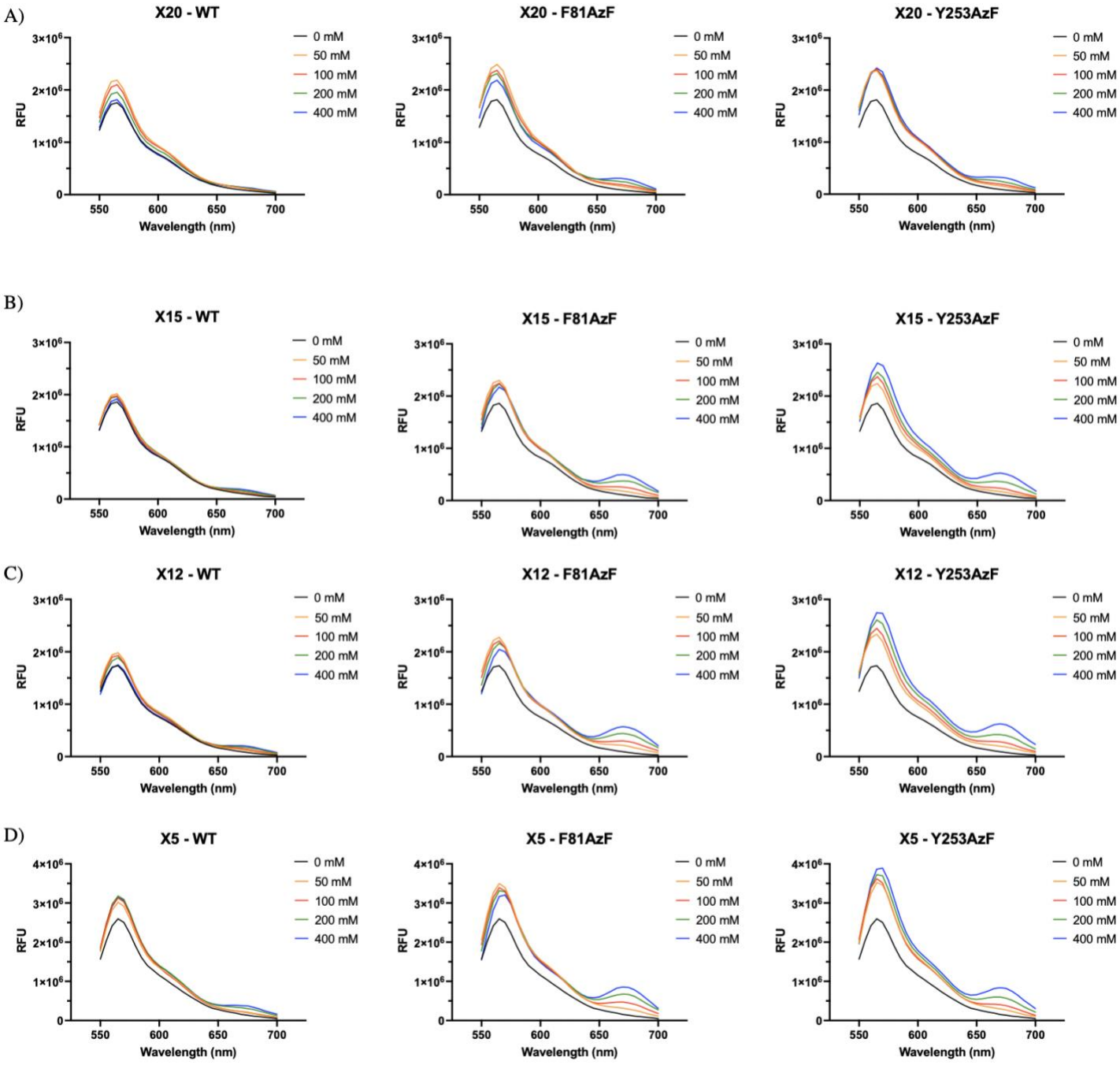

Supplemental Figure 2.3 Binding of Cy5-labelled Nsp13-AzF to Cy3-labelled dsDNA measured by FRET.

The emission spectra for the binding of Cy5-labelled WT Nsp13, F81AzF, and Y253AzF to (A) S20-Cy3/X20, (B) S20-Cy3/X15, (C) S20-Cy3/X12, and (D) S20-Cy3/X5 shows a Cy3 peak at 565 nm and a Cy5 peak at 670 nm.

Supplemental Table 2.1 List of Primers used for Subcloning and Site-directed Mutagenesis.

Oligonucleotide	Sequence (5′ – 3′)
Nsp13 Fwd primer with BamHI	GTGTATGGATCCATGGCTGTTGGTGCATGCGTTTTG
Nsp13 Rev primer with HindIII	ATTTATAAGCTTTTGAAGGGTTGCCACGTTACGGCG
F81AzF Fwd	CATTCGCGCAGAGAGGCTATGAAATCGGCGGCTTATG
F81AzF Rev	CATAAGCCGCCGATTTCATAGCCTCTCTGCGCGAATG
F90AzF Fwd	GGTGTTTTTATACAAACCCTACACCTGGCCATTCGCGCAGA
F90AzF Rev	TCTGCGCGAATGGCCAGGTGTAGGGTTTGTATAAAAACACC
Y205AzF Fwd	ATACTACGGCATCACCCTAGTCGCCTTTCTCAAAG
Y205AzF Rev	CTTTGAGAAAGGCGACTAGGGTGATGCCGTAGTAT
Y246AzF Fwd	AAACCCGTGATACGTACCTAGTGTTCCTGCGGTAC
Y246AzF Rev	GTACCGCAGGAACACTAGGTACGTATCACGGGTTT
Y253AzF Fwd	GTTCAGCGTCGGCTATAAACCCGTGATACGTACATA
Y253AzF Rev	TATGTACGTATCACGGGTTTATAGCCGACGCTGAAC

Supplemental Table 2.2 List of Oligonucleotides used for the Helicase Unwinding Assay.

Helicase Assay Substrates	**Sequence (5′ – 3′)**
Cy3 DNA strand	(Cy3)-GGTAGTAATCCGCTC
BHQ-2 DNA strand	TTTTTTTTTTTTTTTTTTTTGAGCGGATTACTACC-(BHQ-2)
Competitor strand	GAGCGGATTACTACC

Supplemental Table 2.3 List of Oligonucleotides used for the FRET Binding Assay.

FRET Assay Substrates	Sequence (5′ – 3′)
S20-Cy3	GAGCGGATTACTATACTACC-(Cy3)
X20	GGTAGTATAGTAATCCGCTC
X17	GGTAGTATAGTAATCCG
X15	GGTAGTATAGTAATC
X12	GGTAGTATAGTA
X10	GGTAGTATAG
X8	GGTAGTAT
X5	GGTAG

Appendix B

Supplemental Figures and Tables for Chapter 3

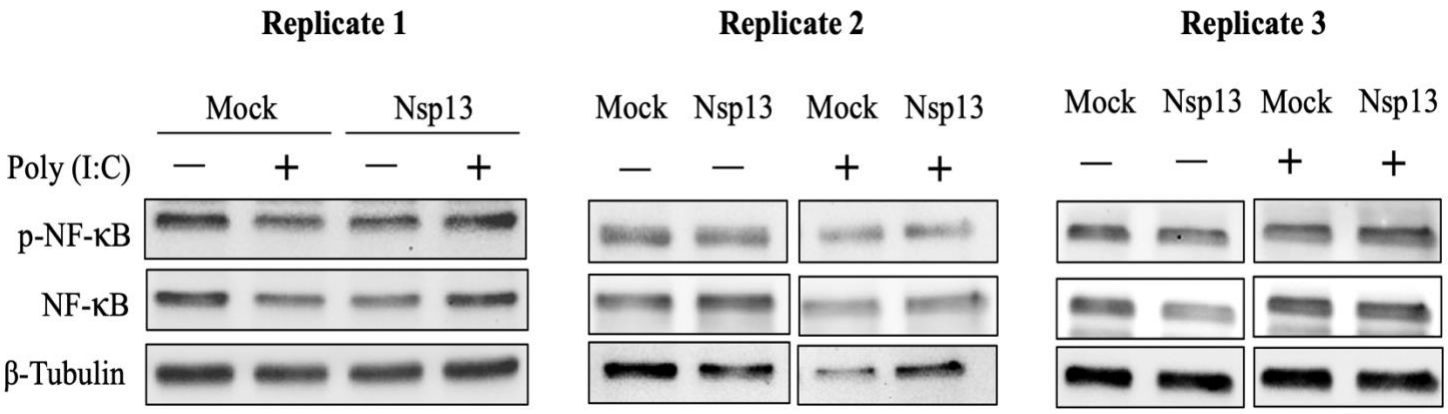

Supplemental Figure 3.1 Western Blot Replicates of p-NF-κB and NF-κB Protein Levels in Nsp13-transfected Cells.

A549 cells were transfected with either a mock or Nsp13 plasmid under two conditions, with and without poly (I:C) treatment for 24 hours. Forty-eight hours post-transfection, cells were lysed and western blot analysis was used to assess the level of phosphorylated NF-κB and total NF-κB in the cells. β-tubulin was used as a loading control.

Supplemental Table 3.1 Gene Ontology Analysis of Molecular Functions and Biological Processes altered by Nsp13 overexpression in A549 cells without poly (I:C) treatment.

General Pathway	Regulation	ID	Name	p-value*
Post-transcriptional gene silencing and translational repression by RNA	↓	GO:0035194	post-transcriptional gene silencing by RNA	2.13E-11
		GO:0016441	post-transcriptional gene silencing	2.66E-11
		GO:0035195	miRNA-mediated gene silencing	5.02E-11
		GO:0031047	gene silencing by RNA	2.50E-10
		GO:1903231	mRNA base-pairing post-transcriptional repressor activity	1.29E-08
		GO:0030371	translation repressor activity	7.79E-08
		GO:0045182	translation regulator activity	1.52E-06
		GO:0003730	mRNA 3'-UTR binding	5.86E-06
		GO:0003729	mRNA binding	6.81E-05
Detection of stimulus in sensory perception and receptor activity	↓	GO:0004984	olfactory receptor activity	4.27E-09
		GO:0050907	detection of chemical stimulus involved in sensory perception	1.31E-08
		GO:0009593	detection of chemical stimulus	7.56E-08
		GO:0050906	detection of stimulus involved in sensory perception	8.39E-08
		GO:0007606	sensory perception of chemical stimulus	3.04E-07
		GO:0007608	sensory perception of smell	6.25E-07
		GO:0050911	detection of chemical stimulus involved in sensory perception of smell	7.23E-07
		GO:0004888	transmembrane signalling receptor activity	1.67E-06
		GO:0004930	G protein-coupled receptor activity	1.78E-06
Immunity	↓	GO:0002250	adaptive immune response	1.58E-06

* p-value adjusted with Bonferroni correction

Supplemental Table 3.2 Gene Ontology Analysis of Molecular Functions and Biological Processes altered by Nsp13 overexpression in A549 cells with poly (I:C) treatment.

General Pathway	Regulation	ID	Name	p-value*
Post-transcriptional gene silencing and translational repression by RNA	↑	GO:0035195	miRNA-mediated gene silencing	3.54E-09
		GO:0035194	post-transcriptional gene silencing by RNA	5.64E-09
		GO:0016441	post-transcriptional gene silencing	6.83E-09
		GO:0031047	gene silencing by RNA	4.57E-08
		GO:1903231	mRNA base-pairing post-transcriptional repressor activity	6.95E-08
		GO:0030371	translation repressor activity	4.01E-07
		GO:0045182	translation regulator activity	2.63E-05
Detection of stimulus in sensory perception and receptor activity	↑	GO:0007608	sensory perception of smell	1.98E-10
		GO:0007600	sensory perception	2.19E-10
		GO:0007606	sensory perception of chemical stimulus	5.47E-10
		GO:0004930	G protein-coupled receptor activity	1.05E-09
		GO:0050907	detection of chemical stimulus involved in sensory perception	3.94E-09
		GO:0050911	detection of chemical stimulus involved in sensory perception of smell	5.99E-09
		GO:0050906	detection of stimulus involved in sensory perception	6.14E-09
		GO:0004888	transmembrane signalling receptor activity	8.29E-09
		GO:0004984	olfactory receptor activity	8.38E-09
		GO:0007186	G protein-coupled receptor signalling pathway	1.39E-08
		GO:0009593	detection of chemical stimulus	2.48E-08
		GO:0051606	detection of stimulus	1.43E-07
Immunity and other host defense responses	↓	GO:0045087	innate immune response	8.44E-11
		GO:0098542	defense response to other organism	1.50E-08
		GO:0042742	defense response to bacterium	5.50E-08
		GO:0002250	adaptive immune response	2.14E-07
		GO:0006959	humoral immune response	6.22E-07
		GO:0009617	response to bacterium	8.89E-07
		GO:0002252	immune effector process	1.21E-06
		GO:0002449	lymphocyte mediated immunity	2.34E-06
		GO:0002443	leukocyte mediated immunity	3.51E-06
		GO:0001911	negative regulation of leukocyte mediated cytotoxicity	4.10E-06
		GO:0001909	leukocyte mediated cytotoxicity	4.32E-06

		GO:0002526	acute inflammatory response	4.65E-06
		GO:0002768	immune response-regulating cell surface receptor signalling pathway	7.75E-06
Other molecular functions and biological processes	↓	GO:0034987	immunoglobulin receptor binding	1.92E-07
		GO:0003823	antigen binding	2.06E-07
		GO:0099024	plasma membrane invagination	3.73E-07
		GO:0006910	phagocytosis, recognition	5.57E-07
		GO:0010324	membrane invagination	7.59E-07
		GO:0006911	phagocytosis, engulfment	8.15E-07
		GO:0005102	signalling receptor binding	7.36E-06

* p-value adjusted with Bonferroni correction

Supplemental Table 3.3 Predicted miRNA-gene Interactions from Nsp13-transfected A549 Cells.

miRNA	Gene Target	Predicted in TargetScan?	Predicted in microRNA.org?
hsa-let-7F-2	ABCA8	No	Yes
hsa-let-7F-2	BLK	No	Yes
hsa-let-7F-2	CACNB2	No	Yes
hsa-let-7F-2	CBFA2T3	Yes	Yes
hsa-let-7F-2	CFP	No	Yes
hsa-let-7F-2	CLEC4M	No	Yes
hsa-let-7F-2	CSRNP3	Yes	No
hsa-let-7F-2	FOXD4L6	No	Yes
hsa-let-7F-2	GLIS3	No	Yes
hsa-let-7F-2	GRAMD1C	No	Yes
hsa-let-7F-2	ITGA11	Yes	No
hsa-let-7F-2	KLHDC8A	No	Yes
hsa-let-7F-2	KLK2	No	Yes
hsa-let-7F-2	KRTAP24-1	No	Yes
hsa-let-7F-2	LCE2B	No	Yes
hsa-let-7F-2	MTUS1	Yes	Yes
hsa-let-7F-2	NOS1	Yes	No
hsa-let-7F-2	NPR 2.00	No	Yes
hsa-let-7F-2	NTRK3	Yes	Yes
hsa-let-7F-2	PDK4	No	Yes
hsa-let-7F-2	PEG10	Yes	No
hsa-let-7F-2	PMFBP1	No	Yes
hsa-let-7F-2	POU2F3	No	Yes
hsa-let-7F-2	RARRES1	No	Yes
hsa-let-7F-2	RTP1	No	Yes
hsa-let-7F-2	SELP	No	Yes
hsa-let-7F-2	SESN3	No	Yes
hsa-let-7F-2	SLAMF6	Yes	Yes
hsa-let-7F-2	SYT2	Yes	No
hsa-let-7F-2	TCEANC	No	Yes

hsa-let-7F-2	TP63	No	Yes
hsa-let-7F-2	TRPC5	No	Yes
hsa-let-7F-2	ZNF443	No	Yes
hsa-let-7F-2	ZNF738	No	Yes
hsa-let-7F-2	ZNF763	No	Yes
hsa-let-7F-2	ZNF806	No	Yes
hsa-mir-130A	ABLIM1	No	Yes
hsa-mir-130A	ADAMTS18	Yes	Yes
hsa-mir-130A	ADCY1	Yes	No
hsa-mir-130A	ADRA2A	No	Yes
hsa-mir-130A	ATXN1	Yes	Yes
hsa-mir-130A	BMP8B	No	Yes
hsa-mir-130A	CHST1	Yes	Yes
hsa-mir-130A	CLEC4M	No	Yes
hsa-mir-130A	COL4A4	No	Yes
hsa-mir-130A	CREB5	Yes	Yes
hsa-mir-130A	FGB	No	Yes
hsa-mir-130A	FLJ42393	No	Yes
hsa-mir-130A	HEY2	No	Yes
hsa-mir-130A	IQGAP2	No	Yes
hsa-mir-130A	IRF4	No	Yes
hsa-mir-130A	ITGA11	Yes	Yes
hsa-mir-130A	ITPKB	Yes	No
hsa-mir-130A	KLHDC8A	Yes	Yes
hsa-mir-130A	KRT38	No	Yes
hsa-mir-130A	LCE2B	No	Yes
hsa-mir-130A	LOC145474	No	Yes
hsa-mir-130A	MAGEB2	No	Yes
hsa-mir-130A	MMP19	No	Yes
hsa-mir-130A	NOS1	No	Yes
hsa-mir-130A	OMG	No	Yes
hsa-mir-130A	PABPC4L	No	Yes
hsa-mir-130A	PEG10	No	Yes

hsa-mir-130A	SLC12A2	No	Yes
hsa-mir-130A	SNX20	No	Yes
hsa-mir-130A	SOD2	No	Yes
hsa-mir-130A	ST3GAL6	No	Yes
hsa-mir-130A	SYT2	Yes	No
hsa-mir-130A	TMEM40	No	Yes
hsa-mir-130A	TMTC1	No	Yes
hsa-mir-130A	TNF	Yes	Yes
hsa-mir-130A	TP63	Yes	Yes
hsa-mir-130A	WFDC13	No	Yes
hsa-mir-130A	ZFYVE9	Yes	Yes
hsa-mir-130A	ZNF738	No	Yes
hsa-mir-133B	ALPI	No	Yes
hsa-mir-133B	CCDC30	No	Yes
hsa-mir-133B	CCT6P1	No	Yes
hsa-mir-133B	CCT6P3	No	Yes
hsa-mir-133B	CXCL11	No	Yes
hsa-mir-133B	FAM71D	No	Yes
hsa-mir-133B	FCAR	No	Yes
hsa-mir-133B	FGF7	No	Yes
hsa-mir-133B	GEM	No	Yes
hsa-mir-133B	GOLGA8B	No	Yes
hsa-mir-133B	HNRNPA3	No	Yes
hsa-mir-133B	MKRN3	No	Yes
hsa-mir-133B	PBOV1	No	Yes
hsa-mir-133B	PPIP5K1	Yes	No
hsa-mir-133B	SIGLEC11	No	Yes
hsa-mir-133B	SLC30A7	Yes	No
hsa-mir-133B	SNORD114-14	No	Yes
hsa-mir-133B	SNORD114-3	No	Yes
hsa-mir-133B	ZEB2	No	Yes
hsa-mir-135B	ADCY1	Yes	No
hsa-mir-135B	ADRA2A	Yes	Yes

hsa-mir-135B	ANGPT1	No	Yes
hsa-mir-135B	BCL11B	No	Yes
hsa-mir-135B	BLK	No	Yes
hsa-mir-135B	C16orf82	No	Yes
hsa-mir-135B	CDH9	No	Yes
hsa-mir-135B	CLEC3A	No	Yes
hsa-mir-135B	CPLX2	Yes	Yes
hsa-mir-135B	CREB5	Yes	No
hsa-mir-135B	DIRAS2	Yes	No
hsa-mir-135B	FGA	No	Yes
hsa-mir-135B	FOXR1	No	Yes
hsa-mir-135B	HHLA3	No	Yes
hsa-mir-135B	KIR2DS4	No	Yes
hsa-mir-135B	KRTAP24-1	No	Yes
hsa-mir-135B	LDHC	No	Yes
hsa-mir-135B	LTB4R2	No	Yes
hsa-mir-135B	MTUS1	Yes	Yes
hsa-mir-135B	OMG	No	Yes
hsa-mir-135B	OTUD7A	No	Yes
hsa-mir-135B	PABPC4L	No	Yes
hsa-mir-135B	PIP5K1A	No	Yes
hsa-mir-135B	PLXNA2	Yes	No
hsa-mir-135B	POM121L9P	No	Yes
hsa-mir-135B	POU2F3	Yes	Yes
hsa-mir-135B	RPL23P8	No	Yes
hsa-mir-135B	SYT2	Yes	Yes
hsa-mir-135B	WFDC13	No	Yes
hsa-mir-135B	ZNF430	No	Yes
hsa-mir-141	BACH1	No	Yes
hsa-mir-141	CAMK1G	No	Yes
hsa-mir-141	CGNL1	No	Yes
hsa-mir-141	FGF7	No	Yes
hsa-mir-141	GEM	No	Yes

hsa-mir-141	GRHL1	No	Yes
hsa-mir-141	HCAR2	Yes	No
hsa-mir-141	HNRNPA3	No	Yes
hsa-mir-141	KBTBD6	No	Yes
hsa-mir-141	LOC284023	No	Yes
hsa-mir-141	LOC344887	No	Yes
hsa-mir-141	MAGEA4	No	Yes
hsa-mir-141	MATN3	No	Yes
hsa-mir-141	MKRN3	No	Yes
hsa-mir-141	MXD1	No	Yes
hsa-mir-141	OR7E5P	No	Yes
hsa-mir-141	PF4V1	No	Yes
hsa-mir-141	PLCL1	No	Yes
hsa-mir-141	PNMAL2	No	Yes
hsa-mir-141	PPP2R5C	No	Yes
hsa-mir-141	PRB4	No	Yes
hsa-mir-141	RBM43	No	Yes
hsa-mir-141	RSAD2	No	Yes
hsa-mir-141	SCG3	No	Yes
hsa-mir-141	SHISA2	No	Yes
hsa-mir-141	SIM1	No	Yes
hsa-mir-141	SLC13A3	No	Yes
hsa-mir-141	SLC30A7	No	Yes
hsa-mir-141	TMEM154	No	Yes
hsa-mir-141	VSNL1	No	Yes
hsa-mir-141	ZEB2	Yes	Yes
hsa-mir-141	ZNF225	No	Yes
hsa-mir-141	ZNF420	No	Yes
hsa-mir-141	ZNF544	No	Yes
hsa-mir-152	ABLIM1	No	Yes
hsa-mir-152	ADAMTS18	Yes	Yes
hsa-mir-152	ADRA2A	No	Yes
hsa-mir-152	ARMCX2	No	Yes

hsa-mir-152	ATXN1	Yes	No
hsa-mir-152	CABP7	Yes	Yes
hsa-mir-152	CBFA2T3	No	Yes
hsa-mir-152	CHST1	Yes	Yes
hsa-mir-152	CSRNP3	No	Yes
hsa-mir-152	CYP2B6	No	Yes
hsa-mir-152	GOLGA7B	No	Yes
hsa-mir-152	GRAMD1C	No	Yes
hsa-mir-152	HEY2	No	Yes
hsa-mir-152	INE1	No	Yes
hsa-mir-152	IRF4	No	Yes
hsa-mir-152	ITGA11	Yes	Yes
hsa-mir-152	KLK2	No	Yes
hsa-mir-152	LOC145474	No	Yes
hsa-mir-152	MMP19	No	Yes
hsa-mir-152	NR1H4	No	Yes
hsa-mir-152	PABPC4L	No	Yes
hsa-mir-152	PDK4	Yes	Yes
hsa-mir-152	RTP1	No	Yes
hsa-mir-152	SELE	No	Yes
hsa-mir-152	ST3GAL6	No	Yes
hsa-mir-152	SYT2	Yes	Yes
hsa-mir-152	TC2N	No	Yes
hsa-mir-152	TNF	No	Yes
hsa-mir-152	TRPC5	No	Yes
hsa-mir-152	TSPY2	No	Yes
hsa-mir-152	ZFYVE9	No	Yes
hsa-mir-152	ZNF806	No	Yes
hsa-mir-191	ADAM7	No	Yes
hsa-mir-191	FCGR1C	No	Yes
hsa-mir-191	NPM1	No	Yes
hsa-mir-191	ZEB2	No	Yes
hsa-mir-196A-1	ANGPT1	No	Yes

hsa-mir-196A-1	BMP4	No	Yes
hsa-mir-196A-1	CACNB2	No	Yes
hsa-mir-196A-1	CBFA2T3	Yes	Yes
hsa-mir-196A-1	CDH17	No	Yes
hsa-mir-196A-1	CFP	No	Yes
hsa-mir-196A-1	COL4A4	No	Yes
hsa-mir-196A-1	FGA	No	Yes
hsa-mir-196A-1	GDPD2	No	Yes
hsa-mir-196A-1	INHBC	No	Yes
hsa-mir-196A-1	KRTAP24-1	No	Yes
hsa-mir-196A-1	NEUROD2	No	Yes
hsa-mir-196A-1	NPR 2.00	No	Yes
hsa-mir-196A-1	PEG10	Yes	Yes
hsa-mir-196A-1	PPP1R2P3	No	Yes
hsa-mir-196A-1	RARRES1	No	Yes
hsa-mir-196A-1	SAMD3	No	Yes
hsa-mir-196A-1	SERPINI1	No	Yes
hsa-mir-196A-1	SLC2A4	No	Yes
hsa-mir-196A-1	TMTC1	No	Yes
hsa-mir-196A-1	TRPC5	No	Yes
hsa-mir-196A-1	WFDC13	No	Yes
hsa-mir-196A-1	ZNF763	No	Yes
hsa-mir-200C	ACSM2A	No	Yes
hsa-mir-200C	ADAMDEC1	No	Yes
hsa-mir-200C	ANKRD62	No	Yes
hsa-mir-200C	ARHGEF1	Yes	Yes
hsa-mir-200C	ARMC3	No	Yes
hsa-mir-200C	ASB5	No	Yes
hsa-mir-200C	BTBD18	No	Yes
hsa-mir-200C	CCT6P1	No	Yes
hsa-mir-200C	CCT6P3	No	Yes
hsa-mir-200C	ELL	Yes	Yes
hsa-mir-200C	GATA2	Yes	Yes

hsa-mir-200C	GEM	Yes	Yes
hsa-mir-200C	GLUD1	No	Yes
hsa-mir-200C	GOLGA8B	No	Yes
hsa-mir-200C	GOLGA8DP	No	Yes
hsa-mir-200C	GRHL1	No	Yes
hsa-mir-200C	HNRNPA3	No	Yes
hsa-mir-200C	HSPA9	Yes	Yes
hsa-mir-200C	IBSP	No	Yes
hsa-mir-200C	IL24	No	Yes
hsa-mir-200C	KBTBD6	Yes	Yes
hsa-mir-200C	KLF8	No	Yes
hsa-mir-200C	LOC284023	No	Yes
hsa-mir-200C	MATN3	No	Yes
hsa-mir-200C	MKRN3	No	Yes
hsa-mir-200C	NPM1	No	Yes
hsa-mir-200C	PCDHB14	No	Yes
hsa-mir-200C	PCDHB15	No	Yes
hsa-mir-200C	PLCL1	Yes	Yes
hsa-mir-200C	PPP2R5C	Yes	Yes
hsa-mir-200C	RBM43	No	Yes
hsa-mir-200C	RSAD2	No	Yes
hsa-mir-200C	SHISA2	No	Yes
hsa-mir-200C	SLC13A3	No	Yes
hsa-mir-200C	SLC30A7	No	Yes
hsa-mir-200C	SMAD4	No	Yes
hsa-mir-200C	SPCS2	No	Yes
hsa-mir-200C	TMEM154	No	Yes
hsa-mir-200C	TMEM236	Yes	No
hsa-mir-200C	VSNL1	No	Yes
hsa-mir-200C	ZEB2	Yes	Yes
hsa-mir-21	ADAMTS18	No	Yes
hsa-mir-21	ARMCX2	No	Yes
hsa-mir-21	BCL11B	Yes	No

hsa-mir-21	CREB5	Yes	No
hsa-mir-21	CSRNP3	Yes	No
hsa-mir-21	CYP2B6	No	Yes
hsa-mir-21	DSG4	No	Yes
hsa-mir-21	FGB	No	Yes
hsa-mir-21	GLRA2	No	Yes
hsa-mir-21	HEY2	No	Yes
hsa-mir-21	KGFLP1	No	Yes
hsa-mir-21	LCE2B	No	Yes
hsa-mir-21	LOC285556	No	Yes
hsa-mir-21	LRRC32	No	Yes
hsa-mir-21	LRRC55	No	Yes
hsa-mir-21	NWD1	No	Yes
hsa-mir-21	PABPC4L	No	Yes
hsa-mir-21	PAX9	No	Yes
hsa-mir-21	RIPPLY1	No	Yes
hsa-mir-21	SELE	No	Yes
hsa-mir-21	SERPINI1	No	Yes
hsa-mir-21	SIGLEC7	No	Yes
hsa-mir-21	SLC12A2	No	Yes
hsa-mir-21	SLCO1B1	No	Yes
hsa-mir-21	ST3GAL6	Yes	Yes
hsa-mir-21	TC2N	No	Yes
hsa-mir-21	TP63	No	Yes
hsa-mir-21	ZFYVE9	No	Yes
hsa-mir-21	ZNF608	No	Yes
hsa-mir-23A	ACSM2A	No	Yes
hsa-mir-23A	ACTBL2	No	Yes
hsa-mir-23A	ADAM7	No	Yes
hsa-mir-23A	ANKRD62	No	Yes
hsa-mir-23A	BACH1	No	Yes
hsa-mir-23A	CD1B	No	Yes
hsa-mir-23A	CENPL	No	Yes

hsa-mir-23A	CLEC2A	No	Yes
hsa-mir-23A	DKFZP434L187	No	Yes
hsa-mir-23A	EPGN	No	Yes
hsa-mir-23A	EXOC4	No	Yes
hsa-mir-23A	FAM71D	No	Yes
hsa-mir-23A	FGF7	No	Yes
hsa-mir-23A	FRMPD4	No	Yes
hsa-mir-23A	GOLGA8B	No	Yes
hsa-mir-23A	GOLGA8DP	No	Yes
hsa-mir-23A	GRHL1	No	Yes
hsa-mir-23A	IBSP	No	Yes
hsa-mir-23A	KLF8	No	Yes
hsa-mir-23A	LOC284023	No	Yes
hsa-mir-23A	LOC344887	No	Yes
hsa-mir-23A	MATN3	No	Yes
hsa-mir-23A	MKRN3	No	Yes
hsa-mir-23A	NEFH	No	Yes
hsa-mir-23A	NPM1	No	Yes
hsa-mir-23A	P2RY10	No	Yes
hsa-mir-23A	POTEC	No	Yes
hsa-mir-23A	PPP2R5C	No	Yes
hsa-mir-23A	SHISA2	No	Yes
hsa-mir-23A	SIM1	No	Yes
hsa-mir-23A	SMAD4	No	Yes
hsa-mir-23A	SPCS2	Yes	Yes
hsa-mir-23A	SPDYE1	No	Yes
hsa-mir-23A	VPS37D	Yes	Yes
hsa-mir-23A	VSNL1	No	Yes
hsa-mir-23A	WDR7	No	Yes
hsa-mir-23A	ZEB2	No	Yes
hsa-mir-23A	ZNF420	Yes	Yes
hsa-mir-23A	ZNF544	No	Yes
hsa-mir-23A	ZNF546	No	Yes

hsa-mir-23A	ZNF572	Yes	Yes
hsa-mir-23B	ACSM2A	No	Yes
hsa-mir-23B	ACTBL2	No	Yes
hsa-mir-23B	ADAM7	No	Yes
hsa-mir-23B	ANKRD62	No	Yes
hsa-mir-23B	BACH1	No	Yes
hsa-mir-23B	CD1B	No	Yes
hsa-mir-23B	CENPL	No	Yes
hsa-mir-23B	CLEC2A	No	Yes
hsa-mir-23B	DKFZP434L187	No	Yes
hsa-mir-23B	EPGN	No	Yes
hsa-mir-23B	EXOC4	No	Yes
hsa-mir-23B	FAM71D	No	Yes
hsa-mir-23B	FGF7	No	Yes
hsa-mir-23B	FRMPD4	No	Yes
hsa-mir-23B	GOLGA8B	No	Yes
hsa-mir-23B	GOLGA8DP	No	Yes
hsa-mir-23B	GRHL1	No	Yes
hsa-mir-23B	IBSP	No	Yes
hsa-mir-23B	KLF8	No	Yes
hsa-mir-23B	KRT34	No	Yes
hsa-mir-23B	LOC284023	No	Yes
hsa-mir-23B	LOC344887	No	Yes
hsa-mir-23B	MATN3	No	Yes
hsa-mir-23B	MKRN3	No	Yes
hsa-mir-23B	MUC15	No	Yes
hsa-mir-23B	NEFH	No	Yes
hsa-mir-23B	NPM1	No	Yes
hsa-mir-23B	P2RY10	No	Yes
hsa-mir-23B	POTEC	No	Yes
hsa-mir-23B	PPP2R5C	No	Yes
hsa-mir-23B	SHISA2	No	Yes
hsa-mir-23B	SIM1	No	Yes

hsa-mir-23B	SMAD4	No	Yes
hsa-mir-23B	SPCS2	Yes	Yes
hsa-mir-23B	SPDYE1	No	Yes
hsa-mir-23B	VPS37D	Yes	Yes
hsa-mir-23B	VSNL1	No	Yes
hsa-mir-23B	WDR7	No	Yes
hsa-mir-23B	ZEB2	No	Yes
hsa-mir-23B	ZNF420	Yes	Yes
hsa-mir-23B	ZNF544	No	Yes
hsa-mir-23B	ZNF546	No	Yes
hsa-mir-23B	ZNF572	Yes	Yes
hsa-mir-23C	ADCY1	Yes	No
hsa-mir-23C	ADRA2A	Yes	No
hsa-mir-23C	ATXN1	Yes	No
hsa-mir-23C	CBFA2T3	Yes	No
hsa-mir-23C	COL4A4	Yes	No
hsa-mir-23C	DIRAS2	Yes	No
hsa-mir-23C	FAM46C	Yes	No
hsa-mir-23C	MAGEB2	Yes	No
hsa-mir-23C	NLGN4Y	Yes	No
hsa-mir-23C	NUDT3	Yes	No
hsa-mir-23C	PAX9	Yes	No
hsa-mir-23C	SLC12A2	Yes	No
hsa-mir-23C	TRIL	Yes	No
hsa-mir-30A	ACSM2A	No	Yes
hsa-mir-30A	ACTBL2	No	Yes
hsa-mir-30A	ADAM7	No	Yes
hsa-mir-30A	ADRB2	No	Yes
hsa-mir-30A	ANKRD62	No	Yes
hsa-mir-30A	BACH1	Yes	No
hsa-mir-30A	CDH13	Yes	No
hsa-mir-30A	CLSTN2	No	Yes
hsa-mir-30A	CSN1S1	No	Yes

hsa-mir-30A	CXCL11	No	Yes
hsa-mir-30A	DKFZP434L187	No	Yes
hsa-mir-30A	ELAVL3	Yes	Yes
hsa-mir-30A	ELL	Yes	Yes
hsa-mir-30A	ELOVL7	No	Yes
hsa-mir-30A	EXOC4	No	Yes
hsa-mir-30A	FAM126A	Yes	Yes
hsa-mir-30A	FAM133B	No	Yes
hsa-mir-30A	FAM71D	No	Yes
hsa-mir-30A	FLJ26850	No	Yes
hsa-mir-30A	FRMPD4	No	Yes
hsa-mir-30A	GBP5	No	Yes
hsa-mir-30A	GLUD1	Yes	Yes
hsa-mir-30A	GOLGA8B	No	Yes
hsa-mir-30A	GRHL1	Yes	Yes
hsa-mir-30A	HNRNPA3	Yes	Yes
hsa-mir-30A	IL24	No	Yes
hsa-mir-30A	KBTBD6	No	Yes
hsa-mir-30A	KLF8	No	Yes
hsa-mir-30A	MATN3	No	Yes
hsa-mir-30A	MKRN3	Yes	Yes
hsa-mir-30A	NPM1	No	Yes
hsa-mir-30A	OR7E5P	No	Yes
hsa-mir-30A	P2RY10	No	Yes
hsa-mir-30A	PBOV1	No	Yes
hsa-mir-30A	PPP2R5C	No	Yes
hsa-mir-30A	RBM43	No	Yes
hsa-mir-30A	RSAD2	No	Yes
hsa-mir-30A	SNORA11B	No	Yes
hsa-mir-30A	TTPA	Yes	No
hsa-mir-30A	UBE2E1	No	Yes
hsa-mir-30A	WDR7	Yes	Yes
hsa-mir-30A	ZEB2	Yes	Yes

hsa-mir-30A	ZNF334	No	Yes
hsa-mir-30A	ZNF544	No	Yes
hsa-mir-30D	ABCA8	No	Yes
hsa-mir-30D	ADRA2A	Yes	Yes
hsa-mir-30D	ATXN1	Yes	No
hsa-mir-30D	BCL11B	Yes	Yes
hsa-mir-30D	CABP7	No	Yes
hsa-mir-30D	CACNB2	Yes	Yes
hsa-mir-30D	CHST1	Yes	Yes
hsa-mir-30D	CLEC3A	No	Yes
hsa-mir-30D	CSRNP3	Yes	No
hsa-mir-30D	FAM46C	Yes	Yes
hsa-mir-30D	FAM47A	No	Yes
hsa-mir-30D	FAM83F	Yes	Yes
hsa-mir-30D	FGB	No	Yes
hsa-mir-30D	FLJ42393	No	Yes
hsa-mir-30D	FSTL4	No	Yes
hsa-mir-30D	GATS	No	Yes
hsa-mir-30D	GRID1	No	Yes
hsa-mir-30D	HEY2	No	Yes
hsa-mir-30D	HNRNPA3P1	No	Yes
hsa-mir-30D	IQGAP2	No	Yes
hsa-mir-30D	IRF4	Yes	Yes
hsa-mir-30D	LEP	No	Yes
hsa-mir-30D	MAGEB2	No	Yes
hsa-mir-30D	MMP19	No	Yes
hsa-mir-30D	NKX2-2	Yes	Yes
hsa-mir-30D	NOX1	No	Yes
hsa-mir-30D	NR1H4	No	Yes
hsa-mir-30D	NTRK3	No	Yes
hsa-mir-30D	OMG	Yes	Yes
hsa-mir-30D	PAX9	No	Yes
hsa-mir-30D	PCDHB12	No	Yes

hsa-mir-30D	PDK4	No	Yes
hsa-mir-30D	PEG10	No	Yes
hsa-mir-30D	PLXNA2	Yes	Yes
hsa-mir-30D	PPP1R2P3	No	Yes
hsa-mir-30D	RARRES1	No	Yes
hsa-mir-30D	S100A7A	No	Yes
hsa-mir-30D	SERPINI1	No	Yes
hsa-mir-30D	SH3GL2	No	Yes
hsa-mir-30D	SLCO1B1	No	Yes
hsa-mir-30D	SOD2	No	Yes
hsa-mir-30D	SSTR1	No	Yes
hsa-mir-30D	TC2N	No	Yes
hsa-mir-30D	TM4SF20	No	Yes
hsa-mir-30D	TMTC1	No	Yes
hsa-mir-30D	TP63	No	Yes
hsa-mir-30D	TRIL	Yes	Yes
hsa-mir-30D	ZNF608	Yes	Yes
hsa-mir-320D-1	ARMCX2	Yes	Yes
hsa-mir-320D-1	CFP	No	Yes
hsa-mir-320D-1	CREB5	Yes	Yes
hsa-mir-320D-1	CSRNP3	Yes	No
hsa-mir-320D-1	DCC	Yes	No
hsa-mir-320D-1	FGB	No	Yes
hsa-mir-320D-1	FGL1	No	Yes
hsa-mir-320D-1	FOXR1	No	Yes
hsa-mir-320D-1	GDPD2	No	Yes
hsa-mir-320D-1	GLIS3	Yes	Yes
hsa-mir-320D-1	GRAMD1C	No	Yes
hsa-mir-320D-1	HHLA3	No	Yes
hsa-mir-320D-1	HSPA7	No	Yes
hsa-mir-320D-1	IRF4	No	Yes
hsa-mir-320D-1	KCNC3	No	Yes
hsa-mir-320D-1	KGFLP1	No	Yes

hsa-mir-320D-1	KRTAP24-1	No	Yes
hsa-mir-320D-1	LOC728208	No	Yes
hsa-mir-320D-1	MMP19	Yes	No
hsa-mir-320D-1	NWD1	No	Yes
hsa-mir-320D-1	NXPH4	No	Yes
hsa-mir-320D-1	PABPC4L	No	Yes
hsa-mir-320D-1	PAX9	No	Yes
hsa-mir-320D-1	PIP5K1A	No	Yes
hsa-mir-320D-1	RTP1	No	Yes
hsa-mir-320D-1	SESN3	No	Yes
hsa-mir-320D-1	SIGLEC7	No	Yes
hsa-mir-320D-1	SLC11A1	No	Yes
hsa-mir-320D-1	SLC26A9	No	Yes
hsa-mir-320D-1	ST3GAL6	No	Yes
hsa-mir-320D-1	TC2N	Yes	Yes
hsa-mir-320D-1	TCEANC	No	Yes
hsa-mir-320D-1	TDRD5	No	Yes
hsa-mir-320D-1	TMTC1	No	Yes
hsa-mir-320D-1	TNF	No	Yes
hsa-mir-320D-1	TRPC5	No	Yes
hsa-mir-320D-1	ULBP2	No	Yes
hsa-mir-320D-1	USH1C	No	Yes
hsa-mir-320D-1	USP50	No	Yes
hsa-mir-320D-1	WNT8B	No	Yes
hsa-mir-320D-1	XAGE3	No	Yes
hsa-mir-320D-1	ZFYVE9	No	Yes
hsa-mir-320D-1	ZNF738	No	Yes
hsa-mir-33B	ABCA8	No	Yes
hsa-mir-33B	ADRA2A	Yes	Yes
hsa-mir-33B	AMELX	No	Yes
hsa-mir-33B	BAGE2	Yes	Yes
hsa-mir-33B	BCL11B	Yes	No
hsa-mir-33B	BMP8B	No	Yes

hsa-mir-33B	CABP7	No	Yes
hsa-mir-33B	CACNB2	No	Yes
hsa-mir-33B	CCL11	No	Yes
hsa-mir-33B	CCL8	No	Yes
hsa-mir-33B	CDH9	No	Yes
hsa-mir-33B	CEACAM3	No	Yes
hsa-mir-33B	CLEC3A	No	Yes
hsa-mir-33B	CREB5	Yes	No
hsa-mir-33B	CSRNP3	Yes	Yes
hsa-mir-33B	DIRAS2	No	Yes
hsa-mir-33B	DSG4	No	Yes
hsa-mir-33B	FAM46C	Yes	Yes
hsa-mir-33B	FGA	No	Yes
hsa-mir-33B	GLIS3	No	Yes
hsa-mir-33B	GLRA2	No	Yes
hsa-mir-33B	KGFLP1	No	Yes
hsa-mir-33B	KLK2	No	Yes
hsa-mir-33B	LOC399900	No	Yes
hsa-mir-33B	LOC728660	No	Yes
hsa-mir-33B	OMG	No	Yes
hsa-mir-33B	S100A7A	No	Yes
hsa-mir-33B	SAMD3	No	Yes
hsa-mir-33B	SH3GL2	No	Yes
hsa-mir-33B	SLAMF6	No	Yes
hsa-mir-33B	SLC12A2	No	Yes
hsa-mir-33B	SOD2	No	Yes
hsa-mir-33B	SUN3	No	Yes
hsa-mir-33B	TNF	No	Yes
hsa-mir-33B	TP63	No	Yes
hsa-mir-33B	TSPY2	No	Yes
hsa-mir-33B	ZNF492	No	Yes
hsa-mir-3529	ARRB1	Yes	No
hsa-mir-370	ACBD7	Yes	Yes

hsa-mir-370	ACP5	No	Yes
hsa-mir-370	ANKRD33	No	Yes
hsa-mir-370	CACNB2	No	Yes
hsa-mir-370	CLEC4M	No	Yes
hsa-mir-370	FSTL4	No	Yes
hsa-mir-370	HNRNPA3P1	No	Yes
hsa-mir-370	KIR2DS4	No	Yes
hsa-mir-370	KLHDC8A	No	Yes
hsa-mir-370	MAGEC2	No	Yes
hsa-mir-370	NLGN4Y	No	Yes
hsa-mir-370	NLRP9	No	Yes
hsa-mir-370	NR1H4	No	Yes
hsa-mir-370	POU2F3	No	Yes
hsa-mir-370	RARRES1	No	Yes
hsa-mir-370	SELE	No	Yes
hsa-mir-370	SLAMF6	Yes	Yes
hsa-mir-370	SLC2A4	No	Yes
hsa-mir-370	TCEANC	No	Yes
hsa-mir-370	TMEM130	No	Yes
hsa-mir-370	TMEM40	Yes	Yes
hsa-mir-370	TRIL	No	Yes
hsa-mir-370	XCR1	No	Yes
hsa-mir-376A-2	ADAMTS18	No	Yes
hsa-mir-376A-2	ANGPT1	No	Yes
hsa-mir-376A-2	CACNB2	No	Yes
hsa-mir-376A-2	CBFA2T3	No	Yes
hsa-mir-376A-2	CDH9	No	Yes
hsa-mir-376A-2	CEACAM3	No	Yes
hsa-mir-376A-2	CMTM5	No	Yes
hsa-mir-376A-2	CT47B1	No	Yes
hsa-mir-376A-2	DIRAS2	No	Yes
hsa-mir-376A-2	HEY2	No	Yes
hsa-mir-376A-2	HSPA7	No	Yes

hsa-mir-376A-2	IL1RN	No	Yes
hsa-mir-376A-2	IQGAP2	No	Yes
hsa-mir-376A-2	ITPKB	No	Yes
hsa-mir-376A-2	KLF15	Yes	Yes
hsa-mir-376A-2	LDHC	No	Yes
hsa-mir-376A-2	LRRC32	No	Yes
hsa-mir-376A-2	NLRP7	No	Yes
hsa-mir-376A-2	NOS1	No	Yes
hsa-mir-376A-2	OTUD7A	No	Yes
hsa-mir-376A-2	PABPC4L	No	Yes
hsa-mir-376A-2	PAX9	No	Yes
hsa-mir-376A-2	PCDHB12	No	Yes
hsa-mir-376A-2	SLCO1B1	No	Yes
hsa-mir-376A-2	ST3GAL6	No	Yes
hsa-mir-376A-2	TMTC1	No	Yes
hsa-mir-376A-2	TP63	No	Yes
hsa-mir-376A-2	ZFYVE9	No	Yes
hsa-mir-376A-2	ZNF492	No	Yes
hsa-mir-376A-2	ZNF608	No	Yes
hsa-mir-378I	FRMPD4	Yes	No
hsa-mir-378I	GSDMC	Yes	No
hsa-mir-381	ADRA2A	No	Yes
hsa-mir-381	ARMCX2	No	Yes
hsa-mir-381	BCL11B	Yes	Yes
hsa-mir-381	CACNA2D2	No	Yes
hsa-mir-381	CACNB2	Yes	Yes
hsa-mir-381	CD207	No	Yes
hsa-mir-381	CDH17	No	Yes
hsa-mir-381	CDH9	No	Yes
hsa-mir-381	CEACAM3	No	Yes
hsa-mir-381	CLEC3A	No	Yes
hsa-mir-381	CSRNP3	Yes	No
hsa-mir-381	DCC	Yes	Yes

hsa-mir-381	FSTL4	No	Yes
hsa-mir-381	GPX2	No	Yes
hsa-mir-381	HNRNPA3P1	No	Yes
hsa-mir-381	HSPA7	No	Yes
hsa-mir-381	IL1RN	No	Yes
hsa-mir-381	KGFLP1	No	Yes
hsa-mir-381	KRT38	No	Yes
hsa-mir-381	LRRC55	No	Yes
hsa-mir-381	MAGEB2	No	Yes
hsa-mir-381	NOTCH3	Yes	Yes
hsa-mir-381	NR1H4	No	Yes
hsa-mir-381	PDCL3	No	Yes
hsa-mir-381	PDK4	No	Yes
hsa-mir-381	PPP1R2P3	No	Yes
hsa-mir-381	SAMD3	No	Yes
hsa-mir-381	SELE	Yes	Yes
hsa-mir-381	SERPINI1	No	Yes
hsa-mir-381	SOD2	No	Yes
hsa-mir-381	SSTR1	No	Yes
hsa-mir-381	TCEANC	No	Yes
hsa-mir-381	TDRD5	No	Yes
hsa-mir-381	TMEM150B	No	Yes
hsa-mir-381	TMPRSS7	No	Yes
hsa-mir-381	ZNF443	No	Yes
hsa-mir-381	ZNF608	No	Yes
hsa-mir-381	ZNF738	No	Yes
hsa-mir-4295	ELL	Yes	No
hsa-mir-4295	MXD1	Yes	No
hsa-mir-4295	SCRT1	Yes	No
hsa-mir-4295	SHANK2	Yes	No
hsa-mir-4295	SMAD4	Yes	No
hsa-mir-4295	WDR7	Yes	No
hsa-mir-4295	ZEB2	Yes	No

hsa-mir-4306	CACNA2D2	Yes	No
hsa-mir-4306	CHRNA10	Yes	No
hsa-mir-4306	NEUROD2	Yes	No
hsa-mir-4306	SYT2	Yes	No
hsa-mir-4306	VWA5B2	Yes	No
hsa-mir-4500	ADRB2	Yes	No
hsa-mir-4500	BACH1	Yes	No
hsa-mir-4500	CGNL1	Yes	No
hsa-mir-4500	KLF8	Yes	No
hsa-mir-4500	MXD1	Yes	No
hsa-mir-4500	SLC30A7	Yes	No
hsa-mir-4500	VSNL1	Yes	No
hsa-mir-494	ADAM7	No	Yes
hsa-mir-494	ANKRD62	No	Yes
hsa-mir-494	BACH1	Yes	Yes
hsa-mir-494	CCDC30	No	Yes
hsa-mir-494	CCT6P3	No	Yes
hsa-mir-494	CDH13	No	Yes
hsa-mir-494	CXCL6	No	Yes
hsa-mir-494	DDR1	No	Yes
hsa-mir-494	DKFZP434L187	No	Yes
hsa-mir-494	ELL	No	Yes
hsa-mir-494	ELOVL7	No	Yes
hsa-mir-494	FAM133B	No	Yes
hsa-mir-494	FCAR	No	Yes
hsa-mir-494	FGF7	Yes	Yes
hsa-mir-494	FLT3	No	Yes
hsa-mir-494	FRMPD4	No	Yes
hsa-mir-494	GATA2	No	Yes
hsa-mir-494	GEM	No	Yes
hsa-mir-494	GLUD1	No	Yes
hsa-mir-494	GRHL1	No	Yes
hsa-mir-494	HNRNPA3	Yes	Yes

hsa-mir-494	KBTBD6	No	Yes
hsa-mir-494	KLF8	No	Yes
hsa-mir-494	KRT6C	No	Yes
hsa-mir-494	MAGEA4	No	Yes
hsa-mir-494	MATN3	No	Yes
hsa-mir-494	MKRN3	No	Yes
hsa-mir-494	MUC15	No	Yes
hsa-mir-494	MXD1	No	Yes
hsa-mir-494	NPM1	No	Yes
hsa-mir-494	PEX10	No	Yes
hsa-mir-494	PF4V1	No	Yes
hsa-mir-494	PRB4	No	Yes
hsa-mir-494	RPRM	No	Yes
hsa-mir-494	RSAD2	No	Yes
hsa-mir-494	SCG3	No	Yes
hsa-mir-494	SDC4	No	Yes
hsa-mir-494	SHANK2	Yes	Yes
hsa-mir-494	SHISA2	Yes	Yes
hsa-mir-494	SPCS2	No	Yes
hsa-mir-494	SSX3	No	Yes
hsa-mir-494	TMEM154	No	Yes
hsa-mir-494	TPI1P3	No	Yes
hsa-mir-494	TTPA	No	Yes
hsa-mir-494	WDR7	No	Yes
hsa-mir-494	ZEB2	No	Yes
hsa-mir-494	ZNF544	No	Yes
hsa-mir-495	ABCA8	No	Yes
hsa-mir-495	ACBD7	No	Yes
hsa-mir-495	ADAMTS18	Yes	Yes
hsa-mir-495	ARMCX2	No	Yes
hsa-mir-495	BCL11B	Yes	Yes
hsa-mir-495	CABP7	No	Yes
hsa-mir-495	CACNB2	No	Yes

hsa-mir-495	CLEC3A	No	Yes
hsa-mir-495	CPS1	No	Yes
hsa-mir-495	CREB5	Yes	No
hsa-mir-495	CSNK1A1L	No	Yes
hsa-mir-495	CST11	No	Yes
hsa-mir-495	CT47B1	No	Yes
hsa-mir-495	DIRAS2	No	Yes
hsa-mir-495	FGB	No	Yes
hsa-mir-495	GLIS3	Yes	Yes
hsa-mir-495	GLRA2	No	Yes
hsa-mir-495	GRAMD1C	No	Yes
hsa-mir-495	GRID1	No	Yes
hsa-mir-495	HAL	No	Yes
hsa-mir-495	HEY2	No	Yes
hsa-mir-495	HSPA7	No	Yes
hsa-mir-495	IQGAP2	No	Yes
hsa-mir-495	IRF4	No	Yes
hsa-mir-495	KCNQ2	No	Yes
hsa-mir-495	KGFLP1	No	Yes
hsa-mir-495	KLK2	No	Yes
hsa-mir-495	KRTAP24-1	No	Yes
hsa-mir-495	KRTAP6-3	No	Yes
hsa-mir-495	LEP	No	Yes
hsa-mir-495	LIPE	No	Yes
hsa-mir-495	LOC285556	No	Yes
hsa-mir-495	MAGEC2	No	Yes
hsa-mir-495	MMP19	No	Yes
hsa-mir-495	MTUS1	No	Yes
hsa-mir-495	NKX2-2	No	Yes
hsa-mir-495	NOS1	No	Yes
hsa-mir-495	NR1H4	No	Yes
hsa-mir-495	PABPC4L	No	Yes
hsa-mir-495	PAX9	No	Yes

hsa-mir-495	PIP5K1A	No	Yes
hsa-mir-495	PLXNA2	Yes	No
hsa-mir-495	PPP1R2P3	No	Yes
hsa-mir-495	RPRML	No	Yes
hsa-mir-495	S100A7A	No	Yes
hsa-mir-495	SESN3	No	Yes
hsa-mir-495	SLC12A2	Yes	Yes
hsa-mir-495	SNX20	No	Yes
hsa-mir-495	SOD2	No	Yes
hsa-mir-495	SSTR1	No	Yes
hsa-mir-495	ST3GAL6	No	Yes
hsa-mir-495	TCEANC	No	Yes
hsa-mir-495	TDRD5	No	Yes
hsa-mir-495	TNF	No	Yes
hsa-mir-495	TP63	No	Yes
hsa-mir-495	TRPC5	No	Yes
hsa-mir-495	WFDC13	No	Yes
hsa-mir-495	ZFYVE9	Yes	Yes
hsa-mir-495	ZNF16	No	Yes
hsa-mir-495	ZNF443	No	Yes
hsa-mir-495	ZNF608	No	Yes
hsa-mir-495	ZNF649	No	Yes
hsa-mir-495	ZNF738	No	Yes

Supplemental Table 3.4 Predicted miRNA-gene Interactions from Nsp13-transfected A549 Cells treated with poly (I:C).

miRNA	Gene Target	Predicted in TargetScan?	Predicted in microRNA.org?
hsa-let-7A-1	AK7	No	Yes
hsa-let-7A-1	ARHGAP25	No	Yes
hsa-let-7A-1	CCL3	Yes	Yes
hsa-let-7A-1	CCT6P1	No	Yes
hsa-let-7A-1	CD209	No	Yes
hsa-let-7A-1	HMGCLL1	No	Yes
hsa-let-7A-1	ISLR	Yes	Yes
hsa-let-7A-1	ITIH1	No	Yes
hsa-let-7A-1	LDB3	Yes	No
hsa-let-7A-1	LOC100270804	No	Yes
hsa-let-7A-1	MSX2P1	No	Yes
hsa-let-7A-1	MXD1	Yes	Yes
hsa-let-7A-1	OOSP1	No	Yes
hsa-let-7A-1	P2RY1	No	Yes
hsa-let-7A-1	PAAF1	No	Yes
hsa-let-7A-1	RABL2B	No	Yes
hsa-let-7A-1	RARRES1	No	Yes
hsa-let-7A-1	RGS21	No	Yes
hsa-let-7A-1	RGSL1	No	Yes
hsa-let-7A-1	RORC	Yes	No
hsa-let-7A-1	SLC27A3	No	Yes
hsa-let-7A-1	SLC32A1	No	Yes
hsa-let-7A-1	SLC6A14	No	Yes
hsa-let-7A-1	SLCO2A1	No	Yes
hsa-let-7A-1	SMAD4	No	Yes
hsa-let-7A-1	SNORD11B	No	Yes
hsa-let-7A-1	SP140L	No	Yes
hsa-let-7A-1	TBC1D8B	No	Yes
hsa-let-7A-1	TMEM25	No	Yes

hsa-let-7A-1	TNFSF10	No	Yes
hsa-let-7A-1	TRIM2	No	Yes
hsa-mir-141	APOLD1	Yes	No
hsa-mir-141	ATP6V1C2	Yes	Yes
hsa-mir-141	CALCRL	No	Yes
hsa-mir-141	CDH17	No	Yes
hsa-mir-141	CEACAM8	No	Yes
hsa-mir-141	CHRDL1	No	Yes
hsa-mir-141	DEFB132	No	Yes
hsa-mir-141	ESYT3	No	Yes
hsa-mir-141	FAM84A	No	Yes
hsa-mir-141	FBXO43	No	Yes
hsa-mir-141	FGA	No	Yes
hsa-mir-141	FGB	No	Yes
hsa-mir-141	FPR3	No	Yes
hsa-mir-141	GPRASP1	No	Yes
hsa-mir-141	HCG27	No	Yes
hsa-mir-141	HLA-L	No	Yes
hsa-mir-141	KCNJ15	No	Yes
hsa-mir-141	LDB3	No	Yes
hsa-mir-141	MXD1	No	Yes
hsa-mir-141	OOSP1	No	Yes
hsa-mir-141	P2RY1	No	Yes
hsa-mir-141	PAAF1	No	Yes
hsa-mir-141	PAX3	Yes	Yes
hsa-mir-141	PCMTD1	No	Yes
hsa-mir-141	PCMTD2	No	Yes
hsa-mir-141	PDGFRA	No	Yes
hsa-mir-141	PPP2R2B	No	Yes
hsa-mir-141	PRB4	No	Yes
hsa-mir-141	PRH2	No	Yes
hsa-mir-141	PSMF1	Yes	Yes
hsa-mir-141	RALYL	No	Yes

hsa-mir-141	RGSL1	No	Yes
hsa-mir-141	SCIN	No	Yes
hsa-mir-141	SLC38A4	No	Yes
hsa-mir-141	SNTN	No	Yes
hsa-mir-141	SP140L	No	Yes
hsa-mir-141	STAT4	Yes	Yes
hsa-mir-141	SULT1C2	No	Yes
hsa-mir-141	TBC1D8B	No	Yes
hsa-mir-141	TESK2	No	Yes
hsa-mir-141	TLX1	No	Yes
hsa-mir-141	TRIM2	Yes	No
hsa-mir-141	WDR31	Yes	Yes
hsa-mir-141	ZNF22	No	Yes
hsa-mir-146A	AK7	No	Yes
hsa-mir-146A	AMBN	No	Yes
hsa-mir-146A	ATP6V1C2	No	Yes
hsa-mir-146A	C15orf62	No	Yes
hsa-mir-146A	CALCRL	No	Yes
hsa-mir-146A	CDH8	No	Yes
hsa-mir-146A	CYP2J2	No	Yes
hsa-mir-146A	DEFB132	No	Yes
hsa-mir-146A	DKFZP434L187	No	Yes
hsa-mir-146A	DNAJC15	No	Yes
hsa-mir-146A	DPPA4	No	Yes
hsa-mir-146A	DPY19L2P4	No	Yes
hsa-mir-146A	FGA	No	Yes
hsa-mir-146A	FGFBP3	No	Yes
hsa-mir-146A	GBP3	No	Yes
hsa-mir-146A	GBP6	No	Yes
hsa-mir-146A	GDNF	Yes	No
hsa-mir-146A	GPR158	No	Yes
hsa-mir-146A	HEY2	No	Yes
hsa-mir-146A	HLA-L	No	Yes

hsa-mir-146A	HMGCLL1	No	Yes
hsa-mir-146A	KRT6B	No	Yes
hsa-mir-146A	KRTAP1-5	No	Yes
hsa-mir-146A	LAIR2	No	Yes
hsa-mir-146A	LDB3	No	Yes
hsa-mir-146A	NHLH1	No	Yes
hsa-mir-146A	PDGFRA	No	Yes
hsa-mir-146A	PLCXD1	No	Yes
hsa-mir-146A	PRH2	No	Yes
hsa-mir-146A	PSMF1	No	Yes
hsa-mir-146A	SCIN	No	Yes
hsa-mir-146A	SLC25A2	No	Yes
hsa-mir-146A	SLC27A3	No	Yes
hsa-mir-146A	SLC2A3	Yes	Yes
hsa-mir-146A	SMAD4	Yes	Yes
hsa-mir-146A	SPDYA	No	Yes
hsa-mir-146A	WDR31	No	Yes
hsa-mir-146A	ZNF529	No	Yes
hsa-mir-146A	ZNF76	No	Yes
hsa-mir-16-2	ARHGEF1	No	Yes
hsa-mir-16-2	ATP6V1C2	No	Yes
hsa-mir-16-2	BCO2	No	Yes
hsa-mir-16-2	BEST4	No	Yes
hsa-mir-16-2	CEACAM7	No	Yes
hsa-mir-16-2	CTH	No	Yes
hsa-mir-16-2	DRP2	Yes	No
hsa-mir-16-2	FBXO43	No	Yes
hsa-mir-16-2	FLRT3	No	Yes
hsa-mir-16-2	GPRASP1	No	Yes
hsa-mir-16-2	HEY2	No	Yes
hsa-mir-16-2	HLA-L	No	Yes
hsa-mir-16-2	HPCAL4	Yes	No
hsa-mir-16-2	ISLR	Yes	Yes

hsa-mir-16-2	ITIH1	No	Yes
hsa-mir-16-2	KIR2DS4	No	Yes
hsa-mir-16-2	KRTAP4-4	Yes	Yes
hsa-mir-16-2	LMOD1	Yes	Yes
hsa-mir-16-2	LOC401463	No	Yes
hsa-mir-16-2	MMP3	No	Yes
hsa-mir-16-2	NHLH1	No	Yes
hsa-mir-16-2	NPM1	No	Yes
hsa-mir-16-2	PAAF1	No	Yes
hsa-mir-16-2	PAK7	Yes	Yes
hsa-mir-16-2	PNRC2	Yes	Yes
hsa-mir-16-2	SCIN	No	Yes
hsa-mir-16-2	SLC25A2	No	Yes
hsa-mir-16-2	SLC2A14	Yes	Yes
hsa-mir-16-2	SLC2A3	Yes	Yes
hsa-mir-16-2	SLC38A4	No	Yes
hsa-mir-16-2	SPRY3	Yes	Yes
hsa-mir-16-2	SULT1C2	No	Yes
hsa-mir-16-2	TMPRSS3	No	Yes
hsa-mir-16-2	TPI1P2	No	Yes
hsa-mir-16-2	TRIM2	Yes	Yes
hsa-mir-16-2	VTCN1	No	Yes
hsa-mir-181B-1	ACAN	Yes	Yes
hsa-mir-181B-1	ADH1A	No	Yes
hsa-mir-181B-1	ANGPT2	No	Yes
hsa-mir-181B-1	ASXL3	No	Yes
hsa-mir-181B-1	BACH2	Yes	Yes
hsa-mir-181B-1	BTNL8	No	Yes
hsa-mir-181B-1	C3orf35	No	Yes
hsa-mir-181B-1	CCDC144NL	No	Yes
hsa-mir-181B-1	CCDC150	No	Yes
hsa-mir-181B-1	CCL8	Yes	Yes
hsa-mir-181B-1	CD69	Yes	Yes

hsa-mir-181B-1	CNP	No	Yes
hsa-mir-181B-1	DMTF1	No	Yes
hsa-mir-181B-1	DRD2	No	Yes
hsa-mir-181B-1	ELAVL2	Yes	Yes
hsa-mir-181B-1	EYA1	No	Yes
hsa-mir-181B-1	FABP7	No	Yes
hsa-mir-181B-1	FAM92A1	No	Yes
hsa-mir-181B-1	FLJ22763	No	Yes
hsa-mir-181B-1	GAB2	No	Yes
hsa-mir-181B-1	GABRA1	Yes	Yes
hsa-mir-181B-1	GAL3ST4	No	Yes
hsa-mir-181B-1	GBA3	No	Yes
hsa-mir-181B-1	GNAT1	No	Yes
hsa-mir-181B-1	GNGT2	No	Yes
hsa-mir-181B-1	GPR85	No	Yes
hsa-mir-181B-1	GRAMD1C	No	Yes
hsa-mir-181B-1	KCNA4	Yes	No
hsa-mir-181B-1	KCNE2	No	Yes
hsa-mir-181B-1	KLHL5	Yes	Yes
hsa-mir-181B-1	KRTAP13-2	No	Yes
hsa-mir-181B-1	LRRC18	No	Yes
hsa-mir-181B-1	LRRC7	No	Yes
hsa-mir-181B-1	MPP7	Yes	Yes
hsa-mir-181B-1	NRXN3	No	Yes
hsa-mir-181B-1	OR51E1	No	Yes
hsa-mir-181B-1	OXTR	No	Yes
hsa-mir-181B-1	PCDH11Y	No	Yes
hsa-mir-181B-1	PCID2	No	Yes
hsa-mir-181B-1	PLA2G3	No	Yes
hsa-mir-181B-1	PODXL	Yes	No
hsa-mir-181B-1	POTEA	No	Yes
hsa-mir-181B-1	PSG1	No	Yes
hsa-mir-181B-1	PXT1	No	Yes

hsa-mir-181B-1	SLC12A5	Yes	Yes
hsa-mir-181B-1	SLC24A4	No	Yes
hsa-mir-181B-1	SLC7A11	Yes	Yes
hsa-mir-181B-1	SLITRK2	No	Yes
hsa-mir-181B-1	SNAI2	No	Yes
hsa-mir-181B-1	SNRPN	No	Yes
hsa-mir-181B-1	SP5	No	Yes
hsa-mir-181B-1	TPD52L3	No	Yes
hsa-mir-181B-1	VGLL2	No	Yes
hsa-mir-181B-1	WDR7	No	Yes
hsa-mir-181B-1	ZNF83	Yes	Yes
hsa-mir-194-2HG	ARHGAP6	No	Yes
hsa-mir-194-2HG	BACH1	No	Yes
hsa-mir-194-2HG	C3orf35	No	Yes
hsa-mir-194-2HG	CCDC144NL	No	Yes
hsa-mir-194-2HG	CCDC150	No	Yes
hsa-mir-194-2HG	CHORDC1	No	Yes
hsa-mir-194-2HG	CIITA	No	Yes
hsa-mir-194-2HG	ENTPD4	No	Yes
hsa-mir-194-2HG	EYA1	No	Yes
hsa-mir-194-2HG	FAM92A1	No	Yes
hsa-mir-194-2HG	GABRA1	No	Yes
hsa-mir-194-2HG	GRAMD1C	No	Yes
hsa-mir-194-2HG	KCNA4	No	Yes
hsa-mir-194-2HG	KLHL5	No	Yes
hsa-mir-194-2HG	MED27	No	Yes
hsa-mir-194-2HG	MEI1	No	Yes
hsa-mir-194-2HG	PCDH11Y	No	Yes
hsa-mir-194-2HG	RAB3B	Yes	Yes
hsa-mir-194-2HG	ROR2	No	Yes
hsa-mir-194-2HG	RPS6KA5	No	Yes
hsa-mir-194-2HG	SLC30A8	Yes	Yes
hsa-mir-194-2HG	SNRPN	No	Yes

hsa-mir-194-2HG	WDR7	No	Yes
hsa-mir-194-2HG	WNK3	No	Yes
hsa-mir-196A-1	AGBL3	No	Yes
hsa-mir-196A-1	APOLD1	No	Yes
hsa-mir-196A-1	ATP6V1C2	No	Yes
hsa-mir-196A-1	BCL2L15	No	Yes
hsa-mir-196A-1	CD209	No	Yes
hsa-mir-196A-1	CDH17	No	Yes
hsa-mir-196A-1	CDH8	No	Yes
hsa-mir-196A-1	CTSO	No	Yes
hsa-mir-196A-1	ESYT3	No	Yes
hsa-mir-196A-1	FGA	No	Yes
hsa-mir-196A-1	GJB2	No	Yes
hsa-mir-196A-1	GPRASP1	No	Yes
hsa-mir-196A-1	GYS2	No	Yes
hsa-mir-196A-1	HMGCLL1	No	Yes
hsa-mir-196A-1	HPCAL4	No	Yes
hsa-mir-196A-1	LOC641367	No	Yes
hsa-mir-196A-1	NUDT4	No	Yes
hsa-mir-196A-1	P2RY1	No	Yes
hsa-mir-196A-1	PCMTD2	No	Yes
hsa-mir-196A-1	PDGFRA	Yes	Yes
hsa-mir-196A-1	RARRES1	No	Yes
hsa-mir-196A-1	RGSL1	No	Yes
hsa-mir-196A-1	SLC38A4	No	Yes
hsa-mir-196A-1	SNORD11B	No	Yes
hsa-mir-196A-1	TCHH	No	Yes
hsa-mir-196A-1	TRIM2	No	Yes
hsa-mir-197	CALCA	No	Yes
hsa-mir-197	CCDC144B	No	Yes
hsa-mir-197	CCDC30	No	Yes
hsa-mir-197	CDH17	No	Yes
hsa-mir-197	CDH8	No	Yes

hsa-mir-197	CNGB1	No	Yes
hsa-mir-197	CX3CR1	No	Yes
hsa-mir-197	DEFB132	No	Yes
hsa-mir-197	EXOC4	No	Yes
hsa-mir-197	FGFR1OP2	No	Yes
hsa-mir-197	GCSH	No	Yes
hsa-mir-197	GPRASP1	No	Yes
hsa-mir-197	GYS2	No	Yes
hsa-mir-197	H3F3C	No	Yes
hsa-mir-197	HLA-L	No	Yes
hsa-mir-197	IFNA4	No	Yes
hsa-mir-197	LOC401463	No	Yes
hsa-mir-197	PAAF1	No	Yes
hsa-mir-197	PAX3	No	Yes
hsa-mir-197	PDGFRA	Yes	Yes
hsa-mir-197	SCIN	No	Yes
hsa-mir-197	SLC32A1	Yes	Yes
hsa-mir-197	SLC47A2	No	Yes
hsa-mir-197	SLC6A14	No	Yes
hsa-mir-197	SLCO2A1	No	Yes
hsa-mir-197	SPDYA	No	Yes
hsa-mir-197	SPRY3	No	Yes
hsa-mir-197	SUPT5H	No	Yes
hsa-mir-197	TCEANC2	Yes	No
hsa-mir-197	TMEM169	No	Yes
hsa-mir-197	TNFSF10	No	Yes
hsa-mir-197	ZNF529	No	Yes
hsa-mir-197	ZNF675	No	Yes
hsa-mir-197	ZNF69	No	Yes
hsa-mir-197	ZNF726	No	Yes
hsa-mir-200A	ADORA1	No	Yes
hsa-mir-200A	ANGPT2	No	Yes
hsa-mir-200A	ARHGAP6	No	Yes

hsa-mir-200A	BACH1	No	Yes
hsa-mir-200A	BACH2	Yes	Yes
hsa-mir-200A	BAGE2	No	Yes
hsa-mir-200A	BMX	No	Yes
hsa-mir-200A	C11orf68	No	Yes
hsa-mir-200A	C9orf152	No	Yes
hsa-mir-200A	CCDC144NL	No	Yes
hsa-mir-200A	CCDC150	No	Yes
hsa-mir-200A	CNP	Yes	Yes
hsa-mir-200A	CRMP1	Yes	Yes
hsa-mir-200A	CSNK1E	Yes	Yes
hsa-mir-200A	CYP2B6	No	Yes
hsa-mir-200A	CYP3A43	No	Yes
hsa-mir-200A	DRD2	Yes	No
hsa-mir-200A	ELAVL2	Yes	Yes
hsa-mir-200A	EYA1	No	Yes
hsa-mir-200A	FAM161A	No	Yes
hsa-mir-200A	FLJ22763	No	Yes
hsa-mir-200A	FLJ26245	No	Yes
hsa-mir-200A	FSIP2	No	Yes
hsa-mir-200A	GABRA1	No	Yes
hsa-mir-200A	GPR55	No	Yes
hsa-mir-200A	HTR2A	No	Yes
hsa-mir-200A	KLHL5	No	Yes
hsa-mir-200A	LOC730668	No	Yes
hsa-mir-200A	LRRC7	No	Yes
hsa-mir-200A	MEI1	No	Yes
hsa-mir-200A	MPP7	No	Yes
hsa-mir-200A	NPY5R	No	Yes
hsa-mir-200A	NRG3	No	Yes
hsa-mir-200A	NRXN3	No	Yes
hsa-mir-200A	OR51E1	No	Yes
hsa-mir-200A	OTX2	No	Yes

hsa-mir-200A	PCDH11Y	No	Yes
hsa-mir-200A	PPP1R3A	No	Yes
hsa-mir-200A	PXT1	No	Yes
hsa-mir-200A	RPL23AP82	No	Yes
hsa-mir-200A	SLITRK2	No	Yes
hsa-mir-200A	SNRPN	No	Yes
hsa-mir-200A	TCP10L2	No	Yes
hsa-mir-200A	TPD52L3	No	Yes
hsa-mir-200A	USP49	No	Yes
hsa-mir-200A	ZNF83	No	Yes
hsa-mir-23C	BACH2	Yes	No
hsa-mir-23C	HIC1	Yes	No
hsa-mir-23C	KLHL5	Yes	No
hsa-mir-23C	NRXN3	Yes	No
hsa-mir-23C	NT5DC3	Yes	No
hsa-mir-23C	RXRG	Yes	No
hsa-mir-23C	VGLL2	Yes	No
hsa-mir-23C	WNK3	Yes	No
hsa-mir-29C	ARSF	No	Yes
hsa-mir-29C	BCO2	No	Yes
hsa-mir-29C	C18orf42	Yes	No
hsa-mir-29C	CTSO	No	Yes
hsa-mir-29C	DCAF4L1	No	Yes
hsa-mir-29C	DKFZP434L187	No	Yes
hsa-mir-29C	DRP2	Yes	No
hsa-mir-29C	FGA	Yes	Yes
hsa-mir-29C	GCSH	Yes	Yes
hsa-mir-29C	H3F3C	No	Yes
hsa-mir-29C	HCG27	No	Yes
hsa-mir-29C	HEY2	No	Yes
hsa-mir-29C	HMGCLL1	No	Yes
hsa-mir-29C	HPCAL4	Yes	Yes
hsa-mir-29C	KIR2DS4	No	Yes

hsa-mir-29C	LAIR2	No	Yes
hsa-mir-29C	LILRA4	No	Yes
hsa-mir-29C	MOG	Yes	Yes
hsa-mir-29C	MXD1	Yes	Yes
hsa-mir-29C	N4BP2L1	Yes	Yes
hsa-mir-29C	P2RY1	No	Yes
hsa-mir-29C	PAX3	No	Yes
hsa-mir-29C	PCMTD2	No	Yes
hsa-mir-29C	PDGFRA	No	Yes
hsa-mir-29C	PGAP1	Yes	Yes
hsa-mir-29C	PSMF1	No	Yes
hsa-mir-29C	RORC	No	Yes
hsa-mir-29C	SCIN	No	Yes
hsa-mir-29C	SLC27A3	No	Yes
hsa-mir-29C	SLC2A3	No	Yes
hsa-mir-29C	SLC6A14	Yes	Yes
hsa-mir-29C	SNORA30	No	Yes
hsa-mir-29C	SNTN	No	Yes
hsa-mir-29C	SP140L	No	Yes
hsa-mir-29C	SPRY3	No	Yes
hsa-mir-29C	SUPT5H	No	Yes
hsa-mir-29C	TBC1D8B	No	Yes
hsa-mir-29C	TMEM169	Yes	Yes
hsa-mir-29C	TMPRSS3	No	Yes
hsa-mir-29C	TRIM2	No	Yes
hsa-mir-300	AADACL4	No	Yes
hsa-mir-300	BCL2L15	No	Yes
hsa-mir-300	C8orf46	No	Yes
hsa-mir-300	CCDC110	No	Yes
hsa-mir-300	CCDC30	Yes	Yes
hsa-mir-300	CCT6P1	No	Yes
hsa-mir-300	CD209	No	Yes
hsa-mir-300	CDH17	No	Yes

hsa-mir-300	CFHR3	No	Yes
hsa-mir-300	CHRDL1	No	Yes
hsa-mir-300	COX6A1	No	Yes
hsa-mir-300	CSRP3	No	Yes
hsa-mir-300	CTH	No	Yes
hsa-mir-300	CX3CR1	No	Yes
hsa-mir-300	CYP2J2	No	Yes
hsa-mir-300	ESYT3	No	Yes
hsa-mir-300	FBXO43	No	Yes
hsa-mir-300	FLRT3	Yes	Yes
hsa-mir-300	GJB2	No	Yes
hsa-mir-300	GPR158	Yes	Yes
hsa-mir-300	GYS2	No	Yes
hsa-mir-300	HMGCLL1	No	Yes
hsa-mir-300	HNRNPA1L2	No	Yes
hsa-mir-300	IL1RN	No	Yes
hsa-mir-300	KCNJ15	No	Yes
hsa-mir-300	LOC401463	No	Yes
hsa-mir-300	MXD1	No	Yes
hsa-mir-300	N4BP2L1	No	Yes
hsa-mir-300	NPFF	No	Yes
hsa-mir-300	NUDT4	Yes	No
hsa-mir-300	OOSP1	No	Yes
hsa-mir-300	PAAF1	No	Yes
hsa-mir-300	PAX3	No	Yes
hsa-mir-300	PDGFRA	No	Yes
hsa-mir-300	PNRC2	No	Yes
hsa-mir-300	PRH2	No	Yes
hsa-mir-300	SLC6A14	No	Yes
hsa-mir-300	SMAD4	Yes	No
hsa-mir-300	SNCA	Yes	No
hsa-mir-300	SNORA33	No	Yes
hsa-mir-300	SPDYA	No	Yes

hsa-mir-300	SPRY3	Yes	Yes
hsa-mir-300	TBC1D8B	No	Yes
hsa-mir-300	TESK2	No	Yes
hsa-mir-300	TLX1	No	Yes
hsa-mir-300	TRIM2	No	Yes
hsa-mir-300	ZNF22	No	Yes
hsa-mir-300	ZNF529	No	Yes
hsa-mir-300	ZNF680	No	Yes
hsa-mir-30C-1	ADH1A	No	Yes
hsa-mir-30C-1	ARHGAP6	No	Yes
hsa-mir-30C-1	ARL 14.00	No	Yes
hsa-mir-30C-1	BACH1	Yes	No
hsa-mir-30C-1	BACH2	Yes	No
hsa-mir-30C-1	CCDC144NL	No	Yes
hsa-mir-30C-1	CHORDC1	Yes	Yes
hsa-mir-30C-1	CRMP1	No	Yes
hsa-mir-30C-1	DMTF1	No	Yes
hsa-mir-30C-1	ELAVL2	No	Yes
hsa-mir-30C-1	ENTPD1	No	Yes
hsa-mir-30C-1	EYA1	No	Yes
hsa-mir-30C-1	FABP7	No	Yes
hsa-mir-30C-1	FAM161A	No	Yes
hsa-mir-30C-1	FAM47A	No	Yes
hsa-mir-30C-1	FAM47C	No	Yes
hsa-mir-30C-1	FLJ22763	No	Yes
hsa-mir-30C-1	FLJ26245	No	Yes
hsa-mir-30C-1	IFNA21	No	Yes
hsa-mir-30C-1	KCNA4	Yes	No
hsa-mir-30C-1	KLHL5	No	Yes
hsa-mir-30C-1	LAMC3	No	Yes
hsa-mir-30C-1	LOC340074	No	Yes
hsa-mir-30C-1	LRRC7	No	Yes
hsa-mir-30C-1	LRRTM1	No	Yes

hsa-mir-30C-1	MED27	No	Yes
hsa-mir-30C-1	MEI1	No	Yes
hsa-mir-30C-1	MPP7	No	Yes
hsa-mir-30C-1	MYL1	No	Yes
hsa-mir-30C-1	NPY5R	No	Yes
hsa-mir-30C-1	NRG3	Yes	Yes
hsa-mir-30C-1	NRXN3	Yes	Yes
hsa-mir-30C-1	PCDH11Y	No	Yes
hsa-mir-30C-1	PODXL	No	Yes
hsa-mir-30C-1	PXT1	No	Yes
hsa-mir-30C-1	RPL23AP82	No	Yes
hsa-mir-30C-1	RPS6KA5	No	Yes
hsa-mir-30C-1	SCN1A	Yes	Yes
hsa-mir-30C-1	SLC12A5	Yes	No
hsa-mir-30C-1	SLC24A4	No	Yes
hsa-mir-30C-1	SLC30A8	No	Yes
hsa-mir-30C-1	SLC7A11	Yes	No
hsa-mir-30C-1	SLITRK3	No	Yes
hsa-mir-30C-1	SNAI2	Yes	Yes
hsa-mir-30C-1	SNRPN	No	Yes
hsa-mir-30C-1	TKTL2	No	Yes
hsa-mir-30C-1	WDR7	Yes	Yes
hsa-mir-30C-1	WNK3	Yes	Yes
hsa-mir-30C-1	ZNF208	No	Yes
hsa-mir-30C-1	ZNF214	No	Yes
hsa-mir-30C-1	ZSCAN12P1	No	Yes
hsa-mir-31	BACH2	Yes	Yes
hsa-mir-31	C3orf35	No	Yes
hsa-mir-31	C6orf10	No	Yes
hsa-mir-31	C9orf152	No	Yes
hsa-mir-31	CCL25	No	Yes
hsa-mir-31	CHORDC1	No	Yes
hsa-mir-31	CNP	Yes	No

hsa-mir-31	CRISPLD2	No	Yes
hsa-mir-31	CSNK1E	No	Yes
hsa-mir-31	CYP4A11	No	Yes
hsa-mir-31	DMTF1	No	Yes
hsa-mir-31	ELAVL2	Yes	Yes
hsa-mir-31	ENPP6	No	Yes
hsa-mir-31	FABP7	No	Yes
hsa-mir-31	FAM47A	No	Yes
hsa-mir-31	FAM47C	No	Yes
hsa-mir-31	FLJ22763	No	Yes
hsa-mir-31	GOLGA6L6	No	Yes
hsa-mir-31	GRAMD1C	No	Yes
hsa-mir-31	LOC340074	No	Yes
hsa-mir-31	LOC653786	No	Yes
hsa-mir-31	MEI1	No	Yes
hsa-mir-31	MTMR7	No	Yes
hsa-mir-31	NBPF22P	No	Yes
hsa-mir-31	NRG3	No	Yes
hsa-mir-31	PCDH11Y	No	Yes
hsa-mir-31	PPP1R3A	No	Yes
hsa-mir-31	PSG1	No	Yes
hsa-mir-31	RPL23AP82	No	Yes
hsa-mir-31	SLC12A5	No	Yes
hsa-mir-31	SLC30A8	No	Yes
hsa-mir-31	SNRPN	No	Yes
hsa-mir-31	VGLL2	No	Yes
hsa-mir-329-1	ABCC6P2	No	Yes
hsa-mir-329-1	ARHGEF35	No	Yes
hsa-mir-329-1	BCL2L15	No	Yes
hsa-mir-329-1	CALCRL	No	Yes
hsa-mir-329-1	CCDC30	No	Yes
hsa-mir-329-1	CHRDL1	Yes	Yes
hsa-mir-329-1	DKFZP434L187	No	Yes

hsa-mir-329-1	FAM66D	No	Yes
hsa-mir-329-1	GFI1	No	Yes
hsa-mir-329-1	HLA-L	No	Yes
hsa-mir-329-1	IVL	No	Yes
hsa-mir-329-1	LDB3	No	Yes
hsa-mir-329-1	LOC645752	No	Yes
hsa-mir-329-1	MXD1	No	Yes
hsa-mir-329-1	NHLH1	No	Yes
hsa-mir-329-1	PAAF1	No	Yes
hsa-mir-329-1	PAX3	No	Yes
hsa-mir-329-1	PDGFRA	No	Yes
hsa-mir-329-1	PGAP1	Yes	No
hsa-mir-329-1	PLA2G4A	No	Yes
hsa-mir-329-1	PLCXD1	No	Yes
hsa-mir-329-1	PLEKHG1	No	Yes
hsa-mir-329-1	PRDM9	No	Yes
hsa-mir-329-1	SLC32A1	No	Yes
hsa-mir-329-1	SNORD114-31	No	Yes
hsa-mir-329-1	TCHH	No	Yes
hsa-mir-329-1	TNFSF10	No	Yes
hsa-mir-329-1	TRIM48	No	Yes
hsa-mir-329-1	ZCCHC16	No	Yes
hsa-mir-329-1	ZNF596	No	Yes
hsa-mir-329-2	ACAN	No	Yes
hsa-mir-329-2	ATAD3B	No	Yes
hsa-mir-329-2	BACH1	No	Yes
hsa-mir-329-2	C9orf62	No	Yes
hsa-mir-329-2	CCDC144NL	No	Yes
hsa-mir-329-2	CCDC150	No	Yes
hsa-mir-329-2	CDYL2	No	Yes
hsa-mir-329-2	CRMP1	Yes	Yes
hsa-mir-329-2	CSNK1E	No	Yes
hsa-mir-329-2	ENPP6	No	Yes

hsa-mir-329-2	FAM92A1	No	Yes
hsa-mir-329-2	FGD2	No	Yes
hsa-mir-329-2	GNAT1	No	Yes
hsa-mir-329-2	GRIK1	No	Yes
hsa-mir-329-2	HRNR	No	Yes
hsa-mir-329-2	KLK11	No	Yes
hsa-mir-329-2	MED27	No	Yes
hsa-mir-329-2	MEI1	No	Yes
hsa-mir-329-2	MPP7	No	Yes
hsa-mir-329-2	NBPF22P	No	Yes
hsa-mir-329-2	NRG3	No	Yes
hsa-mir-329-2	OTX2	No	Yes
hsa-mir-329-2	PCDH11Y	No	Yes
hsa-mir-329-2	SNRPN	No	Yes
hsa-mir-329-2	SPDYE5	No	Yes
hsa-mir-329-2	TMEM201	Yes	No
hsa-mir-329-2	VGLL2	No	Yes
hsa-mir-329-2	ZNF285	No	Yes
hsa-mir-329-2	ZNF876P	No	Yes
hsa-mir-34A	ANKRD33	No	Yes
hsa-mir-34A	ARHGAP25	No	Yes
hsa-mir-34A	BCO2	No	Yes
hsa-mir-34A	CALCA	No	Yes
hsa-mir-34A	CNGB1	No	Yes
hsa-mir-34A	CSRP3	No	Yes
hsa-mir-34A	DGCR6L	No	Yes
hsa-mir-34A	DKFZP434L187	No	Yes
hsa-mir-34A	DMGDH	No	Yes
hsa-mir-34A	ESYT3	Yes	Yes
hsa-mir-34A	FGB	No	Yes
hsa-mir-34A	FLJ40288	No	Yes
hsa-mir-34A	FLRT3	No	Yes
hsa-mir-34A	GCSH	No	Yes

hsa-mir-34A	GOLGA6L4	No	Yes
hsa-mir-34A	GPR158	Yes	Yes
hsa-mir-34A	HLA-L	No	Yes
hsa-mir-34A	HPCAL4	No	Yes
hsa-mir-34A	IL1RN	No	Yes
hsa-mir-34A	ITIH1	No	Yes
hsa-mir-34A	KIR2DS4	No	Yes
hsa-mir-34A	KIR3DL2	No	Yes
hsa-mir-34A	LOC644554	No	Yes
hsa-mir-34A	MOV10L1	No	Yes
hsa-mir-34A	PAK7	No	Yes
hsa-mir-34A	PAX3	No	Yes
hsa-mir-34A	PDGFRA	Yes	Yes
hsa-mir-34A	PIPOX	No	Yes
hsa-mir-34A	RBP5	No	Yes
hsa-mir-34A	SLC27A3	No	Yes
hsa-mir-34A	SLC6A14	No	Yes
hsa-mir-34A	SLCO2A1	No	Yes
hsa-mir-34A	SMAD4	Yes	Yes
hsa-mir-34A	SNCA	No	Yes
hsa-mir-34A	SPRY3	Yes	Yes
hsa-mir-34A	TMEM25	No	Yes
hsa-mir-34A	VTCN1	Yes	Yes
hsa-mir-374A	ACAN	No	Yes
hsa-mir-374A	ANGPT2	No	Yes
hsa-mir-374A	ARHGAP6	No	Yes
hsa-mir-374A	ASPA	No	Yes
hsa-mir-374A	BACH2	Yes	Yes
hsa-mir-374A	C3orf79	No	Yes
hsa-mir-374A	C6orf10	No	Yes
hsa-mir-374A	CCDC150	No	Yes
hsa-mir-374A	CCL8	Yes	Yes
hsa-mir-374A	CD69	No	Yes

hsa-mir-374A	CELA2B	No	Yes
hsa-mir-374A	CIITA	No	Yes
hsa-mir-374A	CYP3A43	No	Yes
hsa-mir-374A	DMTF1	No	Yes
hsa-mir-374A	ELAVL2	No	Yes
hsa-mir-374A	ENPP6	No	Yes
hsa-mir-374A	EYA1	No	Yes
hsa-mir-374A	FABP7	No	Yes
hsa-mir-374A	FAM161A	No	Yes
hsa-mir-374A	FLG2	No	Yes
hsa-mir-374A	GABRA1	No	Yes
hsa-mir-374A	GABRP	No	Yes
hsa-mir-374A	GBA3	No	Yes
hsa-mir-374A	GPR85	No	Yes
hsa-mir-374A	GRAMD1C	No	Yes
hsa-mir-374A	HRNR	No	Yes
hsa-mir-374A	IFNA21	No	Yes
hsa-mir-374A	KCNA4	No	Yes
hsa-mir-374A	KLHL5	No	Yes
hsa-mir-374A	LRRC18	No	Yes
hsa-mir-374A	LRRC7	No	Yes
hsa-mir-374A	MPP7	No	Yes
hsa-mir-374A	MS4A4A	No	Yes
hsa-mir-374A	NBPF22P	No	Yes
hsa-mir-374A	NLRP11	No	Yes
hsa-mir-374A	NRXN3	No	Yes
hsa-mir-374A	OTX2	No	Yes
hsa-mir-374A	OVOS	No	Yes
hsa-mir-374A	PCDH11Y	No	Yes
hsa-mir-374A	PXT1	No	Yes
hsa-mir-374A	RPL23AP82	No	Yes
hsa-mir-374A	RPS6KA5	No	Yes
hsa-mir-374A	SCN1A	No	Yes

hsa-mir-374A	SLC12A5	Yes	Yes
hsa-mir-374A	SLC7A11	No	Yes
hsa-mir-374A	SLITRK3	No	Yes
hsa-mir-374A	SNRPN	No	Yes
hsa-mir-374A	SP5	Yes	Yes
hsa-mir-374A	SPDYE5	No	Yes
hsa-mir-374A	SRD5A2	No	Yes
hsa-mir-374A	SYCP3	No	Yes
hsa-mir-374A	TPD52L3	No	Yes
hsa-mir-374A	USP49	No	Yes
hsa-mir-374A	VGLL2	No	Yes
hsa-mir-374A	VNN 1.00	No	Yes
hsa-mir-374A	WDR7	No	Yes
hsa-mir-374A	ZNF214	No	Yes
hsa-mir-374A	ZNF876P	No	Yes
hsa-mir-429	AMBN	No	Yes
hsa-mir-429	ARHGEF1	Yes	Yes
hsa-mir-429	BCO2	No	Yes
hsa-mir-429	C18orf63	Yes	No
hsa-mir-429	CCT6P1	No	Yes
hsa-mir-429	CDH17	No	Yes
hsa-mir-429	CHRDL1	Yes	Yes
hsa-mir-429	CNGB1	No	Yes
hsa-mir-429	CTSO	No	Yes
hsa-mir-429	DEFB132	No	Yes
hsa-mir-429	DNAJC15	No	Yes
hsa-mir-429	ESYT3	No	Yes
hsa-mir-429	FLRT3	No	Yes
hsa-mir-429	GFI1	Yes	Yes
hsa-mir-429	GOLGA8DP	No	Yes
hsa-mir-429	GPR158	Yes	Yes
hsa-mir-429	GPR183	No	Yes
hsa-mir-429	GPRASP1	No	Yes

hsa-mir-429	GSTA1	No	Yes
hsa-mir-429	GYS2	No	Yes
hsa-mir-429	HLA-L	No	Yes
hsa-mir-429	HMGCLL1	No	Yes
hsa-mir-429	IVL	No	Yes
hsa-mir-429	KCNJ15	No	Yes
hsa-mir-429	LDB3	No	Yes
hsa-mir-429	LOC401463	No	Yes
hsa-mir-429	LOC641367	No	Yes
hsa-mir-429	LPAR5	No	Yes
hsa-mir-429	NPM1	No	Yes
hsa-mir-429	NUDT4	Yes	Yes
hsa-mir-429	P2RY1	No	Yes
hsa-mir-429	PAK7	Yes	Yes
hsa-mir-429	PCMTD1	Yes	Yes
hsa-mir-429	PDGFRA	No	Yes
hsa-mir-429	PGAP1	No	Yes
hsa-mir-429	PNRC2	No	Yes
hsa-mir-429	PSMF1	No	Yes
hsa-mir-429	R3HDML	No	Yes
hsa-mir-429	RALYL	No	Yes
hsa-mir-429	RARRES1	No	Yes
hsa-mir-429	RASSF9	No	Yes
hsa-mir-429	SCARNA1	No	Yes
hsa-mir-429	SLC2A3	No	Yes
hsa-mir-429	SLC38A4	Yes	Yes
hsa-mir-429	SMAD4	No	Yes
hsa-mir-429	SNCA	No	Yes
hsa-mir-429	SNTN	No	Yes
hsa-mir-429	SPDYA	No	Yes
hsa-mir-429	SPRY3	No	Yes
hsa-mir-429	TESK2	No	Yes
hsa-mir-429	TMEM191C	No	Yes

hsa-mir-429	TMEM25	No	Yes
hsa-mir-429	TNFSF10	No	Yes
hsa-mir-429	TRIM2	No	Yes
hsa-mir-429	TUBAL3	No	Yes
hsa-mir-429	ZNF529	No	Yes
hsa-mir-429	ZNF680	No	Yes
hsa-mir-429	ZNF724P	No	Yes
hsa-mir-429	ZNF76	No	Yes
hsa-mir-448	ABCC6P2	No	Yes
hsa-mir-448	AGBL3	No	Yes
hsa-mir-448	ANXA13	No	Yes
hsa-mir-448	ARHGAP25	No	Yes
hsa-mir-448	CALCRL	Yes	Yes
hsa-mir-448	CCDC110	No	Yes
hsa-mir-448	CCDC144B	No	Yes
hsa-mir-448	CYP2J2	No	Yes
hsa-mir-448	CYS1	No	Yes
hsa-mir-448	DCAF4L1	No	Yes
hsa-mir-448	DPY19L2P4	No	Yes
hsa-mir-448	EXOC4	No	Yes
hsa-mir-448	F7	No	Yes
hsa-mir-448	FGFR1OP2	No	Yes
hsa-mir-448	FLRT3	No	Yes
hsa-mir-448	GPR158	Yes	No
hsa-mir-448	GSTA1	No	Yes
hsa-mir-448	H3F3C	No	Yes
hsa-mir-448	HEY2	Yes	Yes
hsa-mir-448	HLA-L	No	Yes
hsa-mir-448	ITIH1	No	Yes
hsa-mir-448	LDB3	No	Yes
hsa-mir-448	LOC401463	No	Yes
hsa-mir-448	MSX2P1	No	Yes
hsa-mir-448	N4BP2L1	No	Yes

hsa-mir-448	NUDT4	No	Yes
hsa-mir-448	PDGFRA	No	Yes
hsa-mir-448	PLA2G4A	No	Yes
hsa-mir-448	RGSL1	No	Yes
hsa-mir-448	SCIN	No	Yes
hsa-mir-448	SLC38A4	No	Yes
hsa-mir-448	SLC6A14	No	Yes
hsa-mir-448	SLCO2A1	No	Yes
hsa-mir-448	SNTN	No	Yes
hsa-mir-448	SPDYA	No	Yes
hsa-mir-448	SPRY3	No	Yes
hsa-mir-448	STAR	No	Yes
hsa-mir-448	STAT4	No	Yes
hsa-mir-448	TBC1D8B	No	Yes
hsa-mir-448	TESK2	Yes	No
hsa-mir-448	ZNF724P	No	Yes
hsa-mir-4500	BACH1	Yes	No
hsa-mir-4500	CDH22	Yes	No
hsa-mir-4500	GAB2	Yes	No
hsa-mir-4500	GNAT1	Yes	No
hsa-mir-4500	HIC1	Yes	No
hsa-mir-4500	PLA2G3	Yes	No
hsa-mir-4500	PXT1	Yes	No
hsa-mir-4500	WNK3	Yes	No
hsa-mir-495	APOLD1	No	Yes
hsa-mir-495	ARHGAP25	No	Yes
hsa-mir-495	BCL2L15	No	Yes
hsa-mir-495	BEST4	No	Yes
hsa-mir-495	C12orf56	No	Yes
hsa-mir-495	C8orf46	No	Yes
hsa-mir-495	CALCRL	No	Yes
hsa-mir-495	CCDC110	No	Yes
hsa-mir-495	CCDC144B	No	Yes

hsa-mir-495	CCDC30	No	Yes
hsa-mir-495	CTH	No	Yes
hsa-mir-495	CTSO	No	Yes
hsa-mir-495	CYS1	No	Yes
hsa-mir-495	DEFB132	No	Yes
hsa-mir-495	DKFZP434L187	No	Yes
hsa-mir-495	DNAJC15	No	Yes
hsa-mir-495	DPPA4	No	Yes
hsa-mir-495	DRP2	Yes	No
hsa-mir-495	FAM66D	No	Yes
hsa-mir-495	FGB	No	Yes
hsa-mir-495	FGFR1OP2	Yes	No
hsa-mir-495	FPR3	No	Yes
hsa-mir-495	GBP6	No	Yes
hsa-mir-495	GFI1	Yes	Yes
hsa-mir-495	GJB2	No	Yes
hsa-mir-495	GK2	No	Yes
hsa-mir-495	GPR158	No	Yes
hsa-mir-495	GPR183	No	Yes
hsa-mir-495	GSTA1	No	Yes
hsa-mir-495	HEY2	No	Yes
hsa-mir-495	HLA-L	No	Yes
hsa-mir-495	HMGCLL1	Yes	Yes
hsa-mir-495	LOC100270804	No	Yes
hsa-mir-495	MAGEB10	No	Yes
hsa-mir-495	MOG	No	Yes
hsa-mir-495	MOV10L1	No	Yes
hsa-mir-495	MSX2P1	No	Yes
hsa-mir-495	MXD1	No	Yes
hsa-mir-495	NAB2	Yes	Yes
hsa-mir-495	NPM1	No	Yes
hsa-mir-495	OCA2	No	Yes
hsa-mir-495	PAAF1	No	Yes

hsa-mir-495	PAX3	No	Yes
hsa-mir-495	PCMTD1	No	Yes
hsa-mir-495	PDGFRA	No	Yes
hsa-mir-495	PGAP1	No	Yes
hsa-mir-495	PIPOX	No	Yes
hsa-mir-495	PLA2G4A	No	Yes
hsa-mir-495	PLEKHG1	No	Yes
hsa-mir-495	PRDM9	No	Yes
hsa-mir-495	PRR23B	No	Yes
hsa-mir-495	RABL2B	No	Yes
hsa-mir-495	RASSF9	No	Yes
hsa-mir-495	SCIN	No	Yes
hsa-mir-495	SLC2A14	No	Yes
hsa-mir-495	SLC2A3	No	Yes
hsa-mir-495	SMAD4	No	Yes
hsa-mir-495	SNCA	Yes	Yes
hsa-mir-495	STAT4	No	Yes
hsa-mir-495	SUPT5H	No	Yes
hsa-mir-495	TCHH	No	Yes
hsa-mir-495	TLX1	No	Yes
hsa-mir-495	TRIM2	No	Yes
hsa-mir-495	ZCCHC16	No	Yes
hsa-mir-495	ZNF22	No	Yes
hsa-mir-495	ZNF680	No	Yes
hsa-mir-495	ZNF726	No	Yes
hsa-mir-7-2	AGBL3	No	Yes
hsa-mir-7-2	APOLD1	No	Yes
hsa-mir-7-2	BCO2	No	Yes
hsa-mir-7-2	C8orf46	Yes	Yes
hsa-mir-7-2	CCDC30	No	Yes
hsa-mir-7-2	CDH8	No	Yes
hsa-mir-7-2	CHRNA10	No	Yes
hsa-mir-7-2	CX3CR1	No	Yes

hsa-mir-7-2	DEFB132	No	Yes
hsa-mir-7-2	DNAJC15	No	Yes
hsa-mir-7-2	DRP2	No	Yes
hsa-mir-7-2	FBXO43	No	Yes
hsa-mir-7-2	FGA	No	Yes
hsa-mir-7-2	FGG	No	Yes
hsa-mir-7-2	HPCAL4	Yes	Yes
hsa-mir-7-2	IFNA16	No	Yes
hsa-mir-7-2	IFNA4	No	Yes
hsa-mir-7-2	KRT27	No	Yes
hsa-mir-7-2	KRTAP1-5	No	Yes
hsa-mir-7-2	LAIR2	No	Yes
hsa-mir-7-2	MOG	No	Yes
hsa-mir-7-2	MRAP2	No	Yes
hsa-mir-7-2	NPM1	No	Yes
hsa-mir-7-2	PAAF1	No	Yes
hsa-mir-7-2	PPP2R2B	No	Yes
hsa-mir-7-2	PRR23B	No	Yes
hsa-mir-7-2	RGS21	No	Yes
hsa-mir-7-2	SCARNA23	No	Yes
hsa-mir-7-2	SCTR	No	Yes
hsa-mir-7-2	SLC38A4	Yes	Yes
hsa-mir-7-2	SLC7A9	No	Yes
hsa-mir-7-2	SNCA	Yes	Yes
hsa-mir-7-2	SNORA33	No	Yes
hsa-mir-7-2	TBC1D8B	No	Yes
hsa-mir-7-2	TCHH	No	Yes
hsa-mir-7-2	ZNF214	No	Yes
hsa-mir-758	AIF1	No	Yes
hsa-mir-758	CALCA	No	Yes
hsa-mir-758	CCDC30	No	Yes
hsa-mir-758	CEACAM7	No	Yes
hsa-mir-758	CHRDL1	No	Yes

hsa-mir-758	DPPA4	No	Yes
hsa-mir-758	ESYT3	No	Yes
hsa-mir-758	EXOC4	No	Yes
hsa-mir-758	FGB	No	Yes
hsa-mir-758	FGFBP3	No	Yes
hsa-mir-758	FLRT3	No	Yes
hsa-mir-758	FPR3	No	Yes
hsa-mir-758	GFI1	No	Yes
hsa-mir-758	GPR158	No	Yes
hsa-mir-758	HLA-L	No	Yes
hsa-mir-758	HMGCLL1	No	Yes
hsa-mir-758	MXD1	Yes	Yes
hsa-mir-758	NAB2	No	Yes
hsa-mir-758	PAAF1	No	Yes
hsa-mir-758	PAK7	No	Yes
hsa-mir-758	PCMTD2	No	Yes
hsa-mir-758	PDGFRA	No	Yes
hsa-mir-758	PGAP1	Yes	Yes
hsa-mir-758	RGS21	No	Yes
hsa-mir-758	SAA1	No	Yes
hsa-mir-758	SLC2A3	No	Yes
hsa-mir-758	SLC47A2	No	Yes
hsa-mir-758	SMAD4	No	Yes
hsa-mir-758	SPDYA	No	Yes
hsa-mir-758	STAT4	No	Yes
hsa-mir-758	TBC1D8B	No	Yes
hsa-mir-758	TRIM2	No	Yes
hsa-mir-874	ARHGAP6	No	Yes
hsa-mir-874	C1orf132	No	Yes
hsa-mir-874	C20orf85	No	Yes
hsa-mir-874	C3orf35	No	Yes
hsa-mir-874	CCDC150	No	Yes
hsa-mir-874	CIITA	No	Yes

hsa-mir-874	CNP	No	Yes
hsa-mir-874	KLK11	No	Yes
hsa-mir-874	LILRB1	No	Yes
hsa-mir-874	LOC340074	No	Yes
hsa-mir-874	PCDH11Y	Yes	Yes
hsa-mir-874	SLC12A5	Yes	Yes
hsa-mir-874	SLC30A8	Yes	Yes
hsa-mir-96	ARHGAP6	Yes	Yes
hsa-mir-96	BACH1	No	Yes
hsa-mir-96	BACH2	Yes	No
hsa-mir-96	CCDC150	No	Yes
hsa-mir-96	CD69	No	Yes
hsa-mir-96	CIITA	No	Yes
hsa-mir-96	DNAJB8	No	Yes
hsa-mir-96	ELAVL2	Yes	No
hsa-mir-96	ENTPD4	No	Yes
hsa-mir-96	FAM92A1	No	Yes
hsa-mir-96	FGD2	No	Yes
hsa-mir-96	FLJ22763	No	Yes
hsa-mir-96	FSIP2	No	Yes
hsa-mir-96	GIPR	No	Yes
hsa-mir-96	GOLGA6L6	No	Yes
hsa-mir-96	GPR85	Yes	Yes
hsa-mir-96	GRAMD1C	No	Yes
hsa-mir-96	HRNR	No	Yes
hsa-mir-96	LRRC7	Yes	Yes
hsa-mir-96	MOGAT2	No	Yes
hsa-mir-96	NRXN3	No	Yes
hsa-mir-96	NT5DC3	Yes	No
hsa-mir-96	PCDH11Y	Yes	Yes
hsa-mir-96	PODXL	Yes	No
hsa-mir-96	SCN1A	Yes	No
hsa-mir-96	SLC12A5	Yes	Yes

hsa-mir-96	SLC24A4	Yes	Yes
hsa-mir-96	SLITRK3	No	Yes
hsa-mir-96	SNAI2	No	Yes
hsa-mir-96	SNRPN	No	Yes
hsa-mir-96	TPD52L3	No	Yes

Supplemental Table 3.5 List of qPCR Primers used.

Gene	Forward Sequence (5' – 3')	Reverse Sequence (5' – 3')
18S	GCGATGCGGCGGCGTTATTC	CAATCTGTCAATCCTGTCCGTGTCC
TRAF6	TTTGCTCTTATGGATTGTCCCC	CATTGATGCAGCACAGTTGTC
IRAK1	AGGTTTCGTCACCCAAACATT	CGGGCTGTACCCAGAAGGA
SMAD4	ACGAACGAGTTGTATCACCTGG	TGCACGATTACTTGGTGGATG

Supplemental Table 3.6 List of Primary Antibodies used.

Primary Antibody	Dilution	Manufacturer (Catalog Number)
FLAG M2	1:2000	Sigma-Aldrich (F1804)
p-NF-κB (p65) (Ser-536)	1:1000	Cell Signalling Technology (3033)
NF-κB (p65) (D14E12) XP	1:1000	Cell Signalling Technology (8242)
β-tubulin	1:5000	Abcam (610621)